

POLITECNICO DI TORINO

Dipartimento di Ingegneria Meccanica e Aerospaziale
Master's Degree in Automotive Engineering

Master's Degree Thesis

Design and Multi-Objective Optimisation of the Axial Flux Machine



**Politecnico
di Torino**



Koenigsegg

Supervisor

Prof. Gianmario PELLEGRINO

Candidate

Jorge Luis LORA

Anno accademico 2023/2024

Abstract

This thesis presents a comprehensive approach to the design and multi-objective optimisation of double stator axial flux permanent magnet machines. Starting with the vehicle's specifications and the given driving cycles, the electric motor's requisite parameters are derived and the operating point that represents the region of highest energy consumption, defined as centroid, is identified. Subsequently, an analytical designed process is performed, considering the requirements of the drive cycle analysis. This stage facilitates the determination of parameters which are then used to model three different motors, each defined by unique combinations of slots and poles, within a quasi-3D FEA software. The performance of these machines is verified to ensure compliance with the torque and power demands of the mission profiles. Finally, a multi-objective optimisation process was executed via the genetic algorithm in conjunction with the quasi-3D FEA software with the aim of obtaining motors that have characteristic curves capable of covering all operating points and exhibit higher efficiency at the centroid to further reduce the total energy consumption throughout the entire driving cycles.

Acknowledgements

It is imperative for duty, affection and admiration to reserve this space for those who made possible, with their indispensable support, my arrival here, to the conclusion of my master thesis.

First of all, my thankfulness and gratitude to my supervisor, Professor Gianmario Pellegrino, for giving me the opportunity to gain experience in this important company where I was lucky to meet, both inside and outside, people of different nationalities. The single but varied life stories made me a more empathetic person, even having to rethink my deepest certainties and understanding how important the life of each of us is.

It was a relatively short but qualitatively intense experience that allowed me to grow up and mature.

Thank you professor because I could interact with engineers of high professional profile who, without hesitation, gave me the right tips to learn more and who, more than a few times, showed me the human side by telling me about their difficulties and successes encouraging me to never give up and always be ready for new challenges.

I will not get tired of thanking you for your valuable suggestions and advice which increasingly enriched my knowledge and analytical skills in the realisation of the elaborate and that I will certainly keep with value for the future.

I thank infinitely for this fervent and rich experience to the company Koenigsegg Automotive AB and with it to the Electrical Machine Design Team and company tutors Bharadwaj Raghuraman, Bruno Ricardo Marques and Dragos-Mihai Postariu whose professionalism and excellence in the field of engineering are also translated into the human and ethical sphere. Thank you for your patient, thank you for your support. I can assert that the fine intelligence is also docile and kind, I am honored and pleased to be part of your acquaintances.

Thanks to those who have been close to me in this intense stretch of life: relatives and friends.

I cannot omit to thank those who are a hymn of courage, strength, tenderness and perseverance, to those for whom I profess an infinite reciprocal love: to my parents, safe harbor of my joys, without whom I would not have learned to face life and I

would not have understood that at the end of the tunnel, there is light, there is hope, that fatigue can be perceived as optimism and that the goal is reached by those who never give up and this is the realisation of oneself.

Thanks to my father Jorge, always ready to lift my difficulties. I also thank myself because I fulfilled my dream with joy, perseverance, effort and passion. I tested my tenacity and strength, I am happy to have succeeded and I am ready for new challenges.

And thanks especially to my mother Fanny because due to her I know that in the depths of life there is only love.

Table of Contents

List of Tables	VIII
List of Figures	IX
Acronyms	XIII
1 Introduction	1
1.1 Objective	1
1.2 Canopy Simulations	1
1.3 MotorXP - AFM	1
1.4 GOSET	2
2 Background	5
2.1 Brushless permanent magnet machines	6
2.2 Axial flux permanent magnet machines	10
2.3 Topologies	12
2.3.1 Single-sided machine	12
2.3.2 Double-stators and one internal rotor	13
2.3.3 Double-rotors and one internal stator	14
2.3.4 Multidisc machine	15
2.4 Materials	16
2.4.1 Soft magnetic materials	16
2.4.2 Hard magnetic materials	18
2.4.3 Windings	19
3 Driving Cycle Analysis	22
3.1 Driving mission profile	22
3.2 Vehicle characteristics	25
3.3 Vehicle model	26
3.4 K-means clustering application	35

4	Analytical design	41
4.1	Phase voltage limit	42
4.2	Slot and pole combination	42
4.3	Sizing of the electrical machines	43
4.4	FEA validation	46
	4.4.1 Results	46
4.5	Torque/speed characteristic curve	47
4.6	Design iterations	53
5	Multi-Objective Optimisation	59
5.1	Optimisation problem	60
5.2	Genetic Algorithm	61
	5.2.1 Objective weighting	62
	5.2.2 Diversity control	62
	5.2.3 Scaling	62
	5.2.4 Selection	63
	5.2.5 Death	63
	5.2.6 Mating cross-over	63
	5.2.7 Mutation	63
	5.2.8 Evaluation	63
	5.2.9 Elitism	65
	5.2.10 Random search	65
5.3	Formulation of design problem	65
	5.3.1 Design metrics	66
	5.3.2 Formulation of the Parameter space	67
	5.3.3 Formulation of the constraint functions	69
	5.3.4 Formulation of the fitness function and the set-up of the optimisation	71
5.4	Results from the genetic algorithm	72
	5.4.1 Pareto Front plot	72
	5.4.2 Genes sorted by Objective 1 - maximisation of the electro- magnetic torque	75
	5.4.3 Genes sorted by Objective 2 - minimisation of the total mass	78
	5.4.4 Genes sorted by Objective 3 - minimisation of the magnet mass	80
	5.4.5 Genes sorted by Objective 4 - minimisation of the stator voltage	82
	5.4.6 Genes sorted by Objective 5 - maximisation of the efficiency at the centroid	84
5.5	Selection	86
	5.5.1 Comparison among the non dominated solutions	86

6	Energy consumed of the optimised e-machines	92
6.1	Losses maps	93
6.2	Results	99
7	Conclusion	102
A	Quotes of the axial flux machine	103
B	Calculation of the current input and advance angle given an operating point	106
C	Comparison of the non dominated solutions	108
	Bibliography	111

List of Tables

4.1	Assumptions	43
4.2	Geometries from analytical design	45
4.3	FEA set-up	46
4.4	FEA results	47
4.5	FEA results improved	57
5.1	Genes to define the Parameter space	68
5.2	Constant parameters	68
5.3	Parameters of the three top e-machines	90
5.4	Objective values of the three top e-machines	90
6.1	Energy consumption of the three optimised machines for Nordschleife driving cycle	99

List of Figures

1.1	Two types of mesh slices [2]	2
2.1	The three key elements transferred to the carmakers	6
2.2	Contemporary technologies	7
2.3	Table to compare different electrical machines	9
2.4	Geometrical comparison between the radial and axial flux machines [11]	11
2.5	Single sided machine [13]	13
2.6	Double stator single rotor: flux paths [13]	14
2.7	Double rotor single stator machine	15
2.8	Multidisc machine [13]	16
2.9	Soft magnetic materials	17
2.10	B-H curves of the NdFeB magnet for different temperatures [9]	19
2.11	Winding types [22]	20
3.1	Driving cycles	24
3.2	Vehicle Gemera [23]	25
3.3	Backward model	27
3.4	WLTC and traction power	29
3.5	Nordschleife and traction power	30
3.6	Drag trip and traction power	30
3.7	WLTC operating points	31
3.8	Nordschleife operating points	32
3.9	Drag trip operating points	33
3.10	Overall operating points	34
3.11	WLTC energy consumption	36
3.12	Nordschleife energy consumption	36
3.13	Drag trip energy consumption	37
3.14	Centroid WLTC	38
3.15	Centroid Nordschleife	39
3.16	Centroid Drag trip	39

4.1	Torque versus speed in 24 slots and 22 poles	50
4.2	Power versus speed in 24 slots and 22 poles	50
4.3	Torque versus speed in 12 slots and 10 poles	51
4.4	Power versus speed in 12 slots and 10 poles	51
4.5	Torque versus speed in 24 slots and 20 poles	52
4.6	Power versus speed in 24 slots and 20 poles	52
4.7	Torque versus speed in 24 slots and 22 poles after the update of the number of turns	54
4.8	Power versus speed in 24 slots and 22 poles after the update of the number of turns	54
4.9	Torque versus speed in 12 slots and 10 poles after the update of the number of turns	55
4.10	Power versus speed in 12 slots and 10 poles after the update of the number of turns	55
4.11	Torque versus speed in 24 slots and 20 poles after the update of the number of turns	56
4.12	Power versus speed in 24 slots and 20 poles after the update of the number of turns	56
5.1	Application of the genetic algorithm	59
5.2	GOSET flowchart	62
5.3	Operating points at which the Quasi-3D FEA software runs Magne- tostatic simulation	67
5.4	Electromagnetic torque versus magnet mass	73
5.5	Efficiency at the centroid versus magnet mass	73
5.6	Electromagnetic torque versus supply voltage	74
5.7	Gene distribution of the e-machines with 24 slots and 22 poles configuration sorted by torque	75
5.8	Gene distribution of the e-machines with 12 slots and 10 poles configuration sorted by torque	75
5.9	Gene distribution of the e-machines with 24 slots and 20 poles configuration sorted by torque	76
5.10	Gene distribution of the e-machines with 24 slots and 22 poles configuration sorted by the total mass	78
5.11	Gene distribution of the e-machine with 12 slots and 10 poles con- figuration sorted by total mass	78
5.12	Gene distribution of the e-machines with 24 slots and 20 poles configuration sorted by the total mass	79
5.13	Gene distribution of the e-machines with 24 slots and 22 poles configuration sorted by magnet mass	80

5.14	Gene distribution for the e-machines with 12 slots and 10 poles configuration sorted by magnet mass	80
5.15	Gene distribution of the e-machines with 24 slots and 20 poles sorted by magnet mass	81
5.16	Gene distribution of the machine with 24 slots and 22 poles configuration sorted by voltage	82
5.17	Gene distribution of the e-machines with 12 slots and 10 poles configuration sorted by voltage	82
5.18	Gene distribution of the e-machines with 24 slots and 20 poles sorted by voltage	83
5.19	Gene distribution of the e-machine with 24 slots and 22 poles sorted by efficiency at the centroid	84
5.20	Gene distribution of the e-machines with 12 slots and 10 poles sorted by efficiency at the centroid	84
5.21	Gene distribution of the e-machines with 24 slots and 20 poles sorted by efficiency at the centroid	85
5.22	Radar plot of non dominated solutions with 24 slots and 22 poles .	86
5.23	Radar plot of non dominated solutions with 12 slots and 10 poles .	87
5.24	Radar plot of non dominated solutions with 24 slots and 20 poles .	87
5.25	electrical machine with 24 slots and 22 poles-Individual 12	88
5.26	electrical machine with 12 slots and 10 poles-Individual 11	89
5.27	electrical machine with 24 slots and 20 poles-Individual 20	89
6.1	DC copper loss maps of the three electrical machines	94
6.2	Hysteresis loss maps of the three electrical machines	95
6.3	Eddy current loss maps of the three electrical machines	96
6.4	Magnet loss maps of the three electrical machines	97
6.5	Total Loss maps of the three electrical machines	98
A.1	Quotes on the stator disc	103
A.2	Quotes on the rotor disc	104
A.3	Quotes on the lateral surface of the e-machine	105
C.1	E-machines with 24 slots and 22 poles	108
C.2	E-machines with 12 slots and 10 poles	109
C.3	E-machines with 24 slots and 20 poles	109

Acronyms

FEA

Finite Element Analysis

AFM

Axial Flux Machine

LMMA

Linear Machine Modelling Approach

GOSET

Genetic Optimization System Engineering Toolbox

MOSFET

Metal-Oxide-Semiconductor Field-Effect Transistor

IGBT

Insulated Gate Bipolar Transistor

AC

Alternate Current

PM

Permanent Magnet

IPM

Internal Permanent Magnet

SPM

Surface Permanent Magnet

SMPM

Surface Mounted Permanent Magnet

SyR

Synchronous Reluctance

DC

Direct Current

MTPA

Maximum Torque Per Ampere

Od

Outer diameter

Id

Inner diameter

Sh

Stator height

Sw

Slot width

Syh

Stator yoke height

Rh

Rotor height

Ms

Magnet spacing

Irms

Phase current

Chapter 1

Introduction

1.1 Objective

The objective of this thesis is to develop and realise a solver in MATLAB, able to design and optimise the axial flux permanent magnet machine by using the genetic algorithm and a Quasi-3D FEA software.

This project allows the engineers to have more than one e-motor as solutions according to their requirements. In order to implement this project effectively, some theoretical aspects of the electrical machines are employed by making scripts.

1.2 Canopy Simulations

Canopy Simulations is a platform used in motor sport teams which evaluates the lap time simulation and vehicle modelling.

Before running the simulation, the user can choose track, weather, set up the powertrain. This is the software used to receive mission profiles to then perform calculations for the design of the electrical machine.

1.3 MotorXP - AFM

The most used technique to simulate the axial flux machine is the 3D FEA. The main drawback is that it is highly time consuming. Another technique is the 2D Linear Machine Modelling Approach which is performed by slicing the machine into cylindrical layers of different radius and then obtaining several linear machines[1]. The magnetic field and the electromagnetic torque are calculated for each slice and the actual torque is the sum of their results. The main problem of this 2D FEA approach is that its results' accuracy is limited because it is not able to capture

the 3D effects.

MotorXP-AFM is a commercial software for electromagnetic design and analysis of the axial flux permanent magnet machines that is accessible both in MATLAB format and as independent program. It is able to include also the 3D effects by implementing the principle of Quasi-3D FEM approach in which it calculates the magnetic field also in the radial cross-section of the motor.

The magnetic field of the machine is split into circumferential and radial components that are observed and calculated by the cylindrical layer mesh (such as the 2D-LMMA) and radial layer mesh respectively. It is only the radial layer mesh that determines most of the time the end effects.

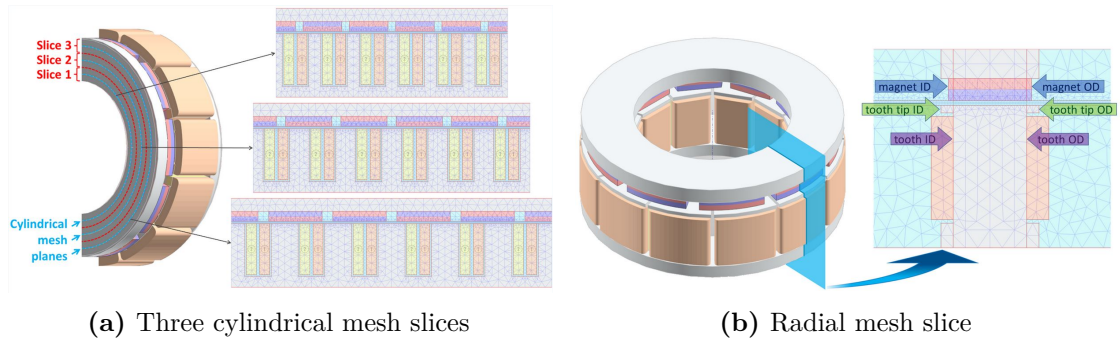


Figure 1.1: Two types of mesh slices [2]

1.4 GOSET

GOSET is a free software package already developed by Purdue University and Office of Naval Research, under the coordination of the professor S.D. Sudhoff, that is implemented for design optimisation in motor design and power electronic applications[3].

GOSET is a MATLAB based code used for solving both single-objective and multi-objective optimisation problems. It contains evolutionary algorithms which allow it to identify global optimum rather than the local optimum. Thus, it is used to solve different engineering problems.

The genetic algorithm is an optimisation method which tries to mimic the evolution: it operates on a population of candidate solutions and applies the principle of survival of the fittest to evolve the candidate solutions towards the desired solutions [4].

The candidate solutions are called as individuals that are encoded to genes that can be presented as a symbol, a binary number, an interger number or a real number. The term population is referred to the group of individuals.

Each individual is a solution of a specific problem and the fitness value is its metric

which says how much the individual is good to solve the problem. The individuals receive that fitness value from a fitness function and those which have a better fitness, they are more likely to survive and reproduce.

All the genetic operators are explained in section 5.2 but for more details they are well explained in the manual [4].

The difference between the single-objective optimisation and the multi-objective optimisation is that in the multi-objective optimisation problem there are more than an objective function and therefore, instead of determining one solution, the result is a set of non-dominated solutions that describe the best trade off between the competing objectives. This specific set of solutions is called the Pareto optimal solution set.

Chapter 2

Background

The propulsion system based on internal combustion engines and mechanical systems has undoubtedly reached a high development and maturity level after more than a hundred years of history. These systems are very well performing and give a satisfactory answer to the main part of the end-user expectation.

Despite these technologies and the distribution fuel infrastructure being very well established, this solution is not the right option.

There are three main elements to be considered:

- Noxious emissions: it is very relevant regarding local impact and air quality. It has a clear connection to the declining health of people living in the vicinity of these vehicles. For many years, there have been standards (applied at large region levels such as Europe, USA and Japan) defining the maximum level of noxious emission that a vehicle can emit under defined conditions. If it is not satisfied, the vehicle cannot be homologated.
- Greenhouse gas emission: it is still an emission issue, but it covers more of a question at the global level and more indirectly. Thus, it can impact the average temperature of the planet and the typology of climate changes. There are voluntary agreements to improve the quality of CO_2 tank to wheel and are becoming more compulsory with penalties to be paid if the carmaker is not in line with the targets.
- Energy efficiencies: it is very important to make wise use of energy due to the continuous increase in the number of people living on the same planet. There is no written rule here, but the local governments are starting to apply logic to recreate green credits on the efficiencies and dependent on which energy classes your vehicle belongs.

These three aspects are transferred to the carmakers from the concept of environmental needs to the concept of compliance through regulations which fix the

targets to be satisfied.

Today, it is possible to make a luxury car having all the performance, style and emotion that you can expect but if it is not compliant with the environmental norm, the effect can become a way to return to the starting point.

Therefore, by considering the modern propulsion systems, it is necessary to find a better solution from the environmental point of view that is able to attract customers and with sustainability for vehicle manufacturers.

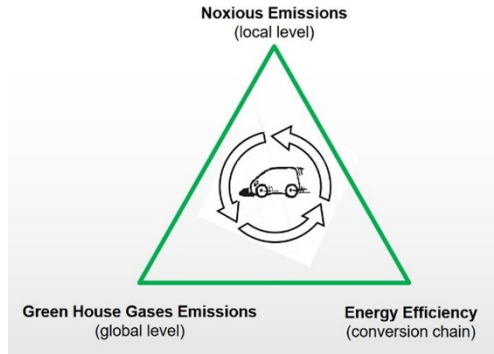


Figure 2.1: The three key elements transferred to the carmakers

2.1 Brushless permanent magnet machines

The electrification of vehicles has been recognised as one of the key parts of meeting climate change targets and sustainable transport. Indeed, the sales numbers of vehicles with electrified powertrains are increasing but not yet replacing the ICE-based technology in the short term [5].

Electric machines are one of the core technologies for electric vehicles and typically, they are connected to the wheels through a mechanical transmission or connected directly in the wheels. The general requirements of electric machines for vehicular applications are much more stringent than those for industrial ones because they demand high power density, wide speed range, high torque at low speed for starting or climbing and high speed at low torque for cruising, high overload capability for overtaking, good integration in a limited space and reasonable cost.

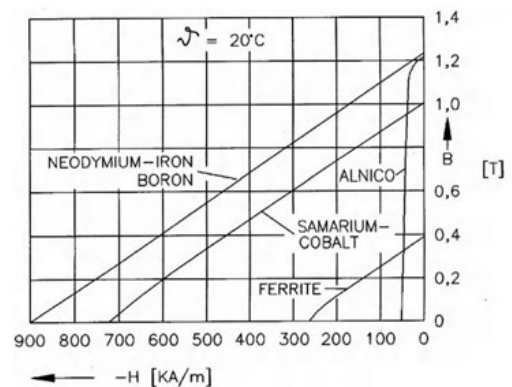
By considering the classification of the electrical machines based on the flux production mechanism, the solutions today adopted for the electric or hybrid propulsion systems are the Induction Machine, the Switched Reluctance Machine and the Permanent Magnet Machine. However, among these solutions, the PM machine dominates more in the automotive market[6].

Two main elements contribute to the development and improvement of brushless

permanent magnet machines: the materials and the power electronic devices. For example, there are evolutions still today on the technology applied mainly for the application in the class of MOSFET and IGBT. Generation by generation, the commutation time is decreasing, the resistance drain-source of MOSFET and the collector-emitter saturation voltage of IGBTs are decreasing to reduce the conduction losses, the devices are able to operate at high temperatures by simplifying the cooling and be more compliant with the harsh automotive environment. Obviously, the IGBTs are very popular but new solutions are coming. In particular, there are GaN solution for low voltage classes and SiC solution for high voltages. SiC are, for instance, used in vehicles inverter and today are applied SiC technologies to MOSFET. They help largely to reduce the losses and improve the performance with low cost. In Figure 2.2a, it is possible to see how impressive the improvement on traditional MOSFET has been, the inverter dimension is well reduced [7]. There is the improvement of some hard magnetic materials such as Samarium-Cobalt and Neodymium-Iron-Boron magnets although there is a concern regarding the limited supply and the demagnetisation issue because of their sensitivity to the temperature. The reduced losses in electrical lamination steels have been achieved through metallurgical and process development[8].



(a) Si IGBT based 200kW inverter on the left and SiC MOSFET based 220 kW inverter on the right



(b) Permanent magnets [9]

Figure 2.2: Contemporary technologies

The main advantages and disadvantages of the brushless permanent magnet machines are listed below:

- Higher torque density due to the presence of the intrinsic flux from permanent magnets in the field excitation system and not the flux generated by the rotor cage or windings.
- Less geometrical constraints because the dimension and shape of the magnets realise flux paths that are less constrained.
- Peak efficiency at peak performance because the flux comes by free in terms of losses.
- Silence because of no generation of torque ripple.

There are also disadvantages to the usage of this type of AC machine:

- Necessary regulation of the flux coming from the magnets. It requires the presence of a current component from armature windings to counteract the flux. Otherwise, if the speed of the machine is very high, the back-emf will be induced in armature windings thereby increasing the machine's supply voltage and generating a short circuit current that cannot be controlled. Thus, an uncontrollable braking torque can be generated (safety problem).
- Constant power region is limited with the distributed windings.
- The price of the magnet and the difficult production process.

From the first two disadvantages, the machine must be equipped with more precise mechanical sensors such as reluctance resolvers and if the winding at the stator level is concentrated and the number of poles is high, it is possible to have a flux regulation over a speed range which is adequate to the requirements.

According to the location of the magnets in the rotor, the Permanent Magnet AC Synchronous Machine can be divided into three categories: Surface Mounted Permanent Magnet, Interior Permanent Magnet and PM assisted Reluctance Machines.

Generally, the first two machines are characterised by high torque density and efficiency. SPM machine can provide the highest possible torque density and high peak efficiency, but it requires a lot of magnets. The structure is isotropic, meaning the phase inductances on the d, q axis are practically the same, so the reluctance torque is null. The IPM machine provides normally high torque density and the structure is slightly anisotropic, producing both magnet and reluctance torque. In this case, the torque maximization requires coordinated control of the two current components i_d , i_q .

The main drawbacks in the SPM with respect to the IPM machines are listed below:

- The high-speed magnet attachment problem due to the rise of the centrifugal forces from the rotor's high rotational speed if the magnets are not properly fixed.
- Thermal challenge because at high-speed operations, the heat generated can degrade the adhesives used for fixing the magnets or even affect the magnetic properties of the magnets themselves.
- More limited maximum speed because the magnets are facing the stator windings.

Overall, there are two different characteristics: on one side, there is the SMPM machine with the highest cost permanent magnets which provides instantaneously the highest possible performance for a given weight and volume at low speed and on the other side, there is the IPM machine which provides a wide constant power area by controlling the current and the flux. The e-machines able to overcome the opposite specific torque and flux weakening limitations are the synchronous mixed e-machines such as the PM-assisted SyR machines that can manage together the isotropy and anisotropy torque.

Figure 2.3 makes it possible to compare the performance of different electrical machines employed in automotive applications[10].









<i>Propulsion Systems</i>				
<i>Characteristics</i>	DC	IM	PM	SRM
<i>Power Density</i>	2.5	3.5	5	3.5
<i>Efficiency</i>	2.5	3.5	5	3.5
<i>Controllability</i>	5	5	4	3
<i>Reliability</i>	3	5	4	5
<i>Technological maturity</i>	5	5	4	4
<i>Cost</i>	4	5	3	4
Σ Total	 22	 27	 25	 23

Figure 2.3: Table to compare different electrical machines

It is possible to notice that the induction machine is never fully poor but is a good average, while the IPM machine is a good compromise which explains why it is the most used. However, the SMPM machine is the king in performance but weak in other aspects and therefore, if it is working on average in different working points, it is worse than IPM.

2.2 Axial flux permanent magnet machines

Typically but not always, the e-machines for automotive applications are radial flux type with internal rotor and external stator. However, in instances necessitating the integration of the e-machine into the car, the ratio between the rotor active length and diameter of the machine, defined as aspect ratio, is critical. The main geometrical options are the “cylindrical” shape with a high aspect ratio between 1 and 2 and the “disc or ring” shape with a low aspect ratio ($\ll 1$). The first type of geometry is for series hybrid and non-coaxial parallel hybrid applications while the second one is for series hybrid in-wheel motors, coaxial parallel hybrid applications and integrated complex split hybrid solutions [9]. The machine can find its place nestled between the engine and transmission by taking advantage of having a large diameter and limiting the length as much as possible. Furthermore, the end windings are very limited.

The operating principle and the control strategy are the same as that of a radial flux machine. The geometry changes from the stator and rotor that are cylinders to the stator and rotor that are disks and this implies a different exploitation of the dimensions in which there is a predominantly radial development and a low axial space.

In the axial flux machine, the magnetic flux crosses the air gap and links the rotor and stator in a direction parallel to the shaft’s rotation axis.

It is worth noticing that having a normal component of the magnetic flux density at the air gap, it results in a magnetic pressure in the axial direction attracting the stator and rotor which does not contribute to torque production but has an order of magnitude higher than the tangential force per unit area. The radial flux electric machine also has a normal component of the magnetic flux density. However, due to the symmetrical geometry, it almost vanishes and is supported by bearings. By contrast, in the axial flux motor, the consequent force from the normal component is not discharged on the bearing but causes a bending of the rotor towards the stator [9].

The reasons for the market dominance of the radial flux machines are several difficulties that the axial flux machine entails. By Moving from cylindrical to discoidal geometry, important geometrical implications change the production technologies and production processes.

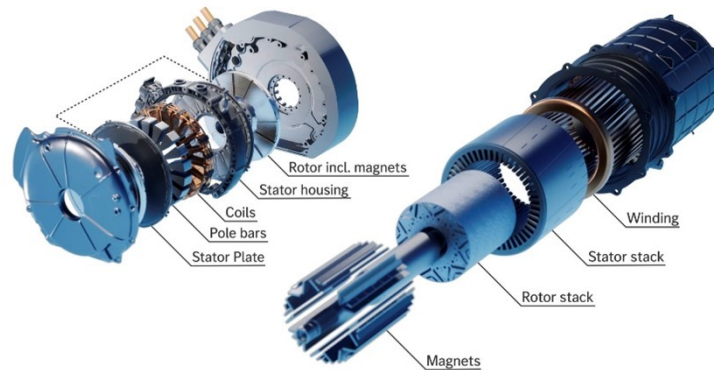


Figure 2.4: Geometrical comparison between the radial and axial flux machines [11]

For example, the stator teeth have a section that varies moving from the external radius to the internal one because the slots must have a constant section to place the coil of conductors whose section cannot change along the radius of the machine. In that case, fabricating metal sheet components and subsequently packaging them, as is done for the radial flux electric machine, presents considerable difficulties. The solution is the use of SMC materials or sheet metal that must be punched with a variable pitch and then wrapped around itself. The complexities inherent in the manufacturing and assembly of the machine are widely recognised, including the necessity to uphold a uniform air gap for optimal performance and to prevent shaft failure [9].

Aside from these shortcomings, the axial flux machine may have a greater specific torque and power with substantial savings in core material which has attracted the attention of military and aircraft applications and is attracting growing attention for automotive applications; the typology of the magnetic circuit of the AFM may be varied so that many different types of AFM may be designed. These indicators support that this type of machine will return to prominence shortly, above all in special-purpose applications where their special features offer distinct advantages. Indeed, it has been proposed for in-wheel motors, e-bikes and hybrid supercar/hype car.

These advantages have been strongly enhanced with the inclusion of permanent magnets in the electrical machine because of technological improvements in this material.

Therefore, in this thesis, the primary consideration is the axial flux permanent magnet machines which have comparable similarities to the radial flux permanent

magnet machines.

2.3 Topologies

The majority of the axial flux machines are Permanent magnet machines. Hence, this paragraph is focused on this technology.

Brushless axial flux permanent magnet machines offer different configurations which are divided into:

- Single-sided structure
- Double-sided structure
 - Double stators and one rotor
 - Double rotors and one stator
- Multistage structure

It is possible to do a further subdivision in each of these typologies according to:

- Presence or not of the stator slots
- If the stator and/or rotor have the back iron
- Winding configuration
- Location of the magnet

2.3.1 Single-sided machine

It is the most straightforward configuration composed of one stator and one rotor. A large aspect ratio with a compact shape and a small torque capacity characterises it. One main drawback is that all local axial forces between the rotor and stator are summed up and not compensated such as in a radial flux machine where all local radial forces are compensated. If this type of machine is large, an axial force of the order of kN will be generated, which could bring mechanical problems. Therefore, it requires more complex bearing arrangements and a thicker rotor disk [12]. In double-sided machines, these local forces can be compensated.

This machine is applied for industrial and traction drives.



Figure 2.5: Single sided machine [13]

2.3.2 Double-stators and one internal rotor

It comprises one rotor containing the permanent magnets sandwiched by two stators.

Different types of magnet arrangement at the rotor level determine the path of the magnetic flux, the thickness and material of the rotor back iron [13]. The magnetic flux flows circumferentially along the rotor back iron if the magnet arrangement is North-North. In North-South arrangement, the flux flows axially through the rotor; in this case, having the rotor's back iron is unnecessary. In the last case, it is possible to save the axial length and weight of the machine and reduce the rotor core losses. The windings can be connected either in parallel or in series. If they are connected in parallel, the reliability is increased because, in case of malfunctioning, one stator can continue to work and the current flowing in each stator is half the total phase current. Therefore, the winding section can be reduced. However, the series connection is preferred because the two stators can produce two equal and opposite axial forces.

In this case, the sum of the two mechanical clearances and the magnet thickness gives the total air gap.

In this configuration, the stators are on the machine's outer sides which facilitates the integration in the vehicle chassis.

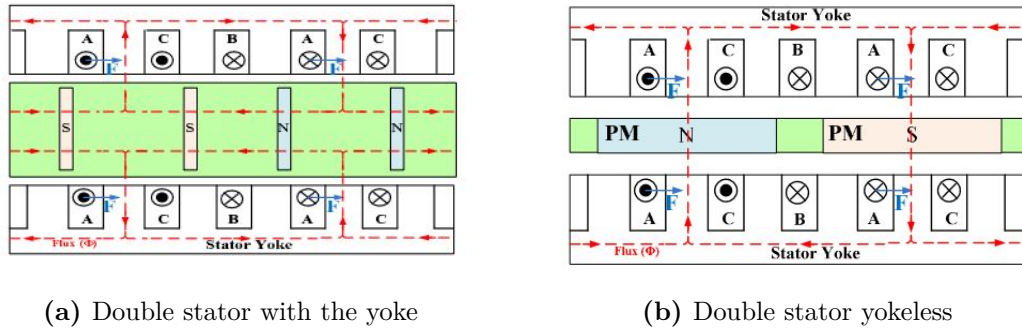


Figure 2.6: Double stator single rotor: flux paths [13]

2.3.3 Double-rotors and one internal stator

This configuration has several motor subgroups according to the stator's structure.

- If the stator is slotless, the armature winding is wound on the stator core (TORUS machine) and the leakage and mutual inductance effect are reduced i.e. there is less variation of the magnetic flux density and therefore, the eddy current and hysteresis rotor losses will be reduced at high frequency and no cogging torque will be generated [13].

In this case, the total air gap is large because the sum of the mechanical clearance with the insulation thickness around the conductor and the magnet thickness gives it. Hence, a larger volume of the permanent magnet is required to increase the average value of the magnetic flux density at the air gap.

- Instead, if the machine is slotted, the air gap is small and therefore, less volume of the permanent magnet is required. It shows higher torque density and efficiency than in the slotless case but this typology presents cogging torque and torque ripple due to the slot effect.

- Lastly, if the machine has a coreless stator, the stator winding wound on a non-magnetic and non-conductive structure or around independent teeth (YASA motor).

In this case, the axial length is reduced and the stator core losses are null. These aspects contribute to increasing the machine's efficiency and reducing the cogging torque [14].

The choice of having or not the core of the stator depends also on the magnet arrangement as explained in the configuration of the double stator and one internal rotor.

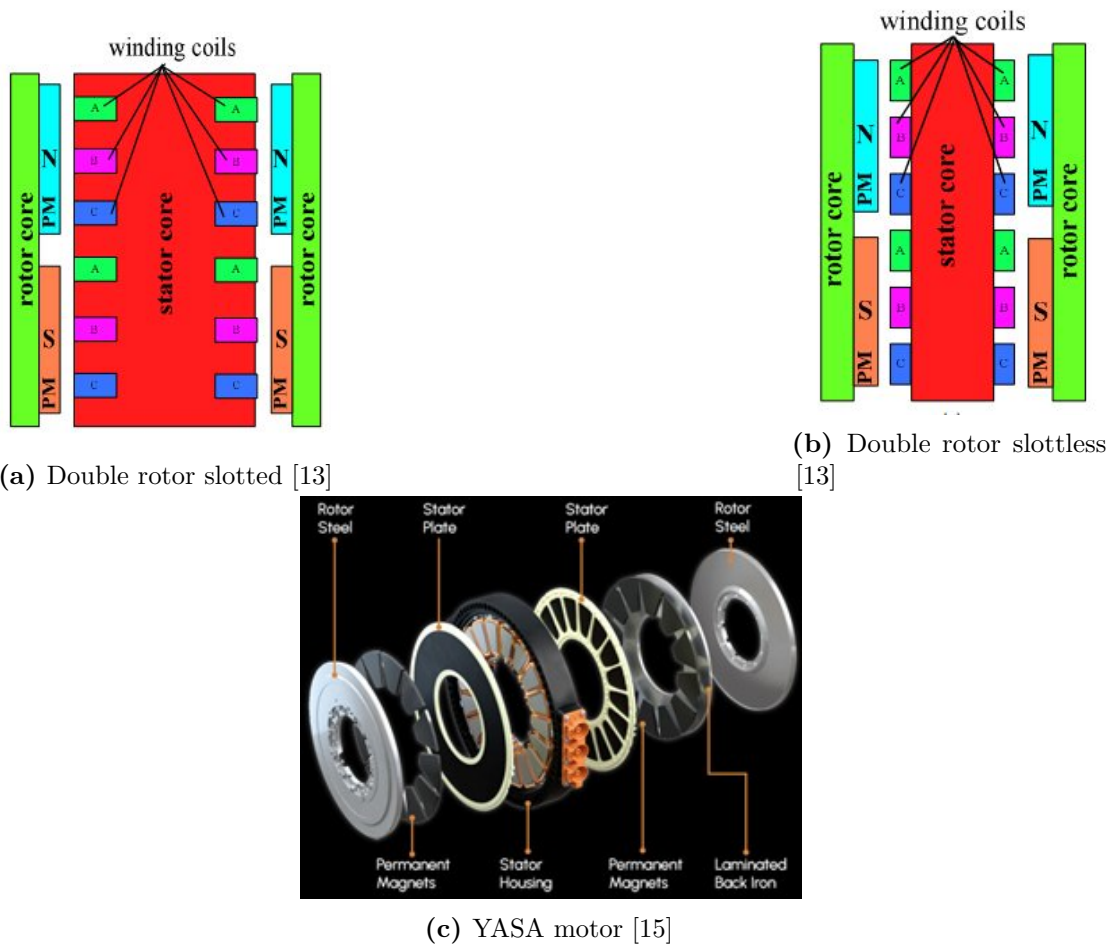


Figure 2.7: Double rotor single stator machine

2.3.4 Multidisc machine

It is a machine built with a certain number of modules i.e. stators and rotors stacked up which can be adjusted to satisfy the requirements. Therefore, it is possible to increase the torque and maximum power without enlarging the diameter due to mechanical constraints.

The size of the discs is limited due to several factors:

- Axial forces acting on the bearings.
- Integrity of the mechanical joints between the rotor and the shaft
- The stiffness of the discs.
- Available space.

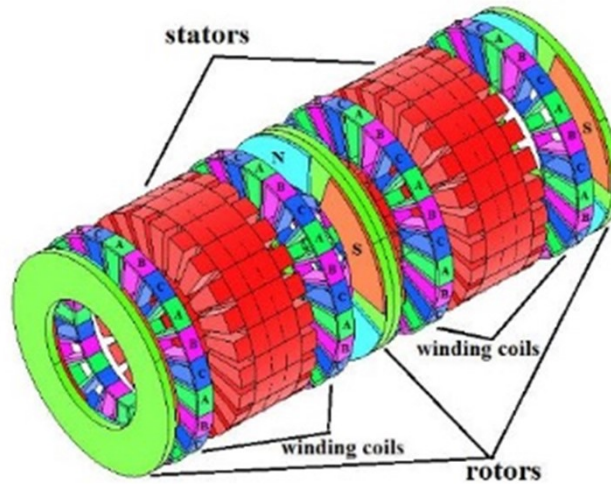


Figure 2.8: Multidisc machine [13]

2.4 Materials

2.4.1 Soft magnetic materials

The stator cores are made of laminated steel or soft magnetic powder materials. Most laminated cores are made of non-oriented silicon steel ribbons which are Fe-Si alloys whose relative magnet permeability is high and independent from the magnetic flux direction in the material.

The laminations are covered with insulating material on at least one of the two faces and then are packed.

These laminations are available as fully processed steels by steel manufacturers or semi-processed if the customer prefers to develop a desired magnetic quality.

Another type of lamination is based on Fe Co and is used for aerospace applications. It presents a residual flux density of about 2.2 or 2.4 T, which means that for the same magnetic flux, it is possible to use it in applications where the weight is important.

The main disadvantages are the material and production costs because the magnetic properties degrade after mechanical processing. In order to restore, the material must be subjected to heat treatments for a while.

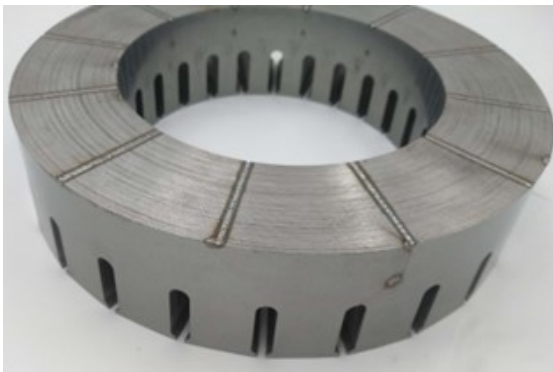
Steel laminated core for axial flux machines is more difficult to fabricate than for radial flux machines [16].

Complex geometries of the stator segments (core and teeth) can be manufactured by compressed soft magnetic powder material as an alternative. It is a powder composed of small isolated iron particles.

This material is suitable for medium or high-speed applications since the isolation covering the particles reduces eddy current losses.

Another advantage is that an arbitrary flux distribution can be developed within the core due to the isotropic properties of this material.

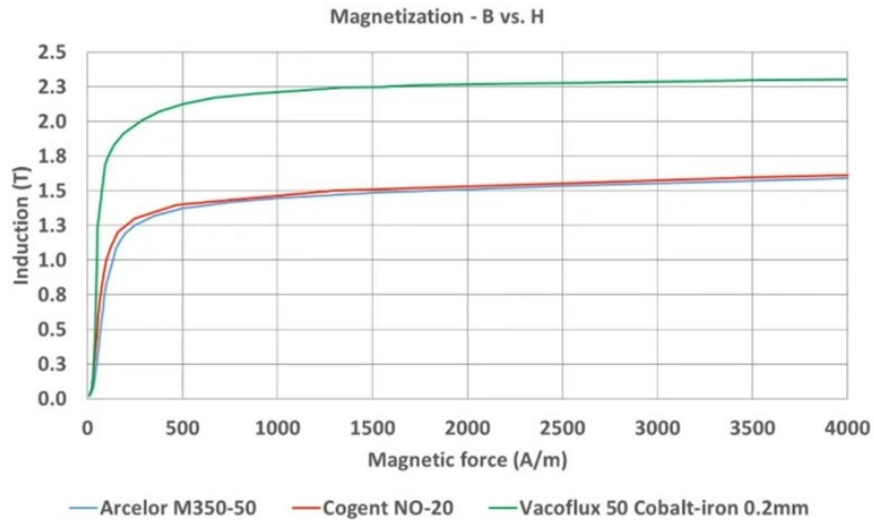
However, due to the presence of isolation between the particles, the magnetic B-H curve can worsen by causing the reduction of the magnetic flux density [17].



(a) Laminated stator [18]



(b) SMC material [19]



(c) B-H curves of different soft magnetic materials [20]

Figure 2.9: Soft magnetic materials

2.4.2 Hard magnetic materials

The magnets can be either glued on the backing rings or rings with cavities of the same shape as magnets. The adhesives used for gluing are epoxy, acrylic or silicon based adhesives but their minimum shear strength is $20 \times 10^6 \text{ Pa}$ [9].

In order to make an internal permanent magnet machine, it is better to use the soft magnetic powder but the rotor's structure high cost discourages its commercialising development.

Today, the most employed permanent magnets of electric machines are Alnicos, Ferrites and Rare earth permanent magnets.

Alnico: its advantage is that it has high residual magnetic flux density and the temperature coefficient is low. The disadvantages are that the coercivity is low and the demagnetisation curve is non-linear, so it is easy to demagnetise this material.

Ferrites: are the cheapest magnet and are available in isotropic and anisotropic grades. Its coercivity is smaller than the Alnico one but its residual magnetic flux density is higher. Its electric resistance is high, so low eddy current losses in the permanent magnet will be generated.

Rare earth: As first generation rare earth permanent magnet, we have the SmCo which is characterised by high residual magnetic flux density and linear demagnetisation curve. It is resistant to corrosion but difficult to manufacture because both samarium and cobalt are expensive due to their supply restrictions. The second generation rare earth permanent magnet is the Neodymium Iron Boron which is the most expensive magnet and has better magnetic properties than SmCo at room temperature only.

It is characterised by high remanence but its defect is strongly dependent on the temperature, so it is easy to demagnetise it at high temperature.

It has a great potential for improving the performance-to-cost ratio for many applications. For this reason, it will have a major impact on the development and application of permanent magnet machines in the future.

One of the main disadvantages is its sensitivity to corrosion. If it is exposed to hydrogen gas at high temperatures, hydrogen reacts with neodymium by leading to porosity in the material [16].

The shapes of the permanent magnets are relevant for the airgap magnetic flux density distribution and cost. The most common shape is trapezoidal but there are also circular, semicircular or rectangular shapes.

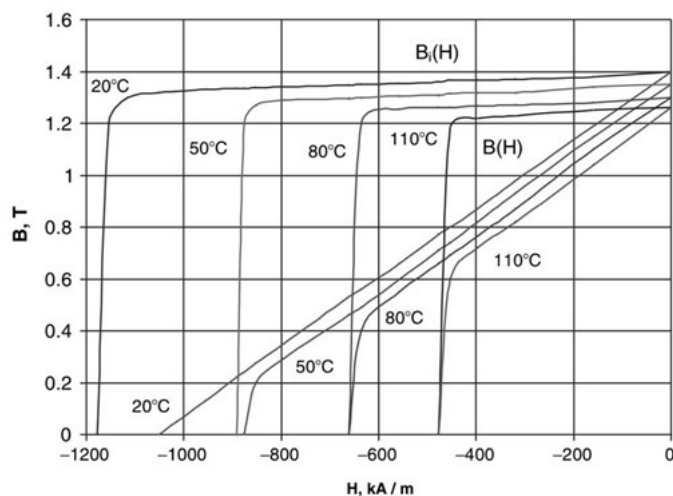


Figure 2.10: B-H curves of the NdFeB magnet for different temperatures [9]

2.4.3 Windings

Armature windings are solid copper conductor wires with round or rectangular cross sections. The temperature limits of insulating materials determine the maximum temperature rise for the windings of the electric machines.

The cross section of the conductor can be circular or rectangular.

If the current density is too high, parallel conductor wires of smaller diameter are recommended rather than one thicker wire.

The armature windings can be either distributed or non-overlap concentrated windings.

Fractional slot winding, with the number of slots per pole per phase smaller than one, presents advantages and disadvantages compared to distributed windings.

First, shorter end windings by causing the reduction of Joule loss, the possibility of achieving higher slot fill factor, lower cogging torque and easy to be produced at low cost.

There is an advantage in reliability because the end windings do not overlap each other and this ensures the reduction of the probability of a phase-to-phase fault. The main disadvantage is that it can produce a non-sinusoidal flux distribution along the airgap compared to distributed winding giving rise to larger iron losses due to the flux harmonic components [21].

The fractional slot concentrated windings are split into two structures that present different features and, hence, are suitable for different applications: single-layer and double-layer windings.

In the first structure, the coils wound on alternate teeth while in the second one,

the coils wound on each tooth.

In the first case, the coils are well isolated magnetically and thermally; indeed, their mutual inductance is very low suggesting the possibility of fault tolerance. The self-inductance can be increased, which is good at high speed values [22].

Otherwise, the second structure is preferable to limit the torque ripple and have a higher fundamental winding factor and the machine's performance can be improved considerably.

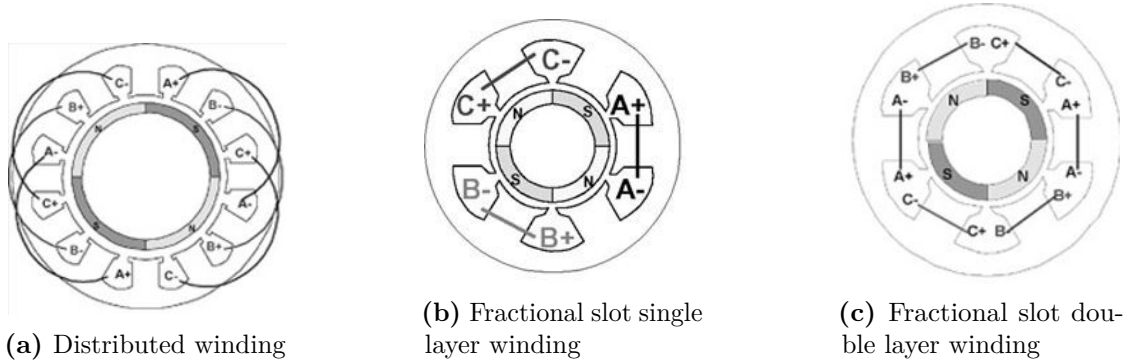


Figure 2.11: Winding types [22]

Chapter 3

Driving Cycle Analysis

This chapter presents a preliminary design model of an electric vehicle.

The main objective is to realise a vehicle model to provide a preliminary evaluation of the electrical machine's performance and energy consumption necessary to move the vehicle and complete specific driving cycles.

The vehicle model has been developed in MATLAB environment whose principles are based on the system's dynamic characteristics.

Its parameters and different powertrain components are defined.

The output data will be used for the calculation of the analytical design of the electrical machine to determine its geometries.

3.1 Driving mission profile

The driving cycles consist of a temporal sequence of speeds a vehicle must satisfy. Those are produced by different countries and organisations and used to assess the vehicles' performance, the mileage and the energy or fuel consumption. There are two main categories of test cycles:

- Legislative cycles: employed in type-approval tests for homologation purposes.
- Non-legislative cycles: mainly used in research and represent a particular operation.

Each of these driving cycles has advantages and disadvantages. For example, NEDC consists of several steady-state test modes and is simple to drive and repeatable. However, it does not represent the real driving behaviour of a vehicle in actual traffic, but it derives from a statistical analysis. Therefore, it does not accurately reflect energy and fuel consumption.

By considering this aspect, the design of a new legislative driving cycle was started to predict fuel and energy consumption more accurately under real-world driving

conditions. The WLTP was derived from real-world driving data from five regions: Europe, Switzerland, USA, India, Korea and Japan.

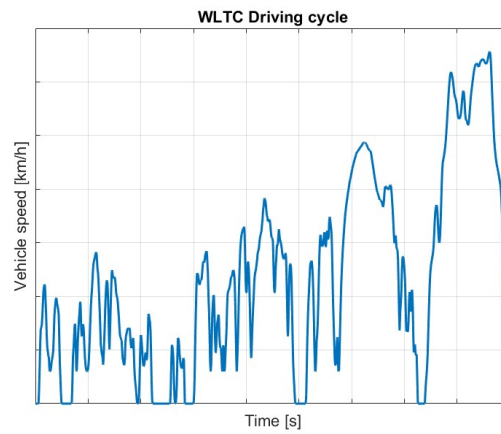
There are infinite driving cycles, some of which are representative of a specific operation on a specific company. Thus, the companies may have internal driving cycles in which speeds and accelerations are customised for design purposes such as definition of the vehicle performance and comparison with other vehicles. In this thesis, two internal driving cycles are considered to design the electrical machines: Nordschleife drive cycle and Drag trip drive cycle.

The former is a racetrack built in the town of Nürburg, Germany, in 1927, used for racing and testing. It is the north loop of Nürburgring track which is currently the longest motorsport racetrack in the world. It is one of the most difficult roads in the world and called by Sir Jackie Stewart as “The Grün Hölle” because it comprises steep elevation changes, jumps, bumps, blind corners and almost complete lack of run-off areas. Nowadays, car manufacturers built research facilities next to the track to test sports cars in the Ring of the track on every driving condition.

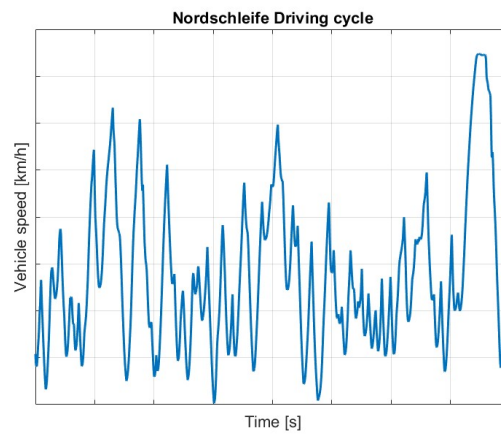
The second drive cycle is a flat track used to perform the ultimate test of acceleration, speed and braking.

In order to approach a specific market, it is necessary to comply with national or European specifications. Therefore, also the WLTP drive cycle is considered.

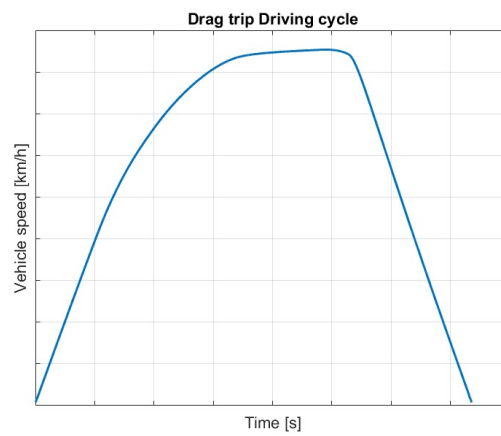
The three drive cycles are shown in the picture below that provide useful information to help understand which driving missions are more demanding regarding power and velocity.



(a) WLTC



(b) Nordschleife



(c) Drag trip

Figure 3.1: Driving cycles

The software Canopy Simulations calculates the speed profiles of the abovementioned non-legislative drive cycles. These data are acquired at variable frequency in the time domain. Thus, before running the simulation, it is necessary to operate a discretisation of the speed profile on the time axis. In this thesis, these input data are filtered at a frequency of 100 Hz.

It is essential to mention that besides the speed profile as input of the simulation, the time series of the braking torque from the mechanical braking system is also considered because the vehicle model developed in MATLAB is simplified as it considers only the traction and regenerative braking modes.

The section 3.3 explains how to use the backward approach model.

3.2 Vehicle characteristics

The vehicle name Gemera comprises two Swedish words “ge” and “mera” which mean “to give more”. This vehicle is the world’s first four-seater mega car, designed to be the fastest car ever produced in acceleration. It beats most two-seater cars on a race track due to its 4WD system. It is all about enjoying the super sports experience extended to four people. The car can run in e-motor mode on all four wheels simultaneously or on the front or rear axle.

As it is widely acknowledged, Koenigsegg Automotive AB once made a megacar with a small engine capacity but what is more impressive is that now the company is making the electrical machine with an outstanding output power, small diameter, small axial length, low weight and super efficient.



Figure 3.2: Vehicle Gemera [23]

In this thesis, the car has four independent brushless axial flux permanent magnet machines customised for racing applications and sending power to each wheel through the final drive transmission system.

On the other side, the machine is electrically connected to the battery through the inverter.

The electrical machine can operate as a motor or generator, according to the driving situation. When the machine works in motor mode, it delivers positive power, which happens when the vehicle moves in pure electric mode. When it works as a generator, it delivers negative power during regenerative braking, providing enough power to restore the battery's state of charge.

The compilation of all requisite parameters for simulating a particular driving cycle is fundamental, as it yields key output data for the subsequent design and optimisation stages of the electrical machine.

For the sake of simplicity, the efficiency of the final drive transmission system is assumed to be constant.

3.3 Vehicle model

In this paragraph, the vehicle model is implemented in MATLAB environment to extract the electrical machine specifications so that the machine can satisfy the speed and torque required of the selected mission profiles.

In order to evaluate the energy flow of the various powertrain components, it is necessary to define the "direction" of the calculation method in the vehicle's various operating conditions.

The forward approach is a method in which the calculation is performed starting from the reference drive cycle and the actual speed cycle given to the driver controller which compares them and gives commands that allow the vehicle to follow the cycle.

The backward method is a method in which the analysis starts from the reference speed profile and is given as input to the vehicle dynamic model producing then the torque at the wheel. It will be managed by the powertrain model to determine the characteristic quantities of various components by considering their losses.

The difference between the two methods is that while an analysis through a forward method requires defining and using a model that emulates the driver's behaviour, a backward method requires only the speed profile of a specific driving cycle.

In this case, it is enough to use a quasi-static backward model in which only the vehicle's longitudinal dynamics and the powertrain components' dynamics are modelled. This model is summarised in the diagram presented in the figure below.

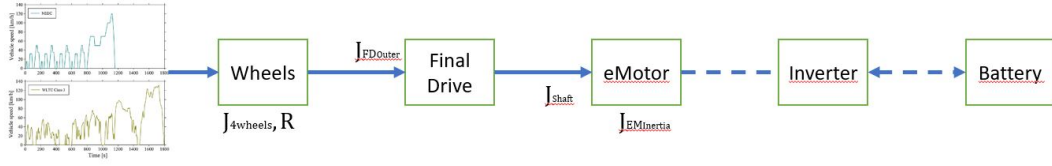


Figure 3.3: Backward model

Since we want to size preliminarily the electrical machine, we are not interested in specific details such as the real shape of the vehicle or the precise effect of the wheel, but it is of interest a global analysis.

The car was simplified to a single point with the same vehicle mass, and the main variables to calculate are the angular speed, torque and power required by each e-machine.

For each time instant of a specific driving cycle, the vehicle is subject mainly to three resistance forces: Rolling, Aerodynamic, and Gradient resistance [24, 25].

- Rolling resistance: it is a resistance due to the deformation that occurs at the tyre contact patch. Being present the hysteresis on the viscoelastic material of the tyre, there is dissipation of energy i.e. the energy absorbed in the deformation is not completely returned when it will go back to its initial shape. At the tyre contact patch, the pressure distribution is asymmetric with respect to the wheel's vertical axis by generating a force which acts against the rotational movement of the tyre.

$$F_{rr} = mgk_r \cos(\alpha) \quad (3.1)$$

Where m is the vehicle mass, g is the gravity acceleration and α represents the slope of the road. The rolling resistance coefficient is affected by several factors such as vehicle speed, tyre pressure, wheel load, wheel size, contact patch, operating temperature, type of road and its condition, tyre wear and tyre material. However, a simplified approach is applied in which we assume that the rolling resistance coefficient k_r is constant and not dependent on the square of the velocity because the tyres were designed for a car going from 0 to 400 km/h. Hence, the rolling resistance will be linear in that specific operating range [26].

- Aerodynamic drag resistance: it is an aerodynamic force that acts against the vehicle motion. It depends on the air density, vehicle speed and vehicle characteristics such as the frontal area and the drag coefficient. The aerodynamic drag is computed as follows:

$$F_a(t) = \frac{1}{2} \rho A_x C_x v_{2w}(t)^2 \quad (3.2)$$

Where v_{v2w} is the vehicle speed with respect to the air, A_x is the frontal area of the vehicle, ρ is the air density which is equal to the standard value $1.225 \frac{kg}{m^3}$ at 25 C and 1 atm of pressure and C_x is the aerodynamic drag coefficient which is determined experimentally according to the vehicle shape.

- Road grade resistance: it is the resistance of the vehicle moving on a sloping road. It is expressed as follows:

$$F_{rr} = mg \sin(\alpha) \quad (3.3)$$

In this simplified vehicle model, further resistances that can be developed at very high speed are assumed negligible such as the aerodynamic lift due to the absence of spoilers. Once all these resistances are calculated for each time instant, the power needed to motion can be evaluated as a product between the sum of all resistance forces and the vehicle speed:

$$P_n(t) = (F_{rr} + F_a(t) + F_g)v(t) \quad (3.4)$$

From the longitudinal dynamic behaviour of the vehicle expressed in the equation below, the traction power can be computed and represents the power that the vehicle must deliver to win against the resistances and the vehicle's inertia if accelerating or decelerating.

$$mv(t) \frac{dv(t)}{dt} = (P_{tract} - P_n(t)) \quad (3.5)$$

The vehicle acceleration can be calculated by taking the derivative of the vehicle speed in the discrete domain.

$$a(t) = \frac{dv(t)}{dt} = \frac{v(t) - v(t-1)}{\Delta t} \quad (3.6)$$

The resulting traction power, vehicle speed and braking torque profiles will be sent to the powertrain dynamics model to run backwardly the simulation from the wheel to the propeller and compute the speed and power for each component.

$$P_{tract}(t) = mv(t) \frac{dv(t)}{dt} + P_n \quad (3.7)$$

$$P_{wheel}(t) = P_{tract}(t) + J_{4wheels} \dot{\omega}_{wheel}(t) \omega_{wheel}(t) \quad (3.8)$$

where $\omega_{wheel}(t) = \frac{v(t)}{R}$ and $\dot{\omega}_{wheel}(t) = \frac{\omega_{wheel}(t) - \omega_{wheel}(t-1)}{\Delta t}$

$$P_{FDOuter}(t) = P_{wheel}(t) + J_{FDOuter} \dot{\omega}_{wheel}(t) \omega_{wheel}(t) \quad (3.9)$$

$$P_{FD_{Inner}}(t) = \frac{P_{FD_{Outer}}(t)}{\eta_{FD}^k} \quad (3.10)$$

where $\omega_{FD}(t) = \frac{\omega_{wheel}(t)}{\tau_{FD}}$, $k=1$ during traction and $k=-1$ during braking.

$$P_{EM_{Mech}}(t) = P_{FD_{Inner}}(t) + J_{Shaft}\dot{\omega}_{EM}(t)\omega_{EM}(t) + J_{EM_{inertia}}\dot{\omega}_{EM}(t)\omega_{EM}(t) \quad (3.11)$$

where $\omega_{EM}(t) = \omega_{FD}(t)$, P_{wheel} is traction power at wheel level, $J_{4wheels}$ is the moment of inertia of the four wheels, ω_{wheel} is the angular speed of the wheel, $P_{FD_{Outer}}(t)$ is the output power of the final drive transmission, $P_{FD_{Inner}}(t)$ is the input power, τ_{FD} is the gear ratio of the final drive transmission, ω_{EM} is the angular speed of the machine, J_{Shaft} is the moment of inertia of the shaft, $J_{EM_{Inertia}}$ is the moment of inertia of the electrical machine and $P_{EM_{mech}}$ is the mechanical output power of the machine.

By implementing these last set of equations, it is possible to compute the angular speed and torque that the electrical machines must supply to the vehicle to maintain a given reference speed for each time instant. Therefore, a set of operating points of torque versus speed and mechanical power versus speed can be collected and are shown from Figure 3.7 to Figure 3.9.

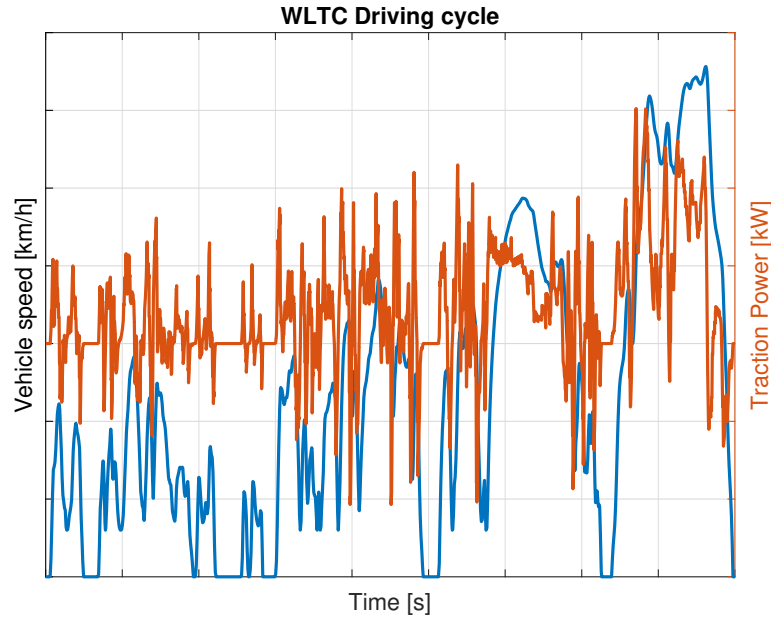


Figure 3.4: WLTC and traction power

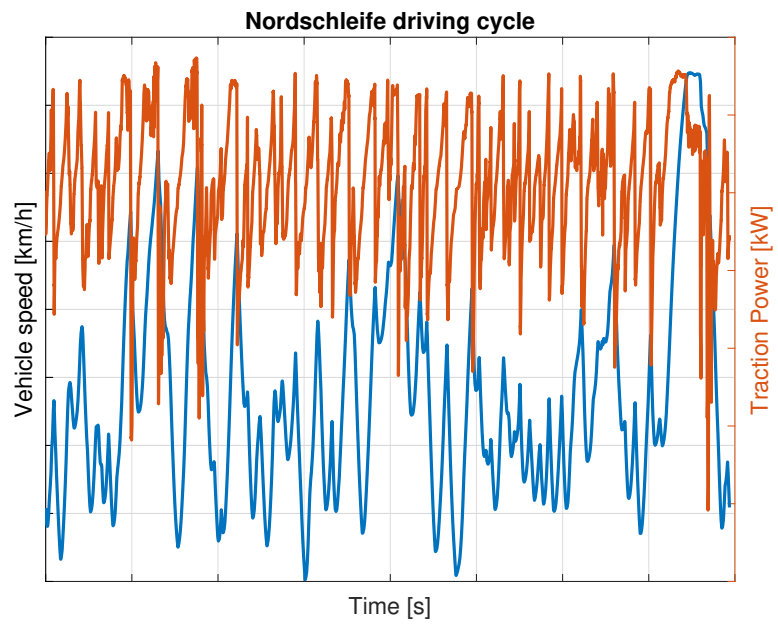


Figure 3.5: Nordschleife and traction power

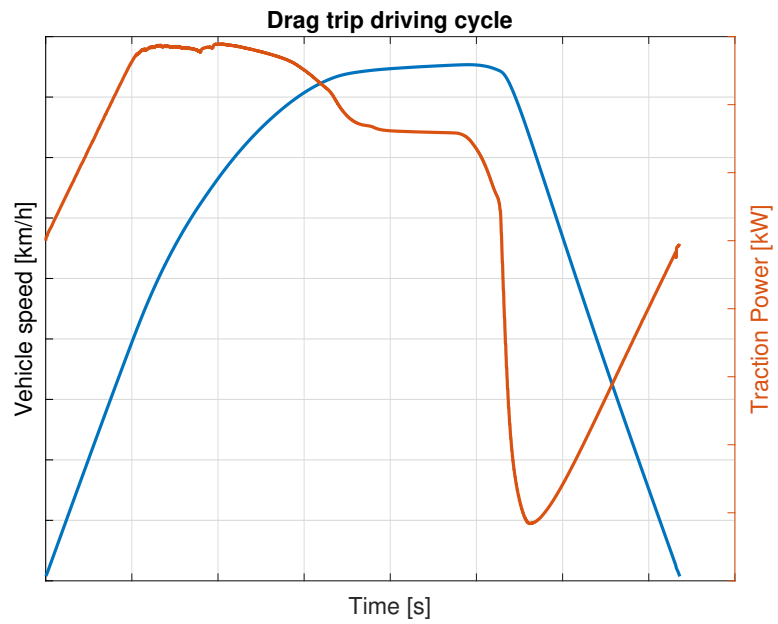
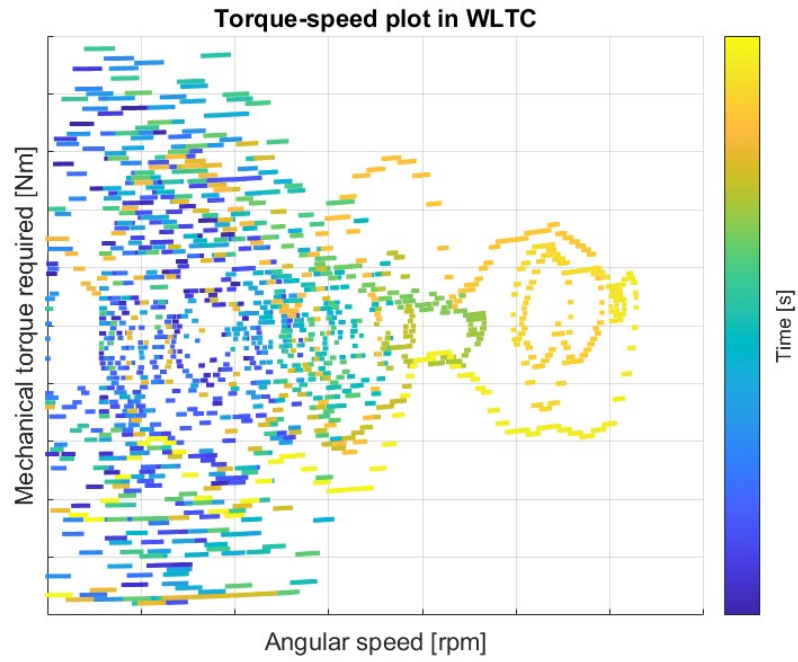
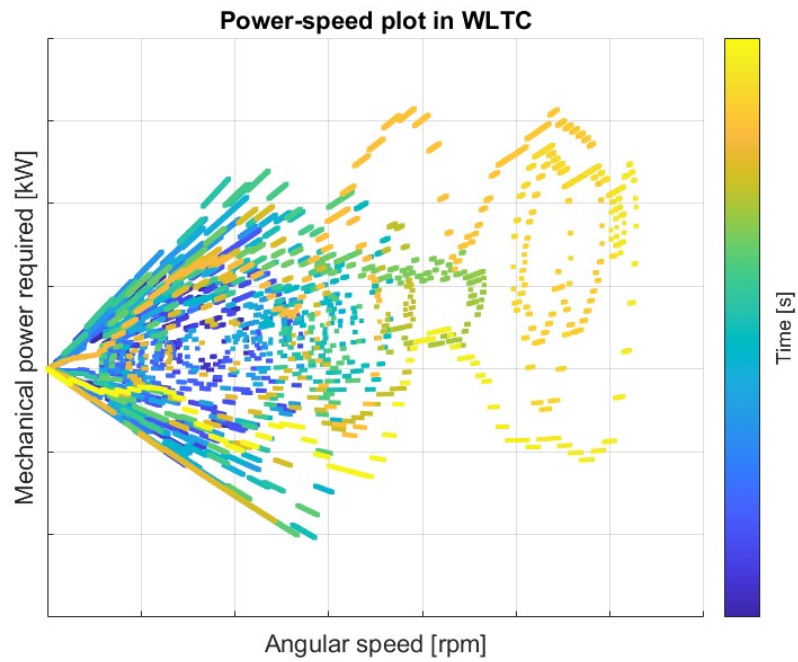


Figure 3.6: Drag trip and traction power

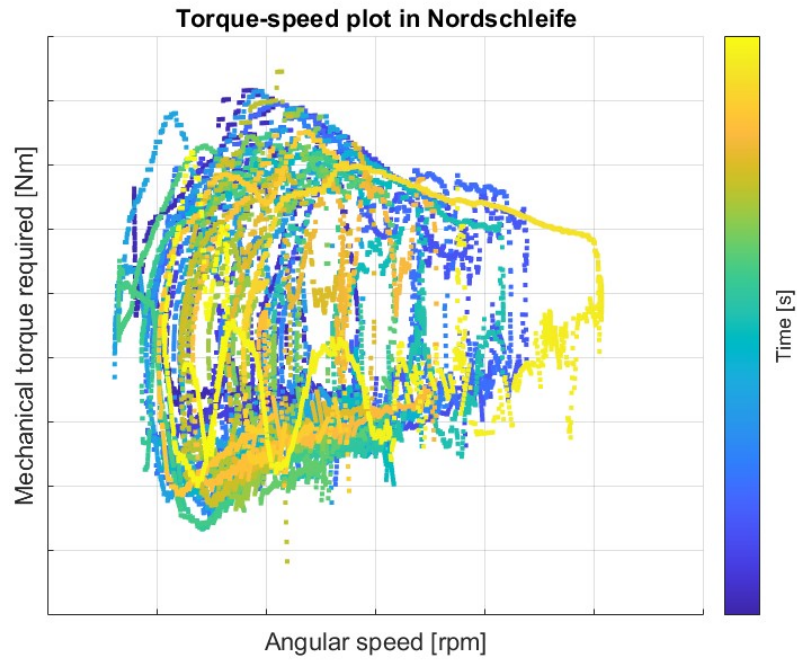


(a) WLTC torque

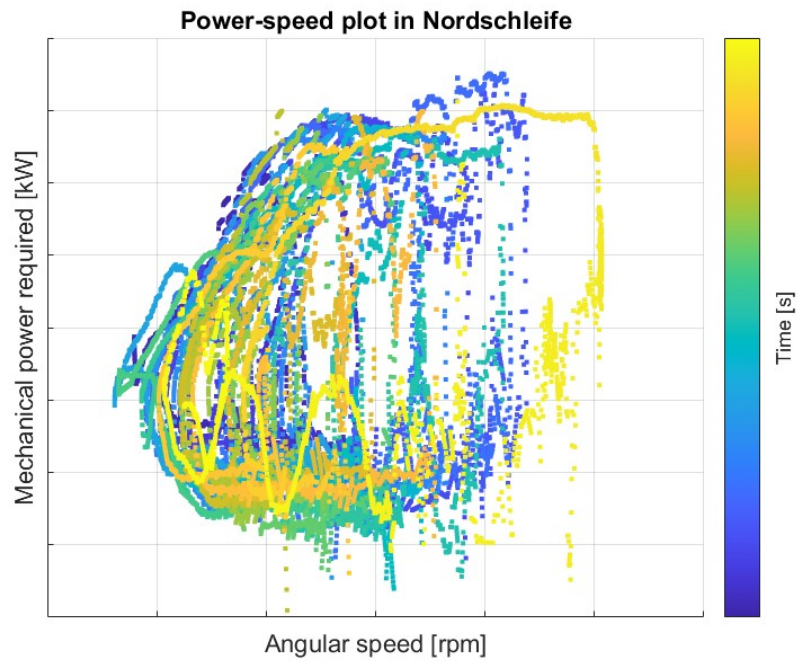


(b) WLTC power

Figure 3.7: WLTC operating points

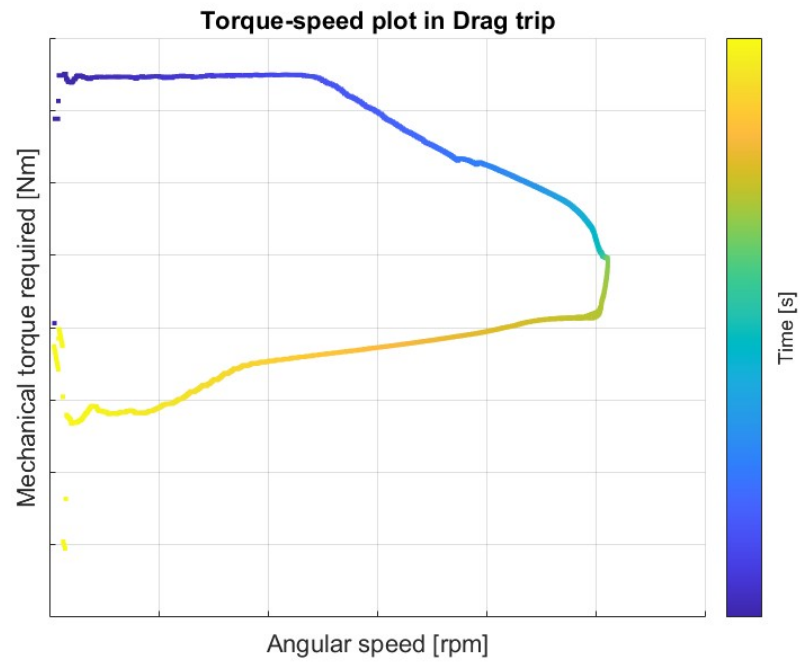


(a) Nordschleife torque

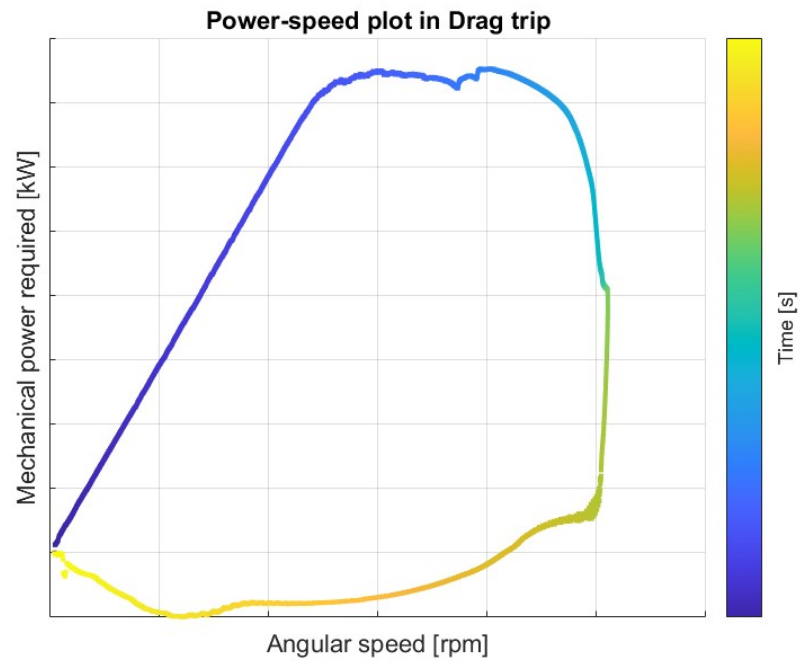


(b) Nordschleife power

Figure 3.8: Nordschleife operating points

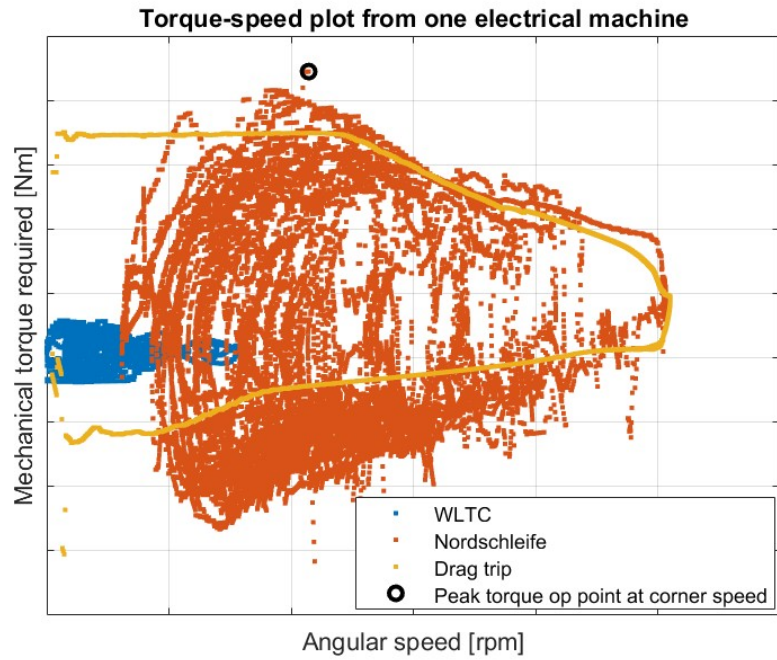


(a) Dragtrip torque

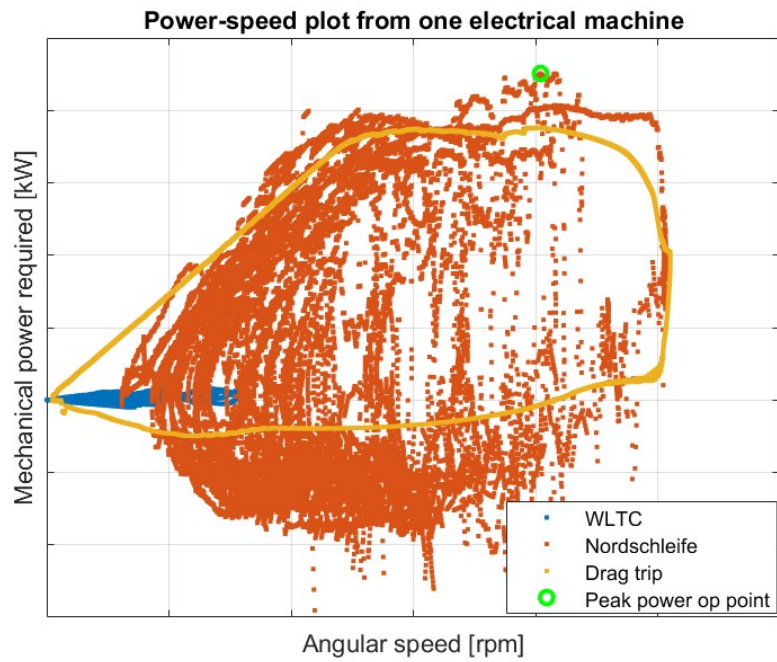


(b) Dragtrip power

Figure 3.9: Drag trip operating points



(a) Overall torque



(b) Overall power

Figure 3.10: Overall operating points

The plots coming from the last two mission profiles offer insights into results which are required to understand the e-machine's behaviour and performance under different conditions. Figure 3.9 illustrates the motor's characteristic transient behaviour, where the vehicle is pushed to its limits, which helps in identifying the maximum speed at which the e-machine has to operate.

On the other hand, Figure 3.8, resulting from the simulation performed on a track under severe conditions, provides the e-machine's peak torque and power, as well as its corner speed.

These results are summarised in Figure 3.10 and give a solid base for the next steps in the analytical design and optimisation phases, ensuring that every aspect of the machine's performance is taken into consideration.

3.4 K-means clustering application

Following the simulation, it is crucial to remember that also the machine efficiency needs to be optimised. The approach of assessing the machine's efficiency at each operating point across a specific drive cycle using finite element analysis is very computationally intensive. However, the machine must be designed so that its maximum efficiency area covers the region where it spends most of its energy. Thus, a more suitable option is to find the region of operating points with large energy consumption in the torque speed map. From that locality, it is possible to define its representative operating point [27], another input for efficiency optimisation. This method, used to find one of the main prerequisites for the optimisation toolbox, is useful to reduce the amount of battery consumption and increase the mileage in driving scenarios [28].

The energy consumption of each operating point is defined as the product between the mechanical power evaluated from the vehicle model and the time interval from the previous time instant to the actual one. This operation is performed in all three driving cycles and the results are shown in the figures below where in the colour bar, the operating point energy consumption value is divided by its maximum value for each drive cycle. It is important to mention that the negative energy points indicate the regenerative braking.

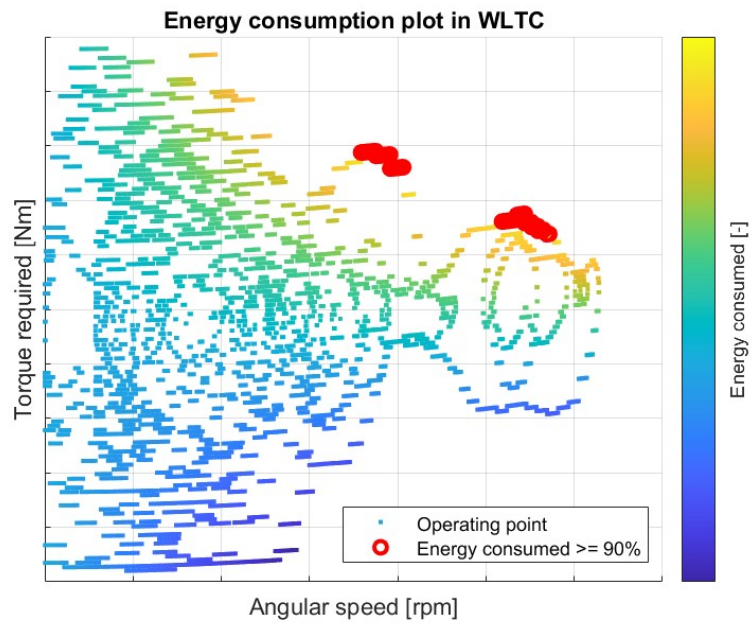


Figure 3.11: WLTC energy consumption

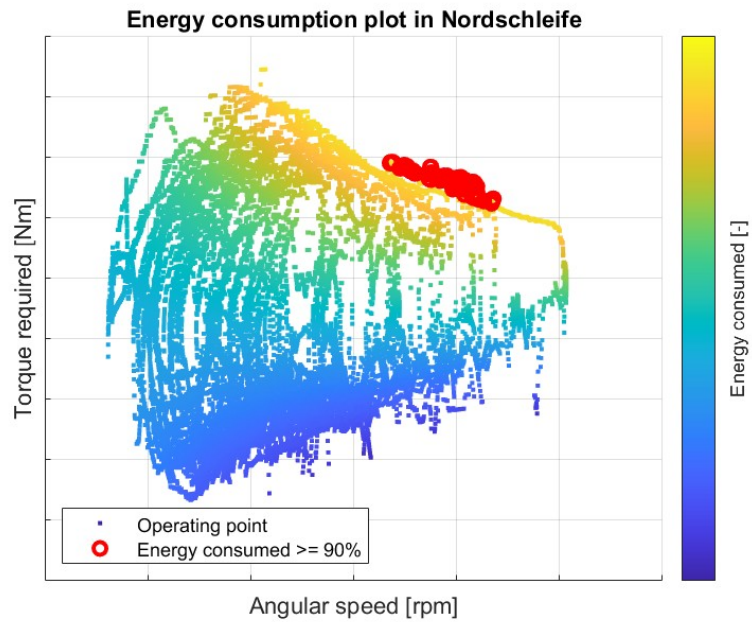


Figure 3.12: Nordschleife energy consumption

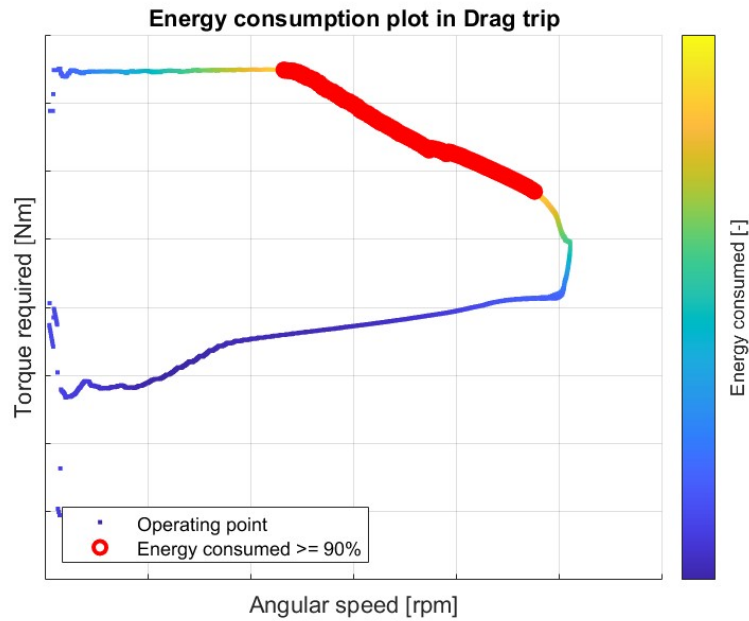


Figure 3.13: Drag trip energy consumption

Then, it is possible to find the operating points whose energy consumption value is between the maximum value and 90% of that value. Once a set of data with a high intra-class similarity is grouped, it is possible to implement an unsupervised learning algorithm called K-means clustering which allows to determine the representative point of that group called as “centroid” [29, 30].

The procedure is the following: with the dataset located in a Euclidean space, it necessitates the decision of the number of clusters of which there is one for this particular case. The process begins by randomly setting the initial position of the centroids of the groups. The next step involves calculating the distances between all operating points and the centroids. Each point is then assigned to the cluster that has the nearest centroid. At the final step, the centroids locations are updated towards the centre of the groups.

The last two steps are repeated many times so that the algorithm tries to understand how this centroid should be positioned in space to represent the group correctly. Given a training set $\{x^{(1)}, x^{(2)}, \dots, x^{(i)}, \dots, x^{(n)}\}$, its mathematical description is as follows:

Algorithm 1 K-means clustering algorithm

Initialise k cluster centroids randomly $\mu_1, \mu_2, \dots, \mu_j, \dots, \mu_k \in R^n$

repeat

Assign each data point to its closest centroid $c^{(i)} \leftarrow \arg \min_j \|x^{(i)} - \mu_j\|^2$

Move each centroid to the mean of the training samples which are assigned to it $\mu_j \leftarrow \frac{\sum_{i=1}^n 1_{\{c^{(i)}=j\}} x^{(i)}}{\sum_{i=1}^n 1_{\{c^{(i)}=j\}}}$

until Convergence

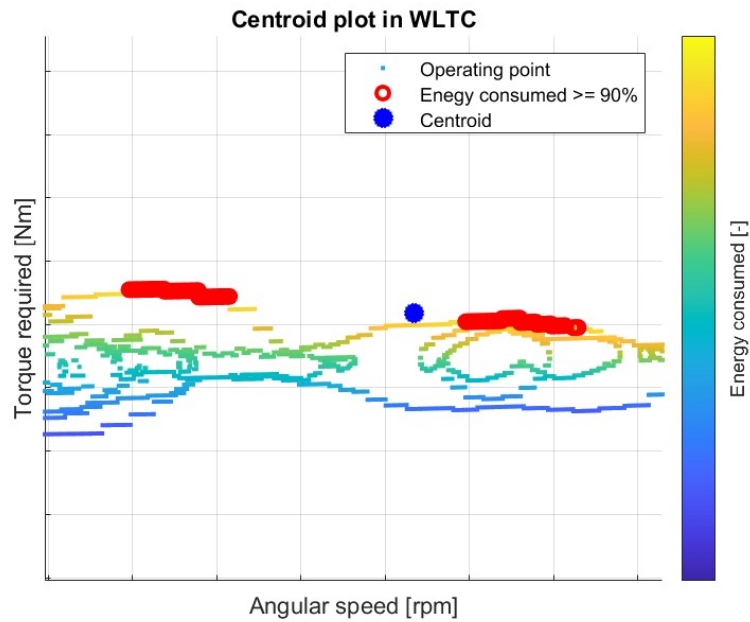


Figure 3.14: Centroid WLTC

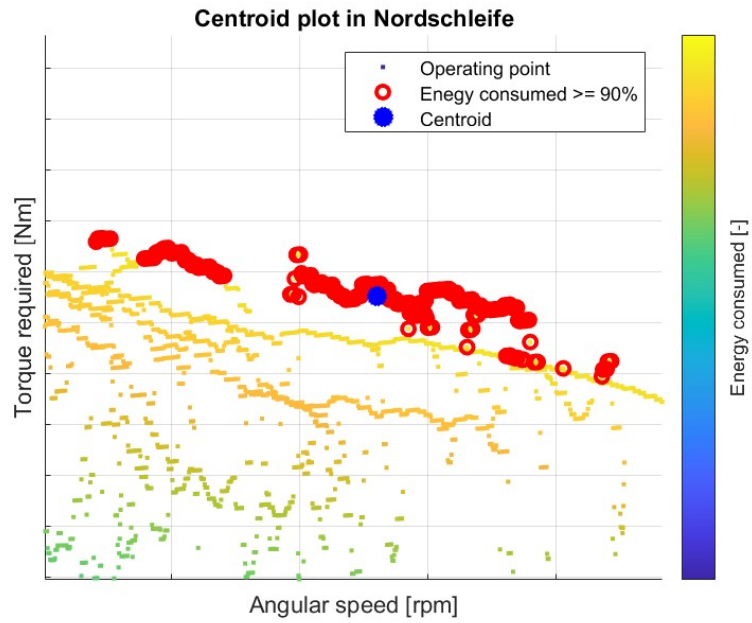


Figure 3.15: Centroid Nordschleife

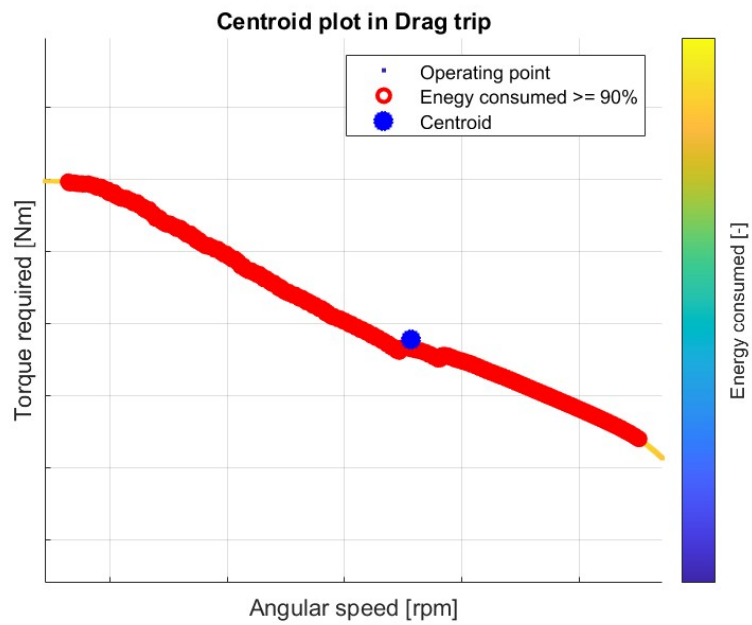


Figure 3.16: Centroid Drag trip

Chapter 4

Analytical design

The goal of this chapter is to obtain, from the analytical calculations, the main dimensions and approximate number of turns per phase for three double-sided double stator and one internal disc rotor PM brushless motors with laminated stator core characterised by different combinations of slots and poles. Once designed and validated by the finite element analysis FEA, the three machines will be optimised to determine the precise values of their geometrical parameters by ensuring specific performance requested by the designer and the driving cycles. Before implementing the analytical design method, there are some design choices for the machine already defined:

- Double slotted stator and one internal disc rotor.
- Laminated stator core and defined its stacking factor.
- Magnet arrangement: North-South arrangement.
- Maximum outer diameter of the stator is defined for packaging constraint.
- Maximum phase current from the inverter limit.
- Maximum DC voltage from the inverter limit.
- Slot fill factor.
- Maximum peak current density of the e-machines.
- The stator windings are connected in parallel.

A MATLAB script is developed to get all parameters required to design an axial flux permanent magnet motor for a specific operating point. All the equations, empirically developed, are taken from scientific papers and thesis [17, 31, 32, 33]

and the book of the authors J. F. Gieras, Rong-Jie Wang and Maarten J. Kamper [9]. These calculations are used to obtain initial approximate solutions to be further analysed using finite element analysis FEA.

In order to avoid a complete redesign of the existing packaging of the machine into the vehicle, the outer diameter of the stator is the main motor dimension to be considered as size constraint.

The required performance parameters of the motor defined from the previous chapter need to be satisfied and are the necessary inputs for the sizing of the machine.

4.1 Phase voltage limit

For a given three phase inverter, the machine characteristics are evaluated for DC link voltage of 700V. The relation between the DC link voltage of the inverter and phase voltage of the electric machine can be expressed as:

$$V_{ph} = V_{phrms} = \frac{V_{DC}}{\sqrt{6}} \quad (4.1)$$

While the maximum phase peak voltage is:

$$V_{phpeak} = V_{phrms} \sqrt{2} \quad (4.2)$$

4.2 Slot and pole combination

In this section, it is necessary to determine the top three combinations of slots and poles. This process starts with an array of different slot and pole combinations within each of which there is a range of different inner-to-outer diameter ratios of the electrical machine. The selection is performed by considering some criteria that are based on the experience.

It is already provided a matrix of different values of the fundamental winding factors for different combinations of slot and pole.

The selection consists in looking for the slot and pole combinations whose value of the fundamental winding factor is larger than 0,9 so that their windings can produce higher torque. Otherwise, there is probability of obtaining slot and pole combinations that are very noisy or do not produce any torque.

However, it is important to be careful in this part because some slot and pole combinations are meaningless causing undesired phenomena such as asymmetry or unbalance magnetic pulls and therefore, some double checks have been performed based on rules which come from different literatures [21].

4.3 Sizing of the electrical machines

Once selected specific slot and pole combinations with different inner-to-outer diameter ratios, the main dimensions of the electrical machines can be determined by using the following experience-based assumptions:

Advance angle ψ (from q axis)	0 deg
Efficiency at corner speed η	0.9
Power factor at corner speed $\cos(\phi)$	0.5
Average magnetic flux density at the airgap B_{avg}	0.82 T
Peak line current density A_m	$150000 \frac{A}{mm}$
Slot fill factor FF	0,6
Maximum peak current density J_a	$40 \frac{A}{mm^2}$
Stacking factor k_i	0.96
Phase EMF to phase Voltage ratio $\epsilon = \frac{E_f}{V_1}$	0.9
Maximum flux density in the stator back iron B_{sy}	2T
Maximum flux density entering in the teeth B_{st}	2.1T

Table 4.1: Assumptions

In Figures 3.10a and 3.10b of the previous chapter, it can be noticed that the operating point of peak torque and the point of peak power are different, as they do not have the same speed. The motor has to be able to cover both, but the bottleneck of implementing these analytical equations is that they are always referred to a single operating point. Therefore, it is necessary to decide whether to design the machine to provide the maximum torque or the maximum power. Nevertheless, the operating point of peak power is in the flux weakening region where the analytical equations cannot be used. Therefore, the significant operating point from which to start designing is that of the peak torque at the corner speed which belongs to Nordschleife driving cycle.

Thus, the stator outer diameter (equal to the outer diameter of the rotor) is expressed as:

$$D_{out} = \sqrt[3]{\frac{\epsilon P_{out}}{\pi k_D k_w 1 n_s B_{mg} A_m \eta \cos(\phi)}} \quad (4.3)$$

where P_{out} is given by the ratio between the peak torque and its corner speed, and n_s is the corner speed in rps.

Also the inner diameter can be calculated as follows:

$$k_d = \frac{D_{in}}{D_{out}} \quad (4.4)$$

As a result, different motors characterised by a specific combination of slot and pole and an outer diameter are obtained. Therefore, it is possible to choose the first three top machines whose outer diameter values are the closest to the maximum one. This last part is performed because the outer diameter of an axial flux machine is the main geometrical parameter which describes the machine performance i.e the electromagnetic torque is proportional to the cubic value of the outer diameter.

For the three top motors, other required parameters can be calculated.

The number of stator turns per phase per stator N_1 is calculated on the basis of the peak line current density equation:

$$A_m = \frac{4\sqrt{2}m_1I_aN_1}{\pi D_{out}(1+k_d)} \quad (4.5)$$

This is an approximate number of turns which can be calculated exactly only after performing detailed electromagnetic and thermal calculations of the machine.

The number of turns in a single coil for one parallel current path a_p is expressed as:

$$N_c = \frac{a_w N_1}{\frac{s_1}{m_1}} \quad (4.6)$$

Given the values of the maximum phase current from the inverter and the peak current density, the cross section area of the stator conductor can be determined:

$$s_a = \frac{I_a}{a_w J_a} \quad (4.7)$$

By assuming that the cross section of the conductors is rectangular, the cross section of the stator slot should be approximately:

$$Stator\ slot\ area = \frac{s_a 2N_c}{FF} \quad (4.8)$$

Where the number of conductors in a single slot is $2N_c$.

The minimum stator slot pitch can be calculated as follows:

$$t_{1min} = \frac{\pi D_{in} k_d}{s_1} \quad (4.9)$$

The values of the magnetic flux density at the stator yoke and tooth are defined from experience and because the stator core is Cobalt Iron steel which has saturation

between 2,2 and 2,3 T. It is desired to design the machine in such a way that it operates at the knee point of the B-H curve.

The narrowest tooth width equation is the following:

$$c_{1_{min}} = \frac{B_{g_{avg}} t_{1_{min}}}{B_{st}} \quad (4.10)$$

The stator slot width can be calculated as:

$$slotwidth = t_{1_{min}} - c_{1_{min}} \quad (4.11)$$

As the consequence, it is possible to calculate also the slot depth having rectangular cross section area of the slot:

$$slotheight = \frac{statorslotarea}{slotwidth} \quad (4.12)$$

Finally, the stator back iron can be calculated as follows:

$$Backiron_{stator} = \frac{\pi D_{out} k_d B_{g_{avg}}}{p B_{sy} k_i} \quad (4.13)$$

The table below summarizes the results that are necessary to draw the three electrical machines in the quasi-3D finite element software and then run the Magnetostatic simulation. In this problem, the magnet thickness is assumed to be

Geometries of the three combinations of slots and poles			
	Combination 1	Combination 2	Combination 3
Number of slots s_1	24	12	24
Number of poles $2p$	22	10	20
Fundamental winding factor k_{w1}	0.949	0.933	0.933
Inner/Outer diameter ratio k_d	0.585	0.585	0.595
Stator outer diameter [mm]	100%	100%	100%
Number of turns	100%	175%	100%
Slot width [mm]	100%	203.43%	101.71%
Slot height [mm]	100%	71.79%	106.52%
Stator yoke height [mm]	100%	223.74%	111.87%
Magnet spacing [mm]	100%	221.4%	110.71%
Magnet thickness [mm]	100%	100%	100%

Table 4.2: Geometries from analytical design

equal to a constant value.

4.4 FEA validation

In this paragraph, the finite element analysis is performed by using the Quasi-3D FEA software which displays the axial flux machine model with pre-defined quotes of the components modified according to the required geometrical parameters from the previous section. The Appendix A shows the quotes that will be varied according to the results from the analytical equations.

One of the main advantages of this software is, besides what is explained in chapter one, the automatic change and adaptation of the coil diameter in the slots and automatic meshing on the model when geometrical parameters are changed. This aspect does not imply the user in changing the calculated geometries due to mesh issues.

These three motors are modelled and simulated with Cobalt Iron as electrical steel and Neodymium Iron Boron as magnet material.

It is worth to consider that the properties of this magnet can change significantly depending on the temperature.

The three machines are tested at a specific operating point which is at peak torque and corner speed defined by the black circle in Figure 3.10a.

The aim of doing the three simulations is to ensure that the three motors can produce the same peak torque at the corner speed calculated in chapter 3.

These simulations have been made by imposing the input current equal to the limit phase current from the inverter (1000 Arms), the advance angle equal to zero, the mechanical angular speed equal to the corner speed and the number of points in one electrical period equal to 48.

FEA set-up	
Input current rms	1000 Arms
Advance angle	0 deg
Mechanical angular speed	Corner speed
Temperature at the copper	180 C
Temperature at the magnet	100 C

Table 4.3: FEA set-up

4.4.1 Results

The required values, the outcomes from the finite element analysis of average electromagnetic torque and mechanical power, and their relative error ϵ_r are reported in the following table:

FEA results of the three combinations of slots and poles				
	Torque [Nm]	ϵ_r of torque	Mechanical power [kW]	ϵ_r of power
Analytical design	100%		100%	
Combination 1	63.55%	-36.45%	63.55%	-36.45%
Combination 2	53.85%	-46.15%	53.85%	-46.15%
Combination 3	61.92%	-38.08%	61.92%	-38.08%

Table 4.4: FEA results

It is possible to notice that the relative errors are very high. The three average electromagnetic torques computed by the FEA software are very small compared to the torque required from the drive cycle analysis. This happens because the three machines are simulated with very high temperatures of the magnet and copper conductors and the number of turns are not calculated precisely.

To deal with this problem, it is necessary to either increase the number of turns and/or decrease the current in order to regulate the average torque calculated from the software. However, it is important to pay attention that their supply voltage and current density do not have to overcome their limits. Before doing this sweep, it is better to consider another important aspect [34] that is explained in the following paragraph.

4.5 Torque/speed characteristic curve

The bottleneck is that the analytical design technique always refers to a single operating point. Therefore, the e-machines are sized in the peak torque operating point at corner speed but are they capable of going at very high speed considering that the inverter has a certain limit of voltage and current? The analytical equations cannot be used in the flux weakening region and it is necessary to verify if the e-motors are able to cover all the operating points of the different driving cycles. The SMPM machine model can be written in phase coordinates (a,b,c) using the following variables:

1. v_{as}, v_{bs}, v_{cs} : stator phase voltages in stator frame.
2. i_{as}, i_{bs}, i_{cs} : stator phase currents in stator frame.
3. $\lambda_{as}, \lambda_{bs}, \lambda_{cs}$: stator flux linkages in stator frame.

It is noticeable that there are a lot of variables. However, the model of an AC machine can be described by the simplest expression in rotating d,q frame. This is possible by performing two transformations that are the Clark transformation (from

three phase a,b,c to two phase machine α, β reference frame) and the Rotational transformation (rotating bi phase d,q frame). Once we go from a,b,c frame to α, β frame and then d,q frame, we are talking about fictitious variables. If we talk about a combination of i_d and i_q , it is necessary to be sure that this combination corresponds to a specific combination of i_a, i_b and i_c . The phase voltage equations for all synchronous machines in dq reference frame is expressed as:

$$v_d = R_s i_d + \frac{d\lambda_d}{dt} - \omega \lambda_q \quad (4.14)$$

$$v_q = R_s i_q + \frac{d\lambda_q}{dt} - \omega \lambda_d \quad (4.15)$$

At steady state, the time derivative of the currents is zero.

In order to know the relationship between the current and flux, we need the magnetic model in dq frame. This model, for SMPM, is expressed as:

$$\lambda_d = L_d i_d + \lambda_m \quad (4.16)$$

$$\lambda_q = L_q i_q \quad (4.17)$$

In SMPM synchronous machine, there is not magnetic anisotropy and therefore, the inductances on the d and q axis are equal, because if we look at the field line on the d axis or q axis, you see that the permeability does not change.

Regardless of the rotor type, the electromagnetic torque in dq frame, if we neglect the cross saturation, is expressed as follows:

$$T_{em} = \frac{3}{2} p [\lambda_m i_q + (L_d - L_q) i_d i_q] \quad (4.18)$$

The total torque is the sum of two components:

1. The PM torque is controlled via the i_q component.
2. The reluctance torque is controlled by the coordination of i_d, i_q .

Considering a SMPM that is isotropic, the torque can be simplified as:

$$T_{em} = \frac{3}{2} p [\lambda_m i_q] \quad (4.19)$$

It is necessary to consider the two inverter constraints in the d,q frame:

Current constraint:

$$i_d^2 + i_q^2 \leq I_{max_peak}^2 \quad (4.20)$$

Voltage constraint:

$$\left(i_d + \frac{\lambda_m}{L_d}\right)^2 + \left(\frac{L_q}{L_d} i_q\right)^2 \leq \left(\frac{V_{max}}{\omega_{el} L_d}\right)^2 \quad (4.21)$$

The first constraint is represented as a circle centred in the origin of the i_d, i_q plane. The radius is the maximum peak current given by the inverter. The second one is a circle, if the inductances on the d,q axis are equal, centred on the d-axis current and whose radius shrinks as the speed increases.

In the speed range from zero to the base speed, what is desirable is that given the torque required, it is important to get it with the minimum stator current amplitude flowing through the machine to minimise the losses. This generic torque control principle for synchronous machine is defined as Maximum Torque per Ampere (MTPA).

If it requested to produce a torque, for SMPM, i_d must be set to zero and only i_q is needed because, otherwise, the flux current would increase the Joule losses without producing any torque.

While for the other synchronous machines, we need to control both i_d and i_q to minimise the current to get a certain torque required.

The operation within that speed range is commonly called as constant torque speed range because, without the voltage limitation, the maximum torque capability is constant and defined by the maximum inverter current.

In high-speed operation, it is possible to rotate faster than the base speed by applying a negative i_d which goes against the flux linkage of the magnet and so reduces the total flux amplitude.

This causes the rotation of the stator current vector from the MTPA locus to the negative d-axis. Due to the reduction of the flux and i_q , the maximum torque capability will also be reduced. In this speed range we have both the current and voltage limits.

For the synchronous machines with magnets, the behaviour at flux weakening depends on the ratio between the maximum current and the machine characteristic current I_0 which is the d-axis current that cancels the machine flux.

$$I_0 = -\frac{\lambda_m}{L_d} \quad (4.22)$$

It is possible to notice that the characteristic current is a parameter that comes from the construction because for a given flux linkage of the magnet, the magnitude of I_0 depends on the inductance.

From this theory above, it is possible to generate the characteristic torque speed curves of the three machines.

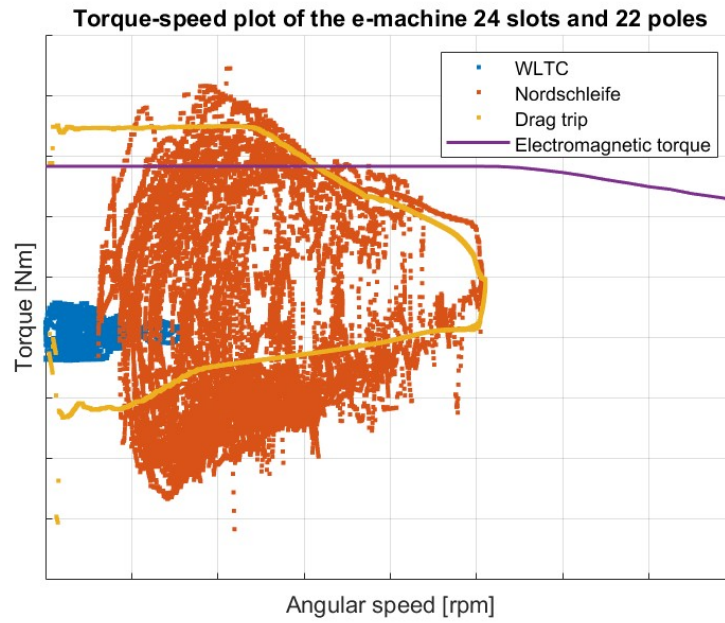


Figure 4.1: Torque versus speed in 24 slots and 22 poles

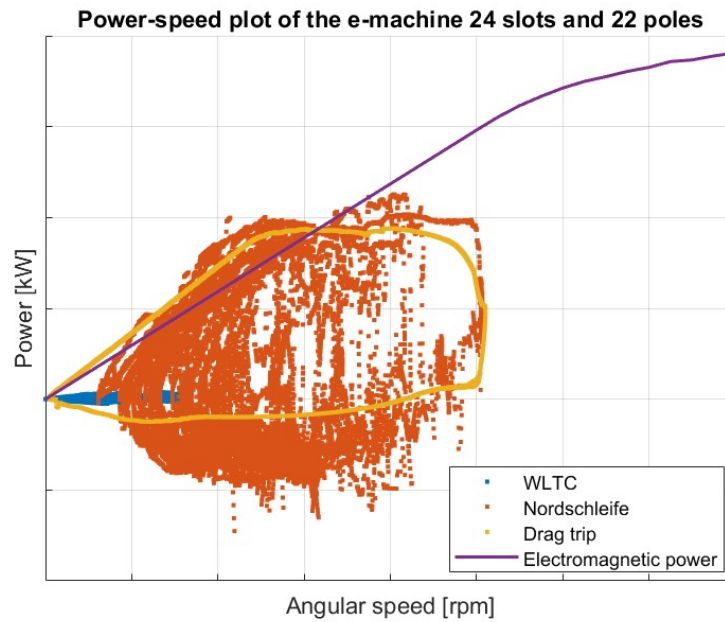


Figure 4.2: Power versus speed in 24 slots and 22 poles

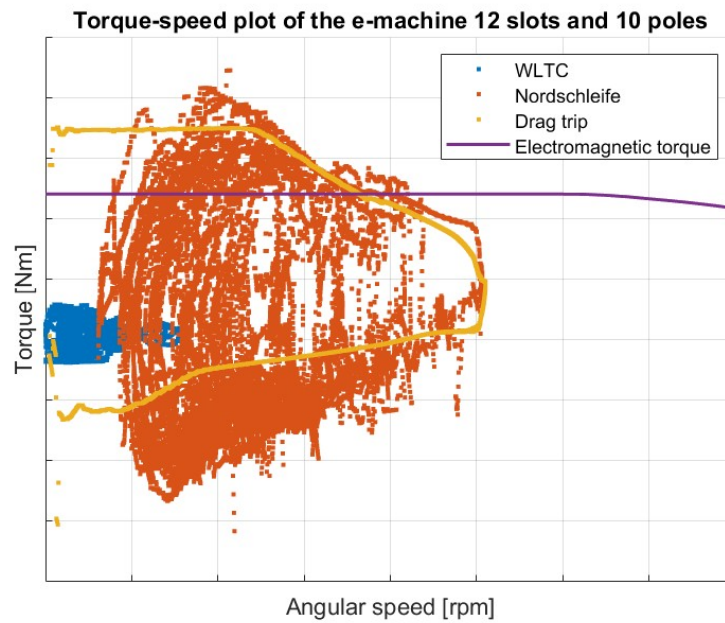


Figure 4.3: Torque versus speed in 12 slots and 10 poles

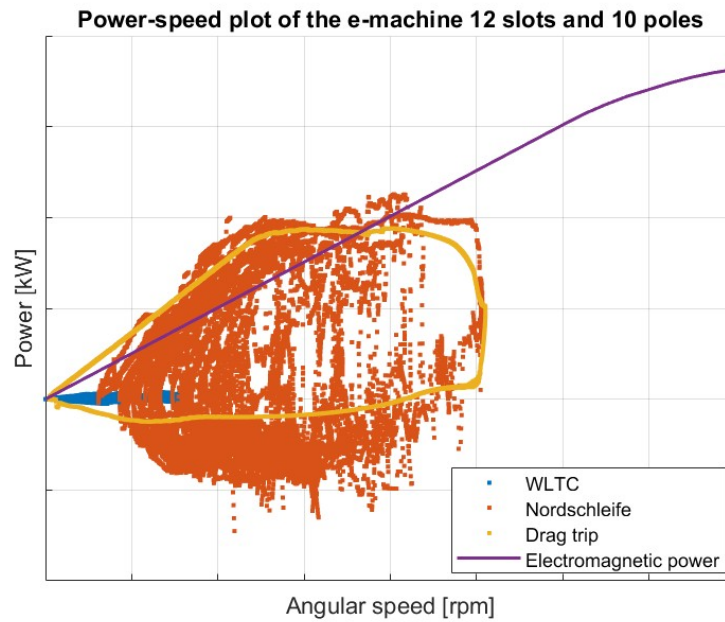


Figure 4.4: Power versus speed in 12 slots and 10 poles

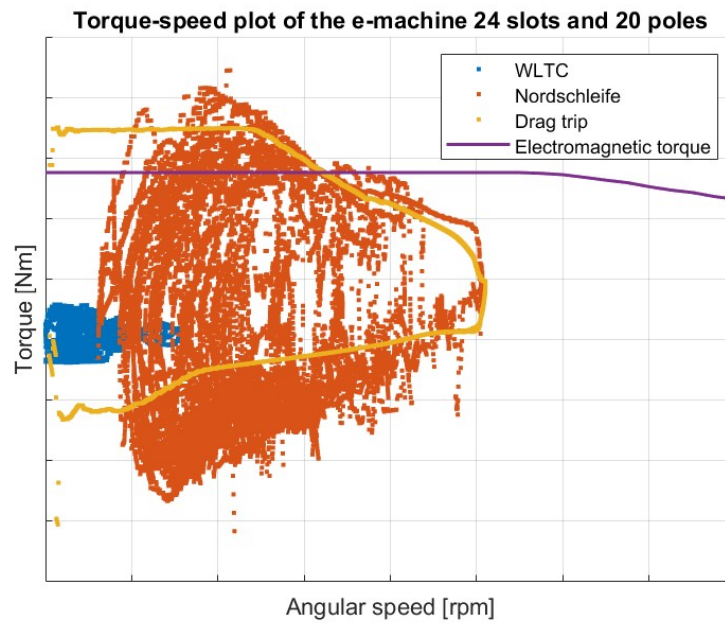


Figure 4.5: Torque versus speed in 24 slots and 20 poles

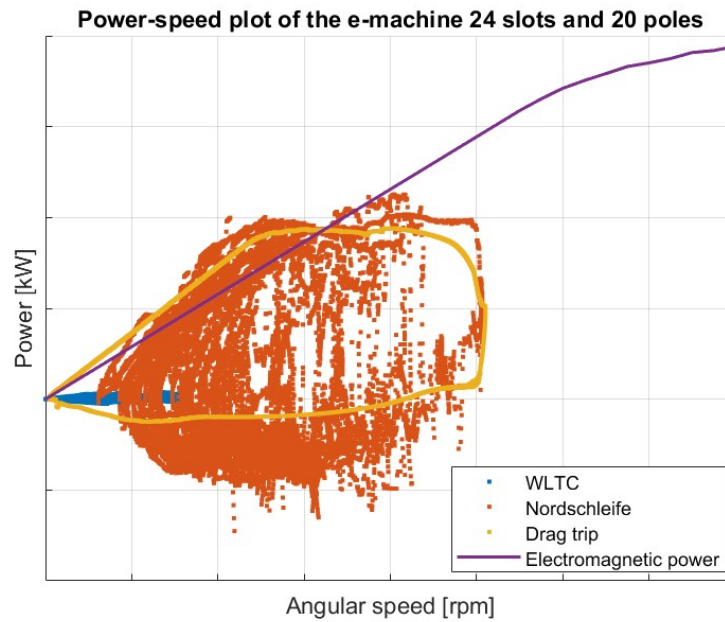


Figure 4.6: Power versus speed in 24 slots and 20 poles

All these three machines are not able to cover all operating points. Their inductances and supply voltages are very low causing the reduction of torque and a big increase of power. Also, the current densities are very low.

4.6 Design iterations

In order to meet the torque-speed requirements, one way is to do an iterative process which consists of increasing the number of turns and reducing the rms phase current input by taking into account the current and voltage limits of the inverter, the current density limit and the supply voltage limit.

As a consequence, from Table 4.5 it is possible to notice that the relative errors are within $\pm 10\%$ which is acceptable.

This iteration process is not aimed to optimise the design but it is done to reach to the requirements.

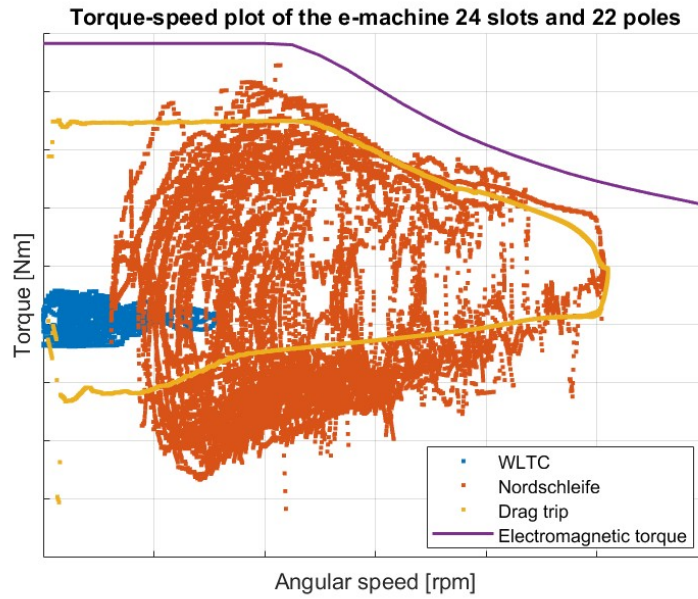


Figure 4.7: Torque versus speed in 24 slots and 22 poles after the update of the number of turns

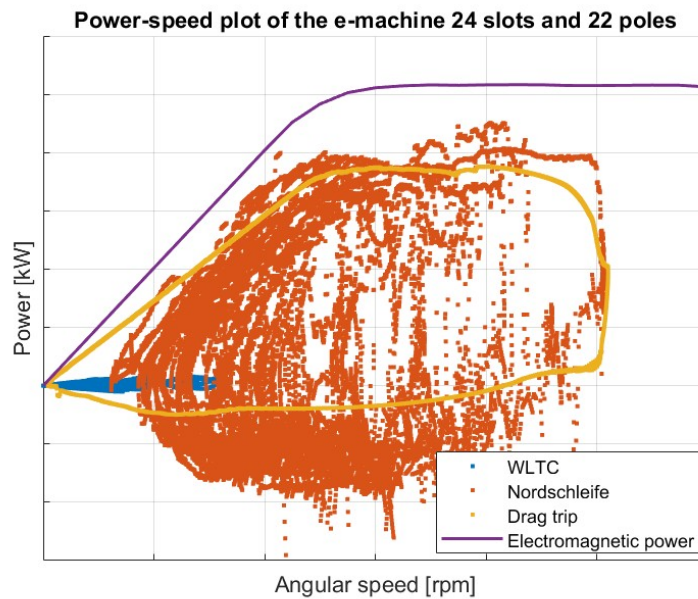


Figure 4.8: Power versus speed in 24 slots and 22 poles after the update of the number of turns

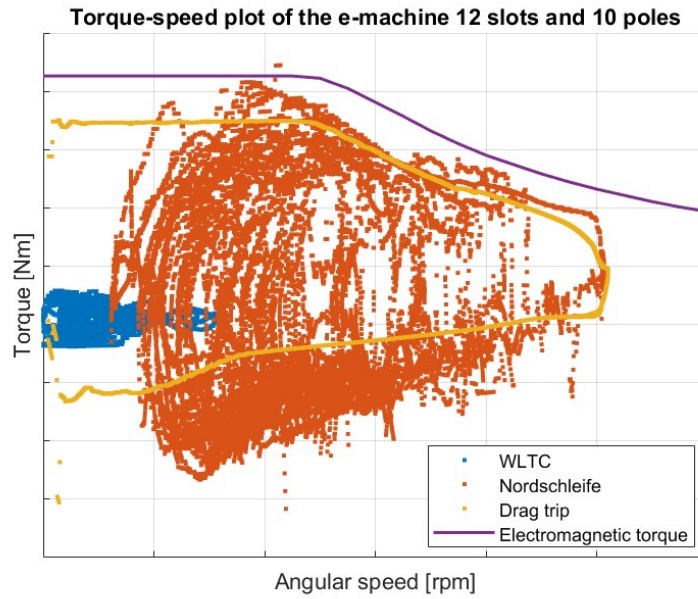


Figure 4.9: Torque versus speed in 12 slots and 10 poles after the update of the number of turns

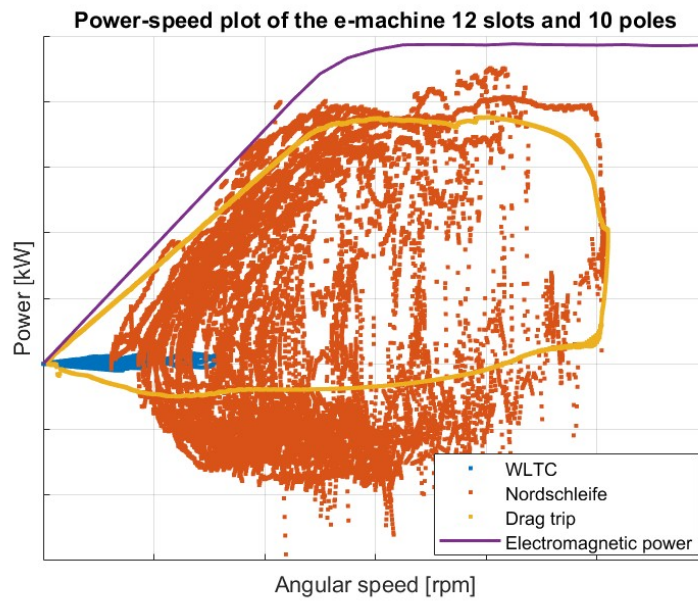


Figure 4.10: Power versus speed in 12 slots and 10 poles after the update of the number of turns

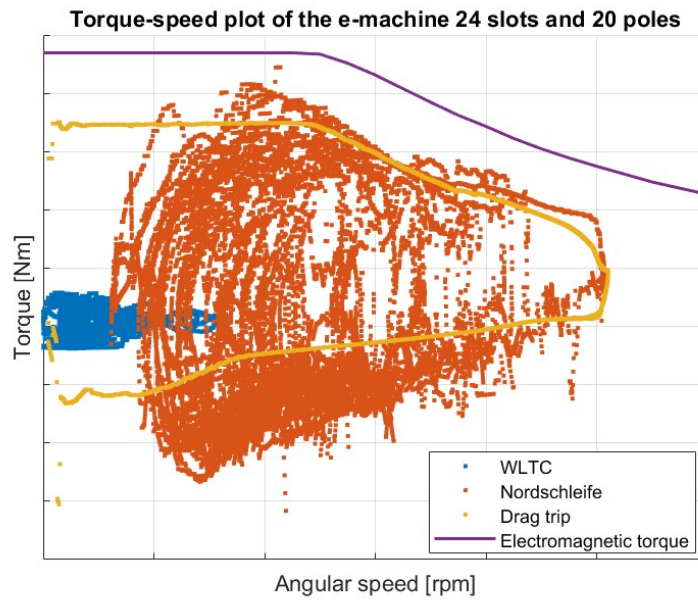


Figure 4.11: Torque versus speed in 24 slots and 20 poles after the update of the number of turns

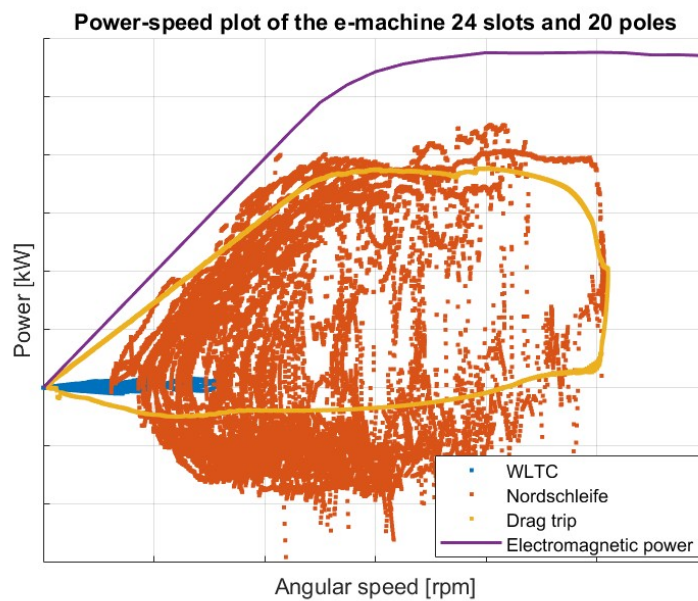


Figure 4.12: Power versus speed in 24 slots and 20 poles after the update of the number of turns

FEA results of the three combinations of slots and poles				
	Electromagnetic torque [Nm]	ϵ_r of torque	Mechanical power [kW]	ϵ_r of power
Analytical design	100%		100%	
Combination 1	108.4%	8.39%	108.4%	8.39%
Combination 2	95.35%	-4.64%	95.35%	-4.64%
Combination 3	105.4%	5.38%	105.4%	5.38%

Table 4.5: FEA results improved

Chapter 5

Multi-Objective Optimisation

In this chapter, the three developed electrical machines are applied in the multi-objective optimisation problem by leveraging the genetic algorithm software package (GOSET) coupled with the Quasi-3D FEA software for precise evaluations. For each machine, multiple individuals will be generated and subject to different genetic processes. In the Evaluation genetic process, the FEA software assesses all these machines, calculating key metrics to determine their fitness values. These fitness values are crucial for deciding which machine are retained for further development and which should be replaced. Prior to running the optimisation process, it is essential to complete several preparatory steps to outline clearly the system. These include identifying the sweep parameters, establishing the objective functions and defining the constraints to find the optimal solutions.

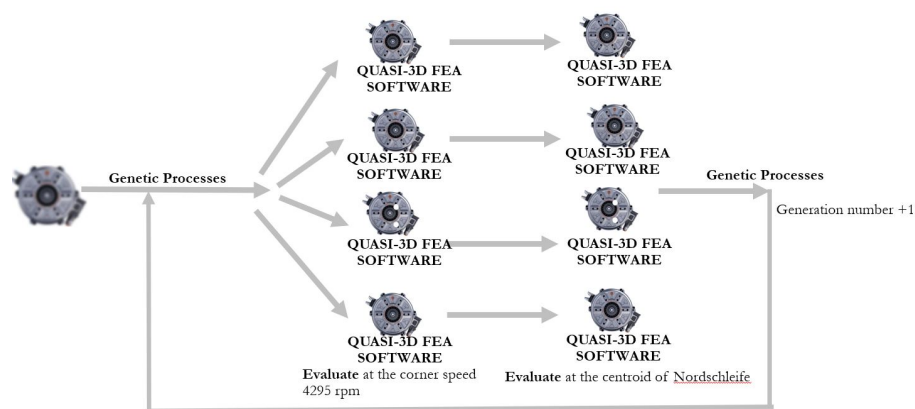


Figure 5.1: Application of the genetic algorithm

5.1 Optimisation problem

The previous chapter focused on the design of the electrical machine according to specific requirements using the "Manual design approach". This approach starts from detailed mathematical analysis of the system, leading to the formulation of design equations for calculating the design parameters .

However, for the correct application of these equations, it is necessary to make several assumptions and approximations. The following step is to validate the designed system using a numerical tool, in particular finite element method based. Based on the results of this analysis, adjustments to the system may be necessary. This iterative process of numerical analysis and system refinement with FEA is repeated until the design fully meets all specifications.

Despite its utility, this approach has two main drawbacks.

- The phase of developing assumptions and adjusting the designed system based on numerical analysis require a high level of engineering experience.
- While this method enables to determine the design, it does not ensure the optimum solution.

This chapter then introduces a different methodology known as "Optimisation-based design process" [35]. In contrast to the Manual design approach, this method does not follow a sequence of steps. It still begins with a detailed mathematical analysis, but rather than generating design equations, it focuses on identifying the metrics for optimisation and system constraints to define the objective function.

An optimisation algorithm is then employed to fine-tune the sweep parameters with the goal of enhancing the objective function.

This method can effectively solve the second shortcoming of the Manual design approach by optimising the system according to the specified design metrics, leading to better solutions.

In order to overcome the first limitation, the Quasi-3D FEA solver is used for metrics calculations, avoiding the need for assumptions inherent in analytical design equations.

However, this method has its own drawback: it requires significant computational time and the results' quality is dependent on the thoroughness of the initial analysis. Therefore, the design experience is still crucial.

5.2 Genetic Algorithm

Genetic Algorithm is an optimisation algorithm which belongs to the category of the population-based optimisation methods. This implies that it searches in the domain not from the single solution estimate but rather from assessing a group of solutions (population). This feature helps to reduce the risk of converging on a local optimal solution, as it explores throughout the feasible domain.

Unlike some optimisation algorithms, it considers the values of the objective functions, but not their derivatives, and uses random operations in each iteration (or generation). As a result, it is suitable to a broader range of engineering problems. In the Genetic Algorithm, the candidate solutions are termed also as individuals and every individual is encoded into a "chromosome". A chromosome is essentially a string where each element, known as "gene", represents a specific parameter of the individual. These genes can be expressed in various forms such as binary, interger or real numbers and are defined by a variation range with upper and lower limits that determine the domain, known as Parameter Space, in which the individuals can explore around to find potential optimal solutions.

A specific fitness value is assigned to each chromosome which measures its effectiveness as a solution of a specific optimisation problem. The higher the fitness value, the more likely the chromosome is to survive and reproduce.

The first step to solve an optimisation problem requires deciding the appropriate number of genes and their variation limits, while also setting the system's constraints. This step is crucial to generate individuals with feasible characteristics. Subsequently, the algorithm starts with the initialisation of the first population that is randomly generated. The fitness values of these individuals are then computed. Based on these evaluations, certain individuals of the population will undergo genetic operators of selection, crossover and mutation, resulting in the production of children and, as a consequence, the formation of a new population.

This procedure is repeated generation by generation until the predefined stopping criterion is fulfilled. The genetic algorithm is effectively summarised by the flowchart depicted in Figure 5.2.

An overview of each genetic operator used in this optimisation algorithm is provided herein for a comprehensive understanding of the entire process.

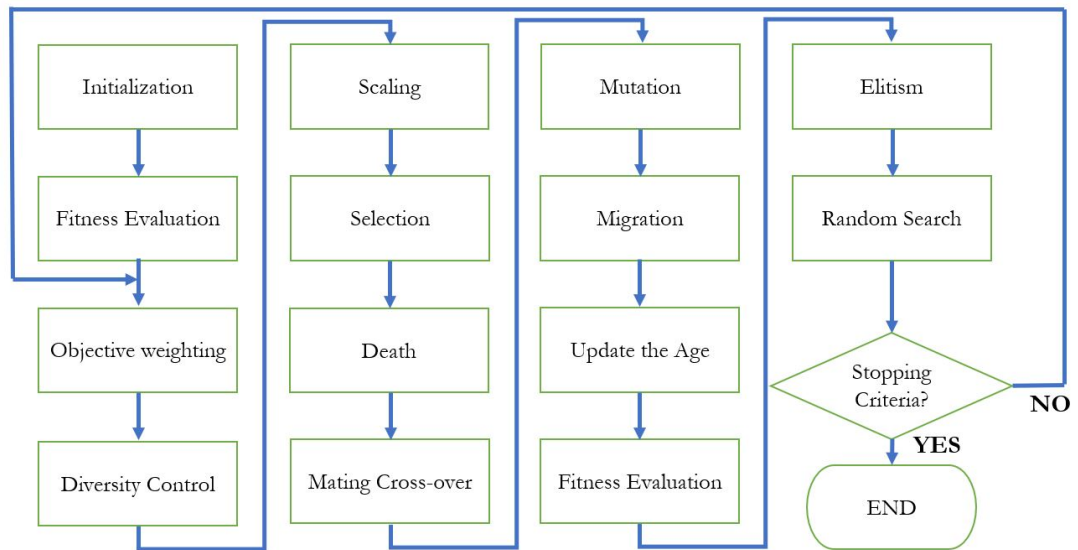


Figure 5.2: GOSET flowchart

5.2.1 Objective weighting

In the multi-objective optimisation problem, a normalised weighting vector is generated randomly to scale the fitness values of each individual.

5.2.2 Diversity control

While the Genetic Algorithm is working, it might happen that most of the candidate solutions converge to one local optimal solution. In order to explore the whole domain, this genetic operator examines the closeness of the candidate solutions. The individuals that are identical are penalised while the under represented individuals are less penalised and have a better chance to survive.

5.2.3 Scaling

During the optimisation process, it might happen that at the early stages of the evolution there is an individual which is the fittest of the population. As a consequence, there will be in the next generations a lot of individuals that are very similar to the fittest one leading to premature convergence and not a full exploration of the domain. In this case, the scaling algorithm is used to reduce the fitness value of the premature fittest individual. However, towards the end of the evolution this algorithm is used to emphasize the fittest individual so that to increase its likelihood of surviving.

5.2.4 Selection

Here, a mating pool is formed from the population by applying one of the two selection schemes. In Roulette wheel selection we select the individuals randomly but their probabilities are proportional to their fitness values. This procedure is repeated N times that corresponds to the size of the mating pool. Another selection scheme is called Tournament scheme in which we select a pair of chromosomes randomly from the population and compare their fitness values. The fitter of the two will be put in the Mating pool.

5.2.5 Death

This genetic operator determines which individual will die and be replaced by the children. They will not undergo any crossover or mutation in the next generations. Those individuals can be either the parents, randomly chosen, the ones with worst fitness values or the oldest ones.

5.2.6 Mating cross-over

This operation takes randomly a pair of chromosomes from the mating pool, called as parents, and gives a pair of offspring chromosomes by exchanging substring of the two parent chromosomes. There are many types of crossover operations. The simplest one is the Single-point crossover in which a crossover point is chosen at random along the chromosome and their genes after the crossover point are interchanged to generate new chromosomes of children.

5.2.7 Mutation

After crossover operation, the children will replace the individuals assigned during death operation and, therefore, the mating pool will be modified by keeping the same number of elements. Subsequently, the Mutation operation is applied which takes a chromosome and randomly changes its genes. Each chromosome has a certain probability of undergoing this mutation.

5.2.8 Evaluation

Through a detailed system analysis, key metrics and operational constraints are identified to formulate a specific fitness function. The fitness function assigns values to each individual based on the metrics, but only if all identified constraints are met.

One effective method to develop this function begins by assessing the status of

each constraint. This i -th constraint function can be described as follows:

$$c_i = lte(x, x_{mx}) = \begin{cases} 1, & \text{if } x \leq x_{mx} \\ \frac{1}{1+x-x_{mx}}, & \text{if } x > x_{mx} \end{cases} \quad (5.1)$$

$$c_i = gte(x, x_{mn}) = \begin{cases} 1, & \text{if } x \geq x_{mn} \\ \frac{1}{1+x_{mn}-x}, & \text{if } x < x_{mn} \end{cases} \quad (5.2)$$

Where the term x is a parameter that can be either the gene, the metric or another variable, x_{mx} is the maximum limit of the parameter and x_{mn} is the minimum limit. From these functions the i th constraint status can be 1 if the constraint is satisfied, otherwise between 0 and 1.

However, these set of constraints are not computed simultaneously but are divided into subgroups based on the different characteristics and theoretical aspects of the system. During the Evaluation phase, only one subgroup of constraint functions is computed at a time. As soon as, an individual does not satisfy one subgroup before reaching the last one, its fitness calculation is terminated prematurely. It is assigned a low fitness value increasing the likelihood of being discarded and replaced by children of fitter individuals in subsequent generation. This approach makes the calculation of remaining constraints unnecessary. This fitness function of the i -th individual calculated prematurely is expressed below:

$$f_i = \epsilon \left(\frac{C_{S_i} - N_C}{N_C} \right) \quad (5.3)$$

Where C_{S_i} is the number of constraints satisfied of the i -th individual, ϵ represents a small number that for MATLAB is 2^{-52} and N_C is the total number of constraints. Conversely, if an individual meets all constraints in the initial subgroups and reaches the final one, its fitness function is expressed as follows:

$$f_i = \begin{cases} \epsilon \left(\frac{C_{S_i} - N_C}{N_C} \right) & \text{if } C_{S_i} < C_I \\ y_i & \text{if } C_{S_i} = N_C \end{cases} \quad (5.4)$$

Where C_I is the number of constraints of one subgroup, y_i is the metric of the i -th individual calculated from the numerical tool or equation if it is a maximisation. In case of minimisation, the fitness value is the inverse of the metric $\frac{1}{y_i}$. This strategy allows to save a lot of time especially when FEA software is employed as numerical tool for metric computation.

In this approach, during the optimisation, individuals which do not adhere all set of constraints receive negative fitness values, while those which meet all constraints are assigned positive fitness values. This assignment process is crucial since, the designs with the lowest fitness values are more likely to be replaced by children generated

in crossover operation. At the beginning of the evolution, all designs may not fulfill all constraints. However, as the evolution progresses with the aim of maximising the fitness function, fitness values of the next generation individuals gradually increase becoming less negative as more constraints will be fulfilled generation by generation.

5.2.9 Elitism

Not always the fittest individual will survive in the whole evolution because of environmental influences. In order to avoid this phenomenon, this genetic operator takes the fittest individual of the new population and the fittest one of the previous population. It compares their fitness value and the fittest between the two will replace the other and so it will be put in the new population.

5.2.10 Random search

It is often the case that the fittest individuals are close to a solution. Therefore, this genetic operator is used to create a set of mutations of these individuals to do local searches around them. If we find mutants that are better, thus the fittest individual will be replaced.

5.3 Formulation of design problem

In this stage, it is possible to start seeking better machine designs through an optimisation-based design process, leveraging the three axial flux permanent magnet machines with different slot and pole combinations obtained from the preceding chapter.

The problem is an optimisation problem in which the objective is to develop machines capable of producing peak torque above the required one from the drive cycle analysis at corner speed. This involves using an inverter with a specified DC link voltage V_{DC} and striving to minimise the supply stator voltage within two specified limits. These limits are set to position the base speed closer to the corner speed deriving from the drive cycle analysis, while also controlling the peak power. It is desirable to minimise the total mass of the machine to increase the torque density and, especially the magnet mass for lessening supply chain dependencies. The aim is also to optimise the efficiency at the centroid operating point from Nordschleife driving cycle. As such, these three machines must be designed to have a certain input current and advance angle to address that load. Additionally, it is also important to ensure that the peak current density of these machines stays below a certain limit at rated current, and the characteristic current is smaller than the peak current input to enable theoretically unlimited speed capabilities.

For this optimisation, a genetic optimisation tool built for MATLAB known as GOSET is employed. In order to execute this code, it is required to identify the free parameters, the metrics and the constraints. Following this, it is possible to formulate the fitness function in the Evaluation block.

5.3.1 Design metrics

The Quasi-3D FEA software outputs several metrics from a Magnetostatic simulation. In this thesis, among these outputs, five design metrics are of interest: torque, voltage, mass, magnet mass and efficiency. The software calculates for each machine the first four metrics at corner speed and peak torque while the last one is computed at the centroid operating point from Nordschleife driving cycle. This necessitates running the Magnetostatic simulation twice for each individual that has respected all subgroups of constraints across all generations during the evolution.

The goal is to maximise torque and efficiency, targeting machines with higher peak torque and optimal efficiency in high energy consumption region. Meanwhile the remaining metrics are intended for minimisation, with the rationale provided in section 5.3.

Furthermore, some of these objectives are subject to constraints that are discussed in the subsection 5.3.3.

In this optimisation problem, the genetic operator Objective weighting (subsection 5.2.1) has another weighting vector applied to the fitness values of the individuals, containing the weight factors that are different in magnitude. The sequential order of the metrics listed below corresponds to the decreasing order of the magnitude of the weight factors:

Electromagnetic torque, stator phase voltage, efficiency at the centroid, magnet mass and total mass.

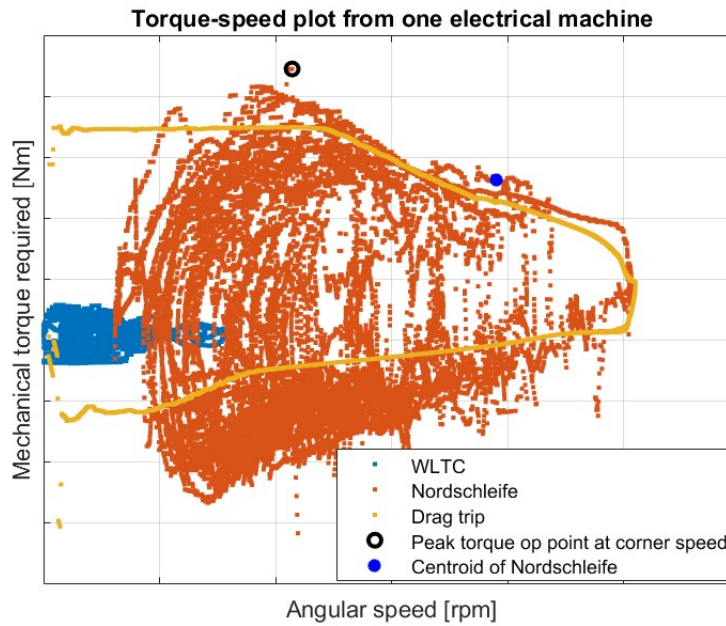


Figure 5.3: Operating points at which the Quasi-3D FEA software runs Magnetostatic simulation

5.3.2 Formulation of the Parameter space

The first step in our design process involves in defining the Parameter space which outlines the limits for the variation of the individuals' genes, which are the geometrical parameters used as input of the Quasi-3D FEA software. This Parameter space is tabulated in Table 5.1.

Some level of engineering experience is required to select a broad reasonable range for these parameters to expand the Parameter space as much as possible and enhance a wider exploration for different solutions. Nevertheless, certain parameters provided by the FEA software to build up a machine are set as constant before the optimisation begins. The fixed variables include the number of slots, number of poles, number of turns, rotor yoke height and the air gap.

For simplification, we assume that stators have not tooth tips which slightly reduces the Parameter space.

All in all, our machine incorporates one discrete variable, that is the current input, and seven continuous variables amounting to eight degrees of freedom.

Gene	Description	Type	Minimum	Maximum
OD	Outer diameter	lin	OD-(30% OD)	OD
ID	Inner diameter	lin	ID-(10% ID)	ID+(30% ID)
h_{st}	Stator height	lin	10 mm	50 mm
w_{sl}	Slot width	lin	10 mm	30 mm
$h_{bi_{st}}$	Stator back iron	lin	3 mm	20 mm
h_{ro}	Rotor height	lin	11 mm	21 mm
M_{sp}	Magnet spacing	lin	2 mm	$\pi \frac{ID_{ro}}{2p} - 1$
I_{rms}	Input current	int	750 Arms	1000 Arms

Table 5.1: Genes to define the Parameter space

Constant parameter	Combination 1	Combination 2	Combination 3
Number of slots	24	12	24
Number of poles	22	10	20
Tooth fillet radius [mm]	100%	100%	100%
Number of magnet segments	100%	100%	100%
Number of turns	100%	185,7%	100%
Rotor yoke height [mm]	100%	100%	100%
Air gap [mm]	100%	100%	100%

Table 5.2: Constant parameters

In this problem, outer diameters of the stators and rotor are equal, as their inner diameters. The variation ranges of these diameters are specifically set to ensure the reduction of the machine's total volume that is very dependent to the outer diameter, with the aim of improving torque density. The maximum limit of the outer diameter is equal to the one obtained from the analytical design also due to packaging constraints.

In addition, while the number turns are constant to position the base speed of the torque speed curve, the current input is designated as a gene with its maximum limit equal to the maximum current that inverters available on the market today can supply. This range is chosen to explore e-machines capable of delivering higher torque with lower input current.

5.3.3 Formulation of the constraint functions

In order to ensure uninterrupted optimisation and the effective functioning of the generated electrical machines, certain constraints are necessary.

These constraints are split into two subgroups: geometrical and output constraints. The geometrical constraints focuses on the proper machine's assembly ensuring that the FEA software can generate mesh layers encompassing the entire machine and run the magnetostatic simulations without errors.

One requirement is that the stator height is always greater than the stator back iron.

$$c_1 = gte(h_{st}, h_{bi_{st}}) \quad (5.5)$$

In order to maintain the structural integrity of the stator with a given outer and inner diameter, the slot width is limited to a maximum value, beyond which the tooth width becomes too narrow. If the maximum slot width is exceeded, the adjacent slots will overlap causing the disappearance of the tooth. To avoid this issue caused by random variation of the genes, the slot width must be kept smaller than the minimum slot pitch.

$$c_2 = lte(w_{sl}, \frac{\pi ID_{st}}{s_1}) \quad (5.6)$$

The last geometrical constraint is keeping the magnet spacing below a maximum limit. If it is too wide, the magnet's inner diameter might be too large with respect to the rotor's inner diameter leading to a situation in which one cylindrical layer mesh does not fully encompass it.

$$c_3 = lte(M_{sp}, \frac{\pi ID_{ro}}{2p}) \quad (5.7)$$

Among the output constraints, there is the maximum allowable value of the current density.

$$c_4 = lte(j, j_{max}) \quad (5.8)$$

For optimal performance, the torque produced by the machine at corner speed has to be larger than the peak torque required from the driving cycle analysis to cover all operating points, but a maximum limit is also set that is 5% more higher than the minimum limit. This is done to compensate losses such as iron, windage and bearing losses which account for about 3% loss in converting from electromagnetic to shaft torque based on engineering experience. These constraints also help to keep the torque within reasonable boundaries.

$$c_5 = gte(Mt, Mt_{req}) \quad (5.9)$$

$$c_6 = lte(Mt, Mt_{req} + (5\%Mt_{req})) \quad (5.10)$$

The next constraint ensures that there is adequate DC link voltage, requiring that the stator phase voltage is less than the DC link voltage and also to reduce the peak power.

$$c_7 = lte(V_s, \frac{V_{DC}MI}{\sqrt{3}}) \quad (5.11)$$

In addition to the constraint above, it is necessary to impose a lower limit to prevent the possibility of generating machines having higher base speed on the electromagnetic torque characteristic curve than the corner speed determined from the drive cycle analysis.

$$c_8 = gte(V_s, \frac{V_{DC}MI}{\sqrt{3}} - (5\% \frac{V_{DC}MI}{\sqrt{3}})) \quad (5.12)$$

As a consequence of the last four constraints, the genetic algorithm will provide e-machines with similar characteristic electromagnetic torque curves that are able to cover all operating points calculated from the driving cycle analysis. Therefore, once the best e-machine is selected among various non-dominated solutions for each slot and pole configuration based on performance, the similarity in the characteristic curves of the three chosen motors simplifies the comparison of their loss maps that is shown in the next chapter.

In order to ensure the electrical machines' capability for infinite speed, the absolute value of the characteristic current has to be less than the peak input current, that is a gene.

$$c_9 = lte(|I_0|, I_{rms}\sqrt{2}) \quad (5.13)$$

In order to have the possibility of optimising the electrical machines in terms of efficiency at the centroid, the last constraint is used to check if the machine has an electromagnetic torque characteristic curve able to cover the centroid operating point. This can be checked by implementing the algorithm shown in Appendix B where it is possible to understand if the e-motor can run at that load with a certain input current and advance angle.

$$c_{10} = \begin{cases} 1 & \text{if } \exists I_{rms_{required}}, \gamma_{required} \\ 0 & \text{otherwise} \end{cases} \quad (5.14)$$

5.3.4 Formulation of the fitness function and the set-up of the optimisation

To formulate the fitness function, it is followed the strategy explained in subsection 5.2.8, where the two subgroups of constraints are computed at specific intervals rather than simultaneously. Before running the simulation, it is necessary to check the geometrical feasibility of the e-machines assembled by the FEA software. If one particular machine does not respect completely the first subgroup, then its fitness function is calculated prematurely following the Equation 5.3.

On the other hand, if the machine assembled respects all geometrical constraints, it can be simulated using the FEA software to calculate its metrics and the fitness function is defined as:

$$f_i = \begin{cases} \epsilon \left(\frac{C_{S_i} - N_C}{N_C} \right) & \text{if } C_{S_i} < C_I \\ [M_{t_i} \ \frac{1}{m_i} \ \frac{1}{m_{pm_i}} \ \frac{1}{V_{s_i}} \ \eta_{centroid_i}]^T & \text{if } C_{S_i} = N_C \end{cases} \quad (5.15)$$

With the fitness function and the genes now established, it is possible to begin the optimisation for the three machines manually designed in the previous chapter. The optimisation was conducted with a population size of 40 over 150 generations. In each generation all individuals, that have respected all constraints, are evaluated through the Magnetostatic simulation in the FEA software. To further save time, these simulations were run in parallel computing by leveraging the number of cores available in the workstation.

5.4 Results from the genetic algorithm

This section presents results provided by GOSET, organised into two parts. The first part includes one subsection which displays Pareto fronts for different objective values combinations where each point corresponds to a non dominated solution.

The second part, instead, includes 5 subsections, and in each, there are three plots which contain the gene distribution of the last generation population of e-machines for three different slot and pole configurations. The genes are sorted by a specific fitness function. This means that, for example, the genes of the motors with higher total mass are the blue colored dots and toward the left of the parameter window, while the genes with lower total mass are the red colored dots and toward right.

Each parameter window is labeled by an acronym. The full list of acronyms is available on page XIII and XIV, providing a useful reference to the reader.

This last part is particularly useful for identifying potential correlations between geometrical parameters and the objective functions.

5.4.1 Pareto Front plot

Figure 5.4 and 5.5, illustrate a trade off between torque and magnet mass, as well as between efficiency at the centroid and the magnet mass. This magnet mass reduction implies a decrease of the magnetic flux density at the air gap. As a result, to generate the same torque, it is necessary to inject higher supply current which in turn leads to greater DC copper loss.

In addition, an increase in the current may also cause saturation on the stator iron leading to an increase of total iron loss.

Electrical machines with higher number of poles exhibit lower efficiency especially at high speeds (centroid operating point of Nordschleife) due to greater magnet and iron loss.

Figure 5.6 is shown to demonstrate that GOSET has correctly respected the torque and voltage constraint functions during the optimisation.

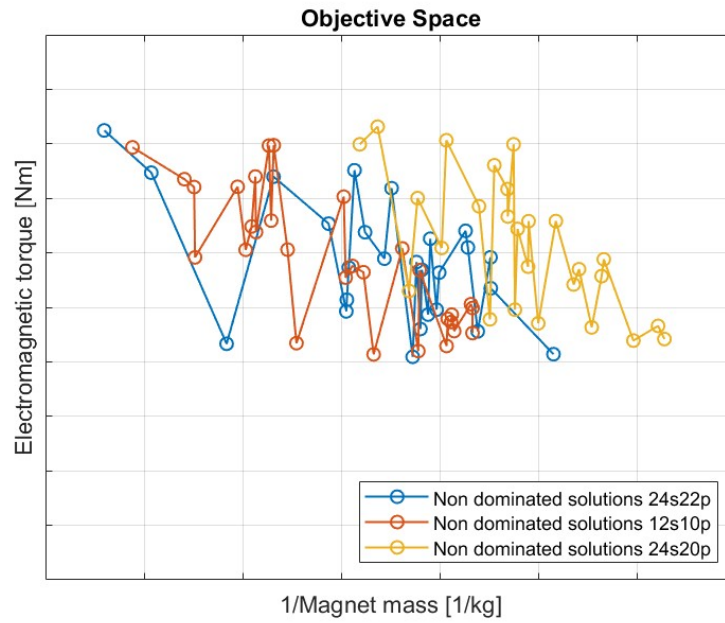


Figure 5.4: Electromagnetic torque versus magnet mass

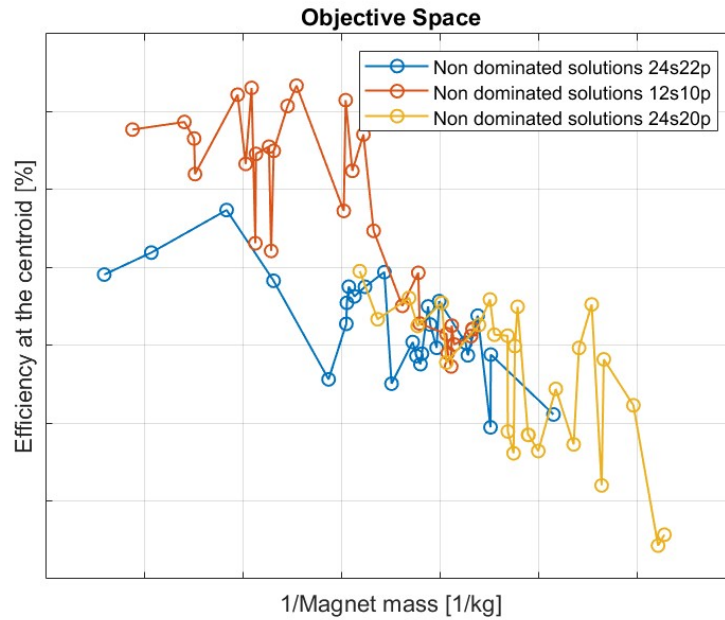


Figure 5.5: Efficiency at the centroid versus magnet mass

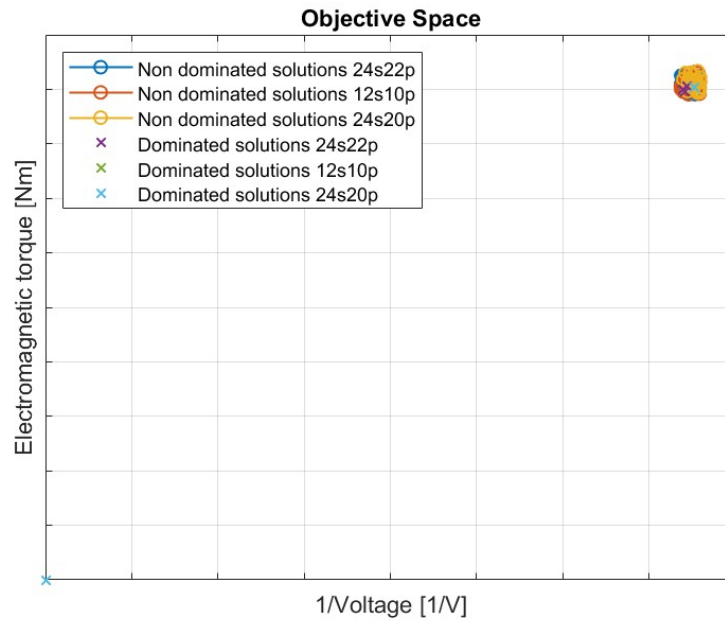


Figure 5.6: Electromagnetic torque versus supply voltage

5.4.2 Genes sorted by Objective 1 - maximisation of the electromagnetic torque

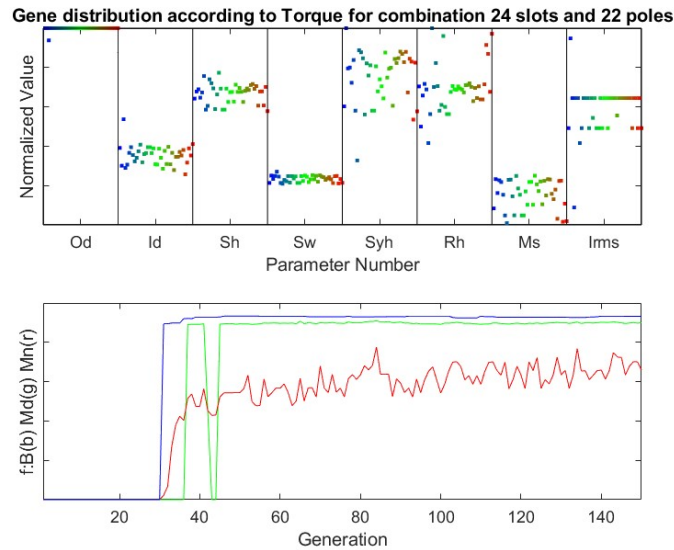


Figure 5.7: Gene distribution of the e-machines with 24 slots and 22 poles configuration sorted by torque

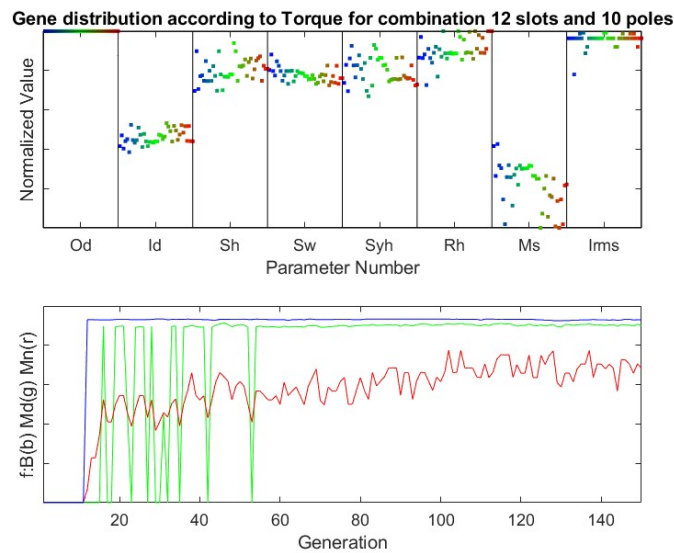


Figure 5.8: Gene distribution of the e-machines with 12 slots and 10 poles configuration sorted by torque

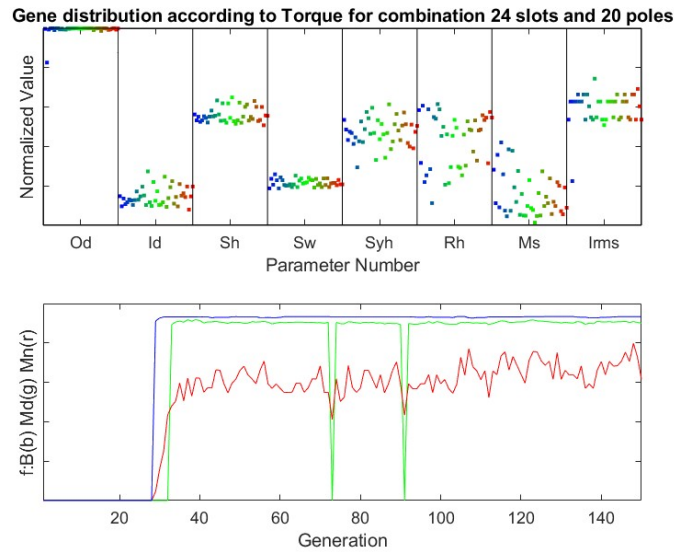


Figure 5.9: Gene distribution of the e-machines with 24 slots and 20 poles configuration sorted by torque

In order to maximise the torque, the clustering of all values of the outer diameter tends to the same value that is the maximum limit, as the torque is proportional to the cubic value of the outer diameter. This result also indicates that the slot width of e-machines with 12 slots and 10 poles is greater than the two other configurations with the same outer diameter.

The genes input current tend to have the same value because they are influenced mainly by the two torque constraints explained in subsection 5.3.3.

The e-machines with 12 slots and 10 poles configuration have the highest input current and thicker magnets to attain the maximum possible total air gap flux density for the required torque. It means that for that aggressive torque target, a machine with 10 poles needs to be close to the limit for input current and magnet thickness. Therefore, if you need to achieve that aggressive target of torque and torque density, an increase on number of poles is necessary. On the other hand, this also leads to increase the electrical frequency which in turn causes larger iron and magnet losses.

If the number of poles increases, the thickness of the stator back iron reduces as it can be seen in the gene distribution. If the number of poles is reduced, it is necessary to have a thicker stator yoke to accommodate the return of the flux lines between poles to ensure that the required torque is met. However, the genes representing the stator yoke height, in the first figure, are scattered and some of them are much larger because a maximum limit on the magnetic flux density at the back iron has not been imposed.

The stator height, that is the sum between the stator yoke and the slot height, is determined by the amount of input current injected because a certain slot area has to be obtained so that the current density can comply with limit. In 12 slots and 10 poles configuration, the supply current genes are very high and thus, it is necessary to have both stator height and slot width large enough to generate a big slot area, reducing the current density. In the other two configurations, the slot width is narrower, due to the higher number of slots, meaning that a large stator height is needed because of high number of poles.

5.4.3 Genes sorted by Objective 2 - minimisation of the total mass

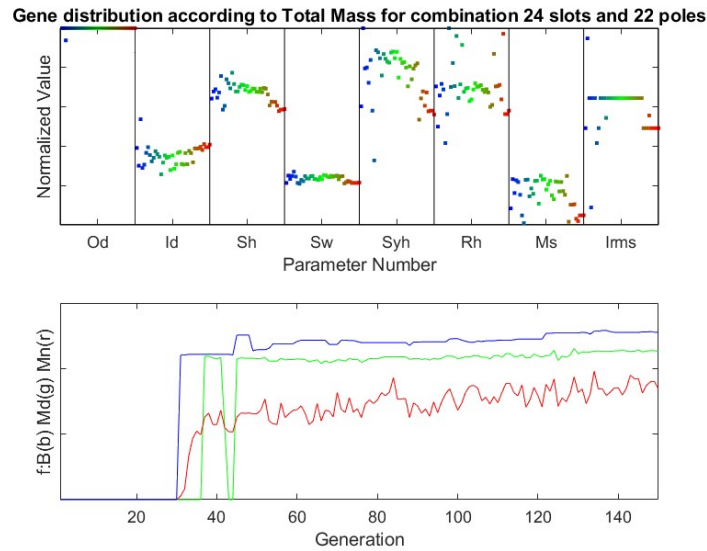


Figure 5.10: Gene distribution of the e-machines with 24 slots and 22 poles configuration sorted by the total mass

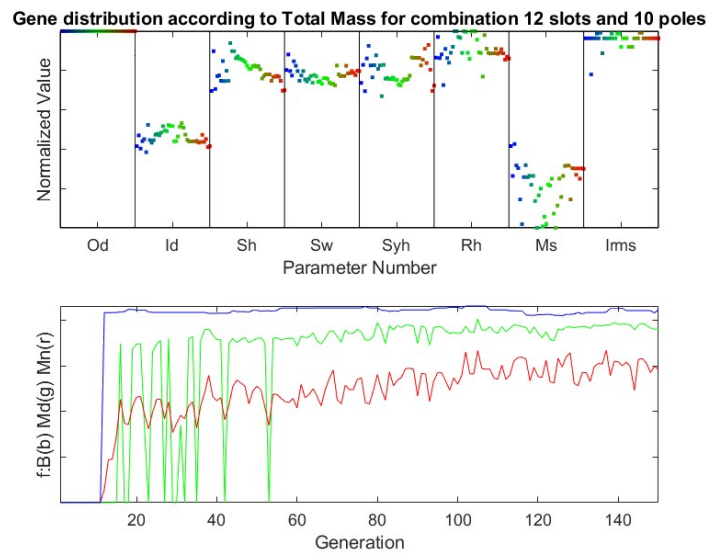


Figure 5.11: Gene distribution of the e-machine with 12 slots and 10 poles configuration sorted by total mass

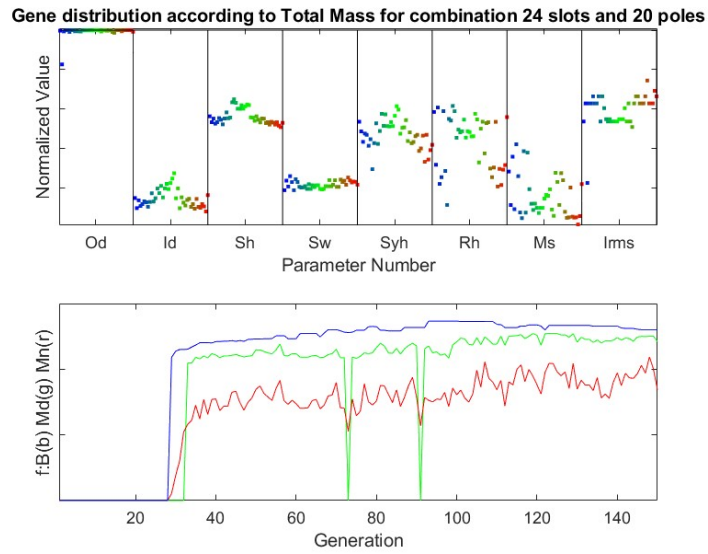


Figure 5.12: Gene distribution of the e-machines with 24 slots and 20 poles configuration sorted by the total mass

In these three figures, it is possible to notice that the most affected genes are the geometrical parameters of the stators.

By increasing the number of poles, it is more visible the upward slope of the inner diameter moving from a higher total mass motor to a lower total mass motor. In this case, the volume of the machines is decreased having fixed outer diameter. Same effect occurs to the stator and yoke height having a downward slope.

5.4.4 Genes sorted by Objective 3 - minimisation of the magnet mass

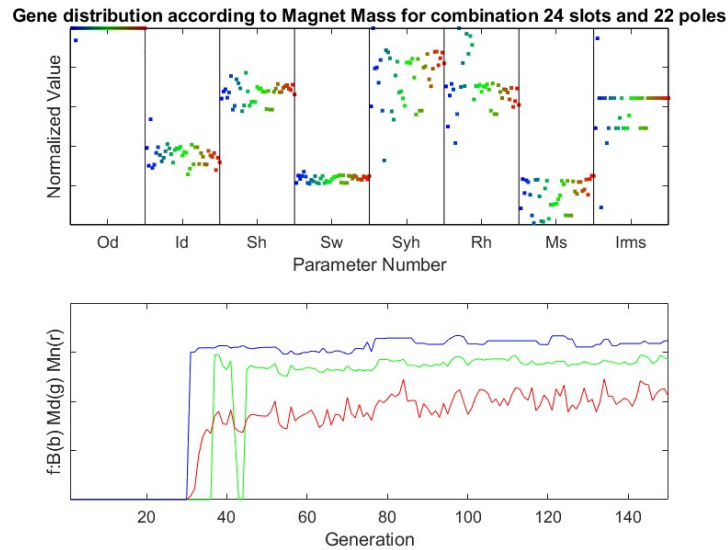


Figure 5.13: Gene distribution of the e-machines with 24 slots and 22 poles configuration sorted by magnet mass

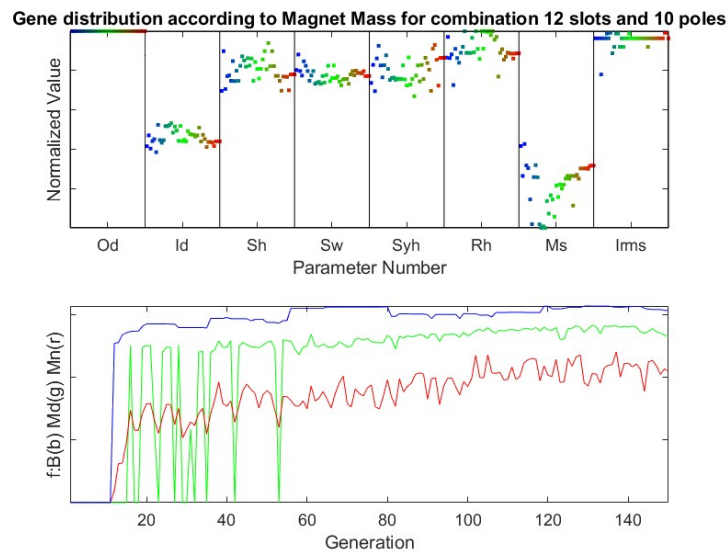


Figure 5.14: Gene distribution for the e-machines with 12 slots and 10 poles configuration sorted by magnet mass

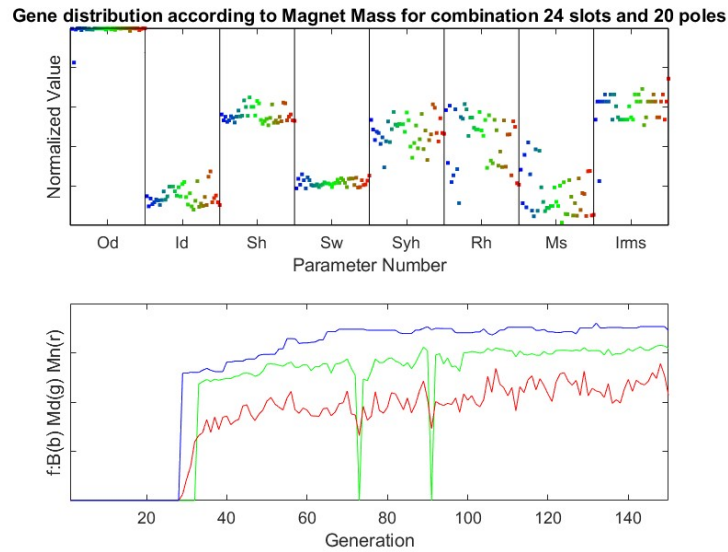


Figure 5.15: Gene distribution of the e-machines with 24 slots and 20 poles sorted by magnet mass

In this objective function, The most affected genes are those related to the magnet size.

Overall in the three configurations, it is possible to notice the increase of magnet spacing from the red points. However, in e-machines with 12 slots and 10 poles configuration, it is more evident the upward slope of the magnet spacing because there is more area available per magnet pole when comparing to the e-motors with higher number of poles.

In the other two configurations, even though there are machines having magnet spacing that are slightly bigger, it is possible to achieve the minimisation of the magnet mass by reducing their magnet thickness.

5.4.5 Genes sorted by Objective 4 - minimisation of the stator voltage

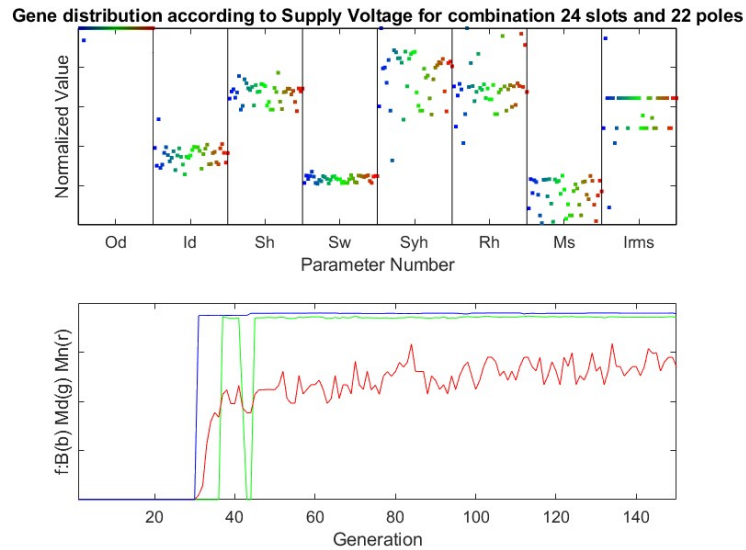


Figure 5.16: Gene distribution of the machine with 24 slots and 22 poles configuration sorted by voltage

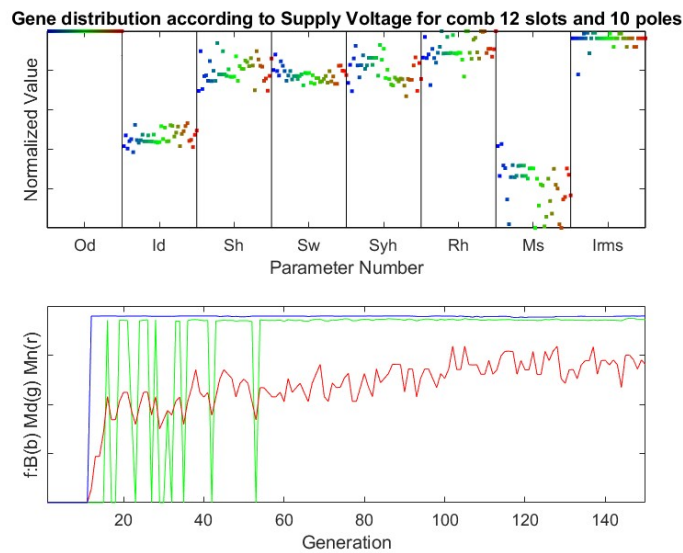


Figure 5.17: Gene distribution of the e-machines with 12 slots and 10 poles configuration sorted by voltage

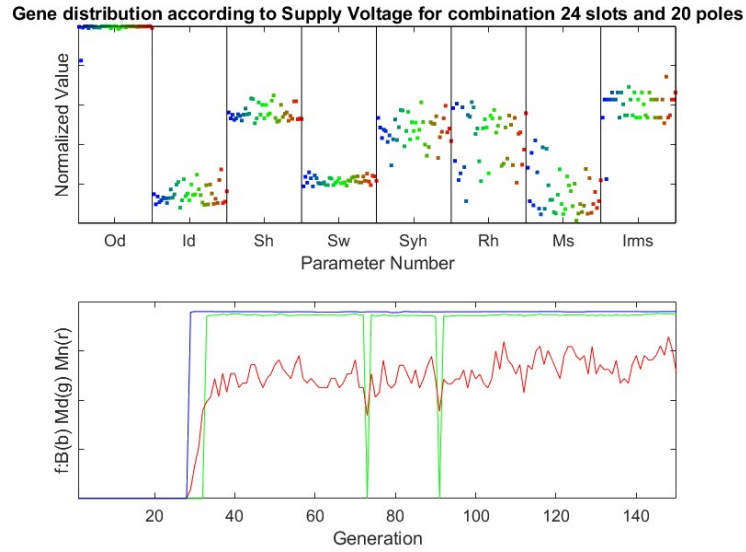


Figure 5.18: Gene distribution of the e-machines with 24 slots and 20 poles sorted by voltage

In this optimisation problem, the number of turns and the mechanical speed are fixed. By recalling the permanent magnet machine equivalent circuit model, the minimisation of the voltage affects the flux from the magnet which in turn it is proportional to its volume. It means that the two constraints applied on the stator voltage imply a specific range of variation for the rotor height and magnet spacing genes.

In addition, the dots representing the stator yoke height, rotor height and magnet spacing are not showing a specific trend but scattered. This happened because no constraints on the magnetic flux density at the back iron and at the tooth have been set, and therefore, these genes are more widespread. These last two constraints are not considered to avoid further reduction of the Parameter space.

5.4.6 Genes sorted by Objective 5 - maximisation of the efficiency at the centroid

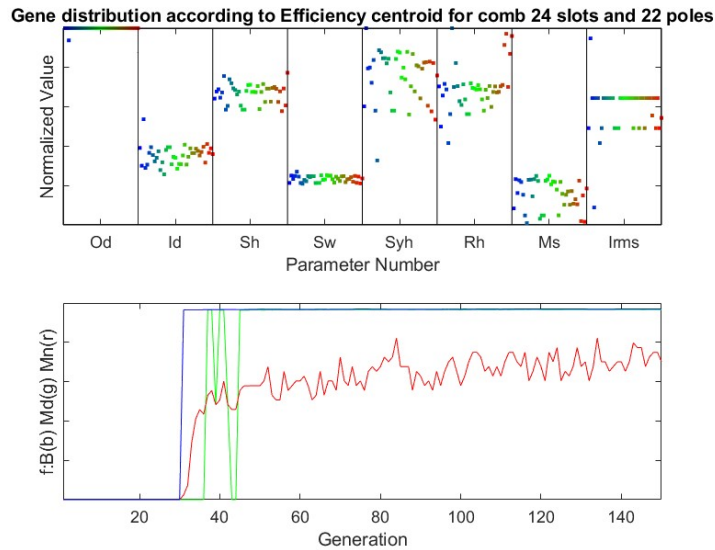


Figure 5.19: Gene distribution of the e-machine with 24 slots and 22 poles sorted by efficiency at the centroid

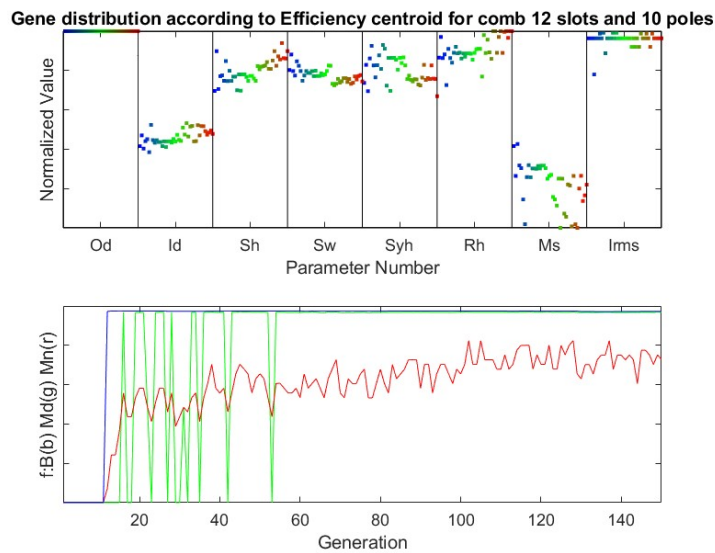


Figure 5.20: Gene distribution of the e-machines with 12 slots and 10 poles sorted by efficiency at the centroid

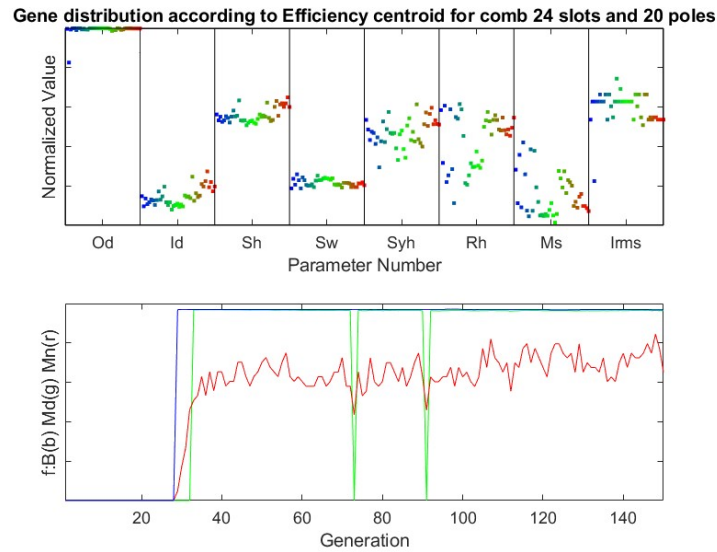


Figure 5.21: Gene distribution of the e-machines with 24 slots and 20 poles sorted by efficiency at the centroid

The maximisation of the efficiency at high speed operating point leads to reduce the total mass and the current input. In this problem, the current supplied at corner speed operating point is fixed due to the torque and current density constraints. As a consequence, only the stator geometrical parameters are influenced by this objective function. Indeed, it is possible to see the increase of the machines' inner diameter and the reduction of the stator yoke height moving rightward.

It is possible to recognise that this multi-objective optimisation problem, with these member genes presented above, is very well suited for simple motor geometries. However, if this problem is applied to radial flux machines which have more geometrical parameters to consider (particularly in the slots geometry), the situation becomes more complicated.

5.5 Selection

Once obtained successfully multiple solutions that align with our targets, the main task is selecting the most suitable machine for the car. The decision-making criterion involves choosing the best performing e-machine for each slot and pole combination based on a thorough comparison of their objective values.

Subsequently, it is also crucial to assess their energy consumption. This dual consideration enables the designer to choose a machine that not only excels in performance as required but also minimises the energy use.

The in depth analysis of energy consumption among the three best machines will be examined in the next chapter.

5.5.1 Comparison among the non dominated solutions

There are several approaches to analyse multi-dimensional data. One effective method employed to compare the objective values of all non dominated solutions is the so called radar or polar plot, as displayed below.

Due to the large number of non dominated solutions obtained in each of the three optimisation problems, only the top five machines with the highest torque from each optimisation are shown in the radar plots. For a complete view of all non dominated solutions, refer to the radar plots in the Annex C.

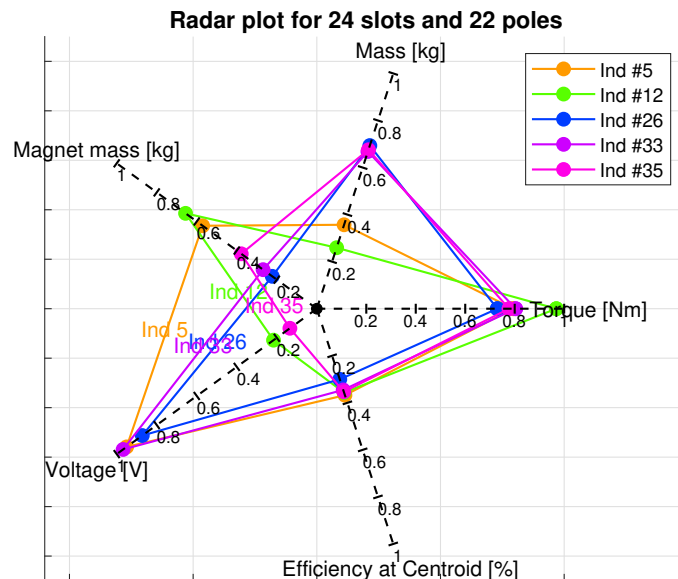


Figure 5.22: Radar plot of non dominated solutions with 24 slots and 22 poles

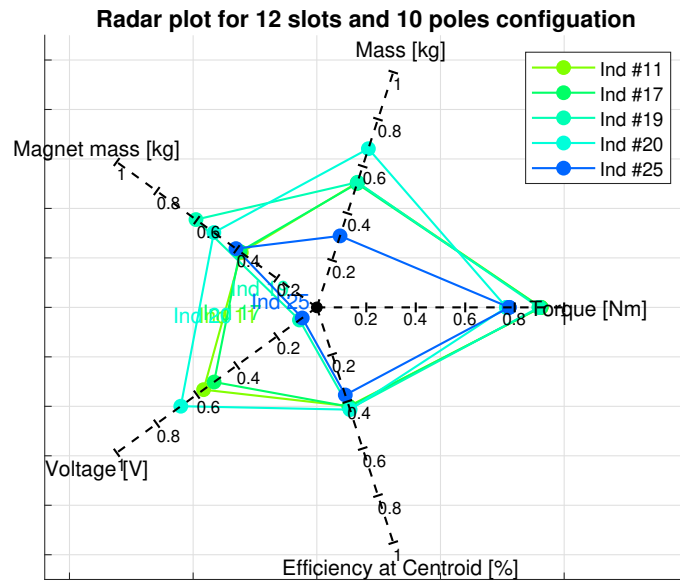


Figure 5.23: Radar plot of non dominated solutions with 12 slots and 10 poles

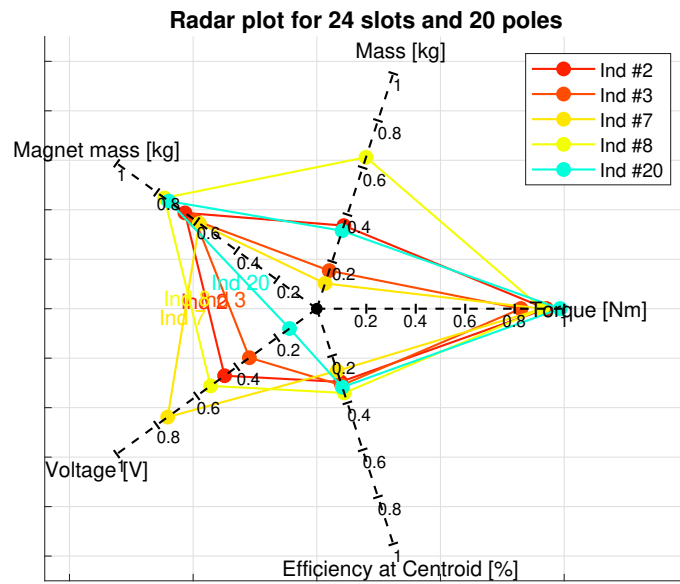


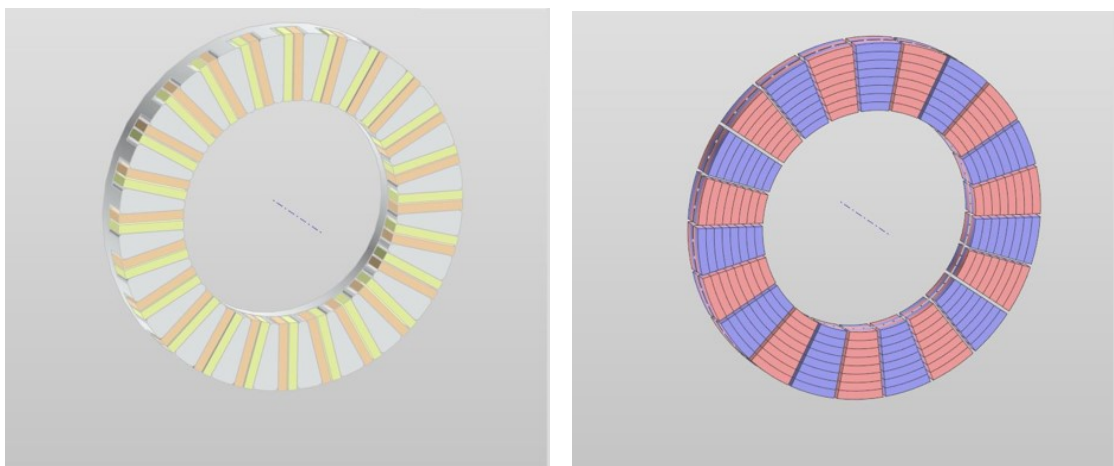
Figure 5.24: Radar plot of non dominated solutions with 24 slots and 20 poles

Each axis on the plots corresponds to a metric defined within a range set by the maximum and minimum values derived from the constraints. For metrics with one or no constraints, their axis limits are set to the nearest rounded numbers i.e. rounding up for the maximum and down for the minimum, based on the actual maximum and minimum values of these metrics among the last generated e-machines. This approach helps to focus on the range showing a clearer visualisation of variations. The range of the magnet mass is of two kilograms while it is five kilograms for the total mass and 5 % for the efficiency at the centroid.

By observing the voltage and torque axis, the plot clearly shows that GOSET has adhered our constraints during the optimisation. The first and third plots immediately reveal the best machine offering the highest torque, low total mass and high efficiency at the centroid. In contrast, the second plot features machines with torque values close to the the maximum limit and similar mass. In this particular case, the choice is based on the comparison of the torque magnitude, thus machine with the highest torque were chosen.

It is evident in all three plots that the machines have a mid-low total mass but their magnet mass are the highest among the five non dominated solutions. This outcome is partly due to the different weight factors applied to the fitness values of the individuals: a higher weight is applied on the minimisation of the total mass compared to the minimisation of the magnet mass, while the maximisation of the electromagnetic torque receives the highest weighting.

After this comparative analysis, the best machines for the three different slot and pole configurations, along with their geometrical parameters and objective values are displayed below.



(a) One stator

(b) Rotor

Figure 5.25: electrical machine with 24 slots and 22 poles-Individual 12

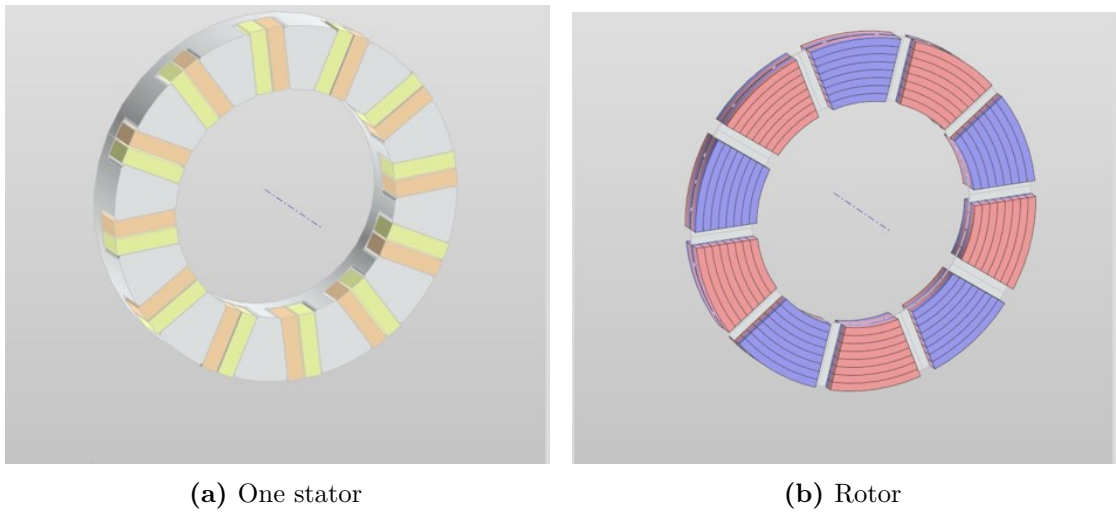


Figure 5.26: electrical machine with 12 slots and 10 poles-Individual 11

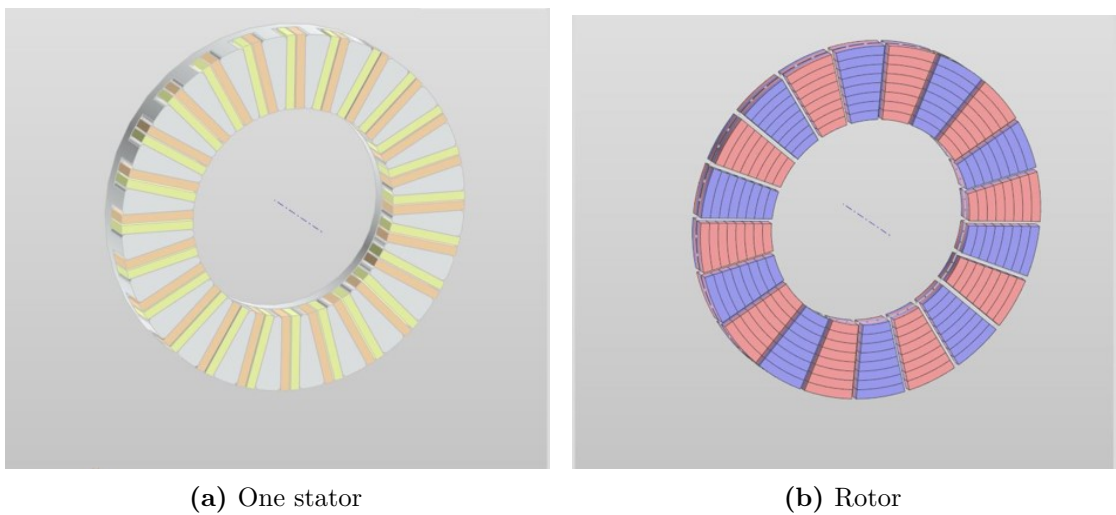


Figure 5.27: electrical machine with 24 slots and 20 poles-Individual 20

	e-Motor 24 slots and 22 poles	e-Motor 12 slots and 10 poles	e-Motor 24 slots and 20 poles
Number of slots	24	12	24
Number of poles	22	10	20
Outer diameter [mm]	100%	100%	99,96%
Inner diameter [mm]	100%	102,82%	93,53%
Slot width [mm]	100%	176,6%	99,08%
Stator height [mm]	100	127,82	97,22
Stator yoke [mm]	100%	120,16%	90,33%
Rotor height [mm]	100%	101,46%	78,48%
Magnet spacing [mm]	100%	503%	164,12%
Current input [Arms]	100%	113,52%	101,26%
Phase resistance [Ω]	100%	93.14%	105.4%

Table 5.3: Parameters of the three top e-machines

	e-Motor 24 slots and 22 poles	e-Motor 12 slots and 10 poles	e-Motor 24 slots and 20 poles
At corner speed			
Electromagnetic torque [Nm]	100%	99,7%	100,07%
Mech. power [kW]	100%	99,7%	100,07%
Supply voltage [V]	100%	101,07%	99,75%
Total mass [kg]	100%	128,96%	98,47%
Magnet mass [kg]	100%	87%	80,74%
Efficiency [%]	100%	99,05%	99,6%
Power factor	100%	88,05%	99,53%
Current density [$\frac{A}{mm^2}$]	100%	84,84%	100,7%
Flux linkage of the magnet [Wb]	100%	193,2%	108,75%
At the Nordschleife centroid			
Efficiency [%]	100%	100,33%	99,92%

Table 5.4: Objective values of the three top e-machines

Chapter 6

Energy consumed of the optimised e-machines

In the design of the electrical machines, the focus is not only on optimising motor performance but also on the calculation of the energy consumption. This calculation is crucial as it determines the energy required on the battery and consequently influencing the driving range of the vehicle.

The widespread customer acceptance of battery electric vehicles is still limited due to ongoing challenges which includes:

- Limited driving range and dependant on the ambient conditions and driving style.
- The increase in the price of raw materials and battery components.
- The impact on driving range can be even more relevant if additional thermal energy is required to manage the battery and electronics operation.

In order to mitigate the range anxiety, researchers are exploring three main approaches:

- Employment of advanced production technologies to increase the battery energy density and fast recharge without affecting ageing.
- Improvement of the efficiency of the main powertrain components to better utilise the energy.
- Urban planning to design the city and have more recharging infrastructure and standards.

Focusing on the second solution, the overall efficiency of the electrical drives is affected by the efficiencies of both the inverter and the e-machine. More attention is

given to the e-machine as it shows greater variability in performance across different driving cycles, in contrast to the consistently high efficiency of the inverter.

This section presents a method for calculating the cumulative energy consumption of the three leading machines, each featuring different slot and pole configurations, over the Nordschleife driving cycle. The final aim is to identify the machine which offers the lowest energy consumption, thus determining the most efficient option. This involves the use of their different loss maps, which are generated through repetitive runs of finite element software by varying different combinations of d and q axis currents and speed.

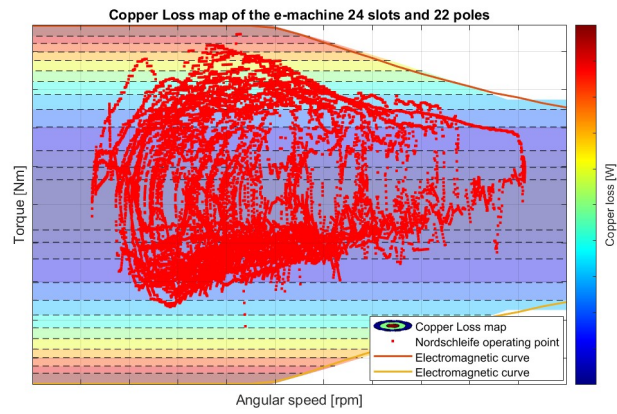
6.1 Losses maps

In order to produce a desired torque and speed combination, various i_d and i_q combinations can be obtained using Matlab. Among these control combinations, the one that ensures Maximum Torque Per Ampere (MTPA) is selected and at the same time satisfying the voltage and current limits of the inverter. That specific combination is then used as input for loss calculation via FEA.

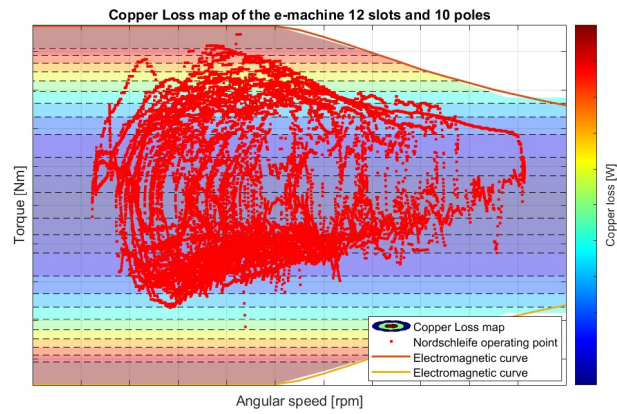
After conducting multiple simulations for varied combinations of torque and speed required, contour plots of the different loss components can be generated. These iterative simulations enable the comparison of the loss maps for the three machines. It is important to mention that, the decision of imposing a maximum torque limit and specifying minimum and maximum voltage values during the optimisation process is made also to ensure that the three machines have similar characteristic electromagnetic torque curves. This similarity allows for an effective analysis of how the different loss maps of each machine impact their cumulative energy consumption [36].

Below, four sets of three plots representing the three selected machines are displayed. Every set is dedicated to a specific loss component calculated using the Quasi-3D FEA software: DC copper loss, Eddy current loss at the stator iron, Hysteresis loss at the stator iron, Magnet loss due to the eddy current and Total loss.

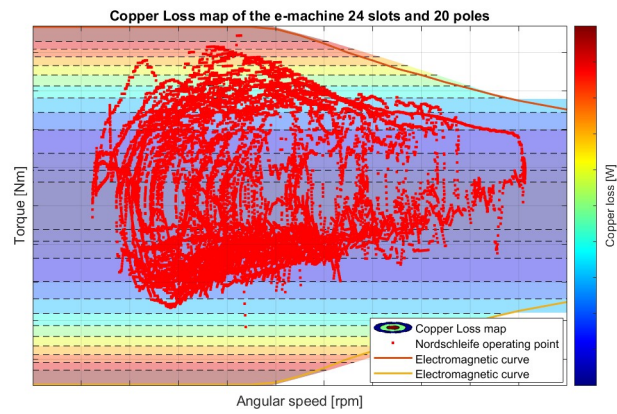
For each group, the scale of the colorbar in the plots is defined by the largest value of the respective loss component found among the three machines, thus facilitating a detailed comparison of each loss component across the three machines. In the Hysteresis and Eddy current loss maps at the stator iron, their colorbar are defined by the largest value of the Eddy current loss found among the three machines.



(a) DC copper loss map of the e-machine 24 slots and 22 poles

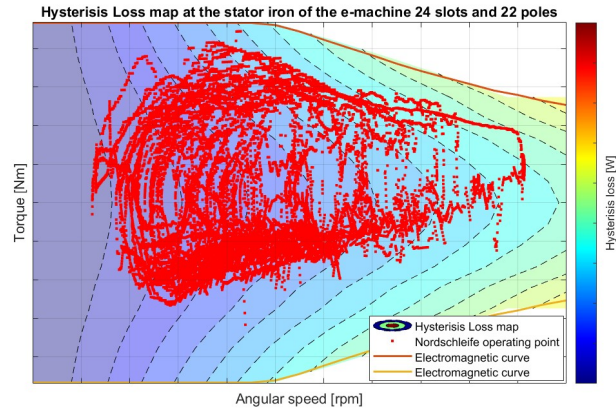


(b) DC copper loss map of the e-machine 12 slots and 10 poles

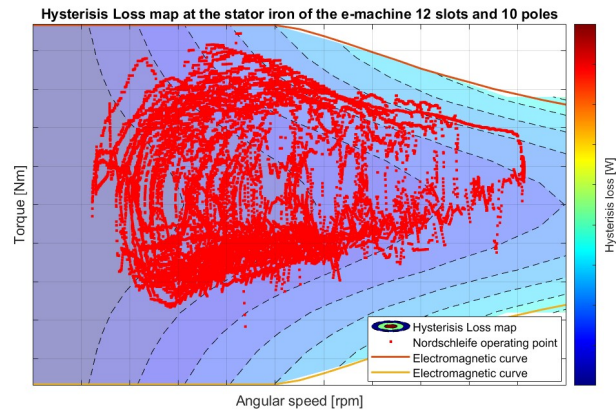


(c) DC copper loss map of the e-machine 24 slots and 20 poles

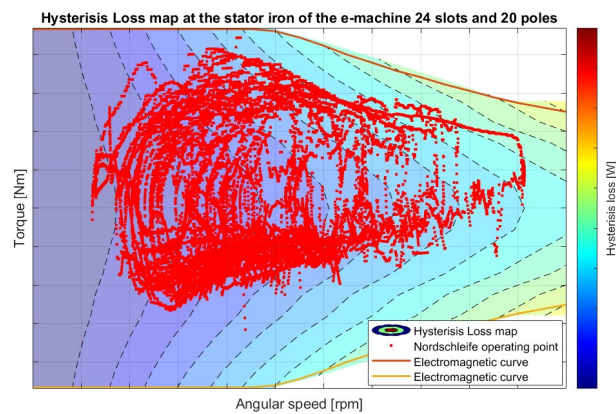
Figure 6.1: DC copper loss maps of the three electrical machines



(a) Hysteresis loss map of the e-machine 24 slots and 22 poles

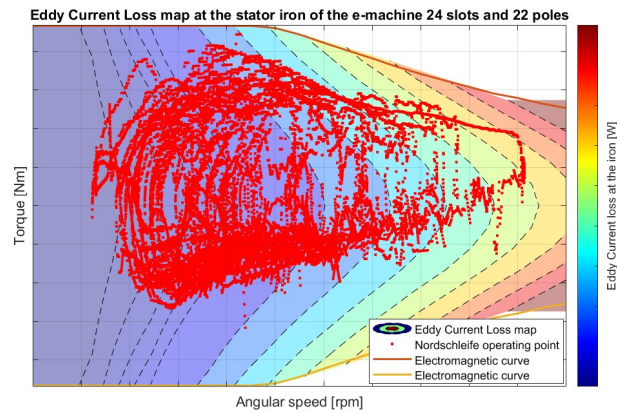


(b) Hysteresis loss map of the e-machine 12 slots and 10 poles

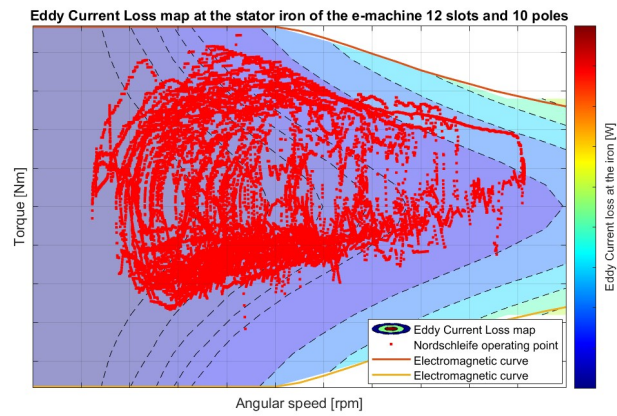


(c) Hysteresis loss map of the e-machine 24 slots and 20 poles

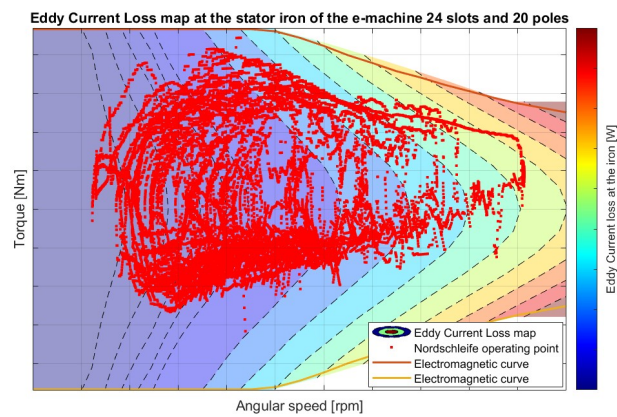
Figure 6.2: Hysteresis loss maps of the three electrical machines



(a) Eddy current loss map of the e-machine 24 slots and 22 poles

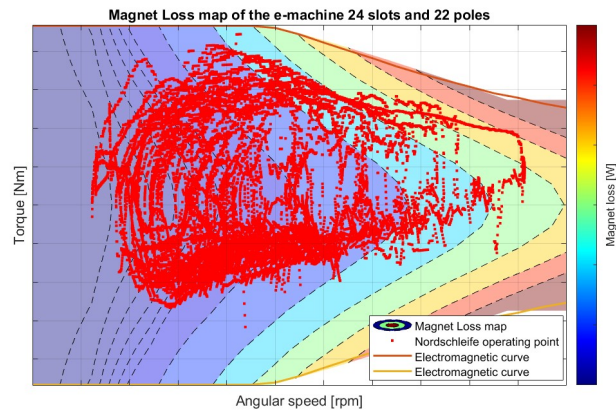


(b) Eddy current loss map of the e-machine 12 slots and 10 poles

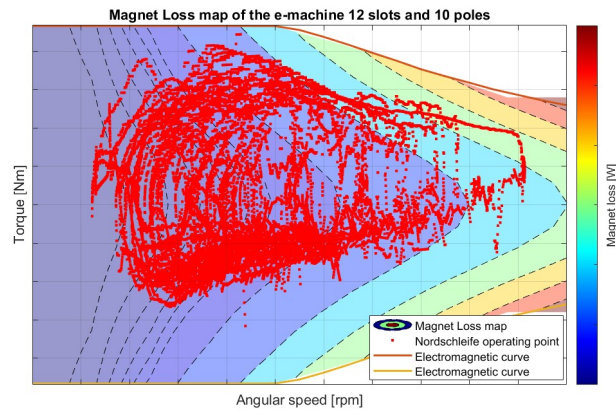


(c) Eddy current loss map of the e-machine 24 slots and 20 poles

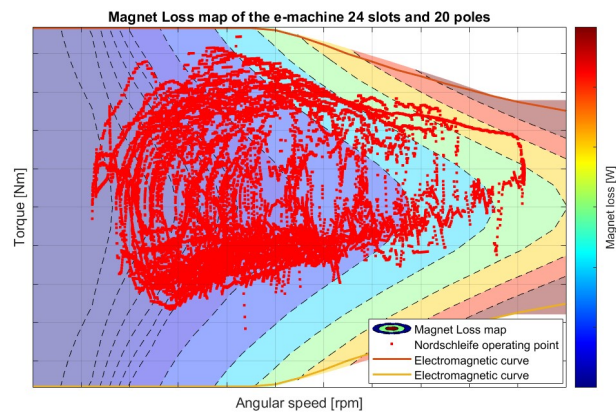
Figure 6.3: Eddy current loss maps of the three electrical machines



(a) Magnet loss map of the e-machine 24 slots and 22 poles

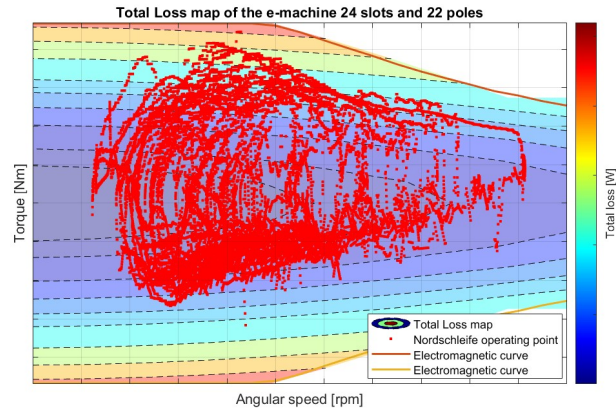


(b) Magnet loss map of the e-machine 12 slots and 10 poles

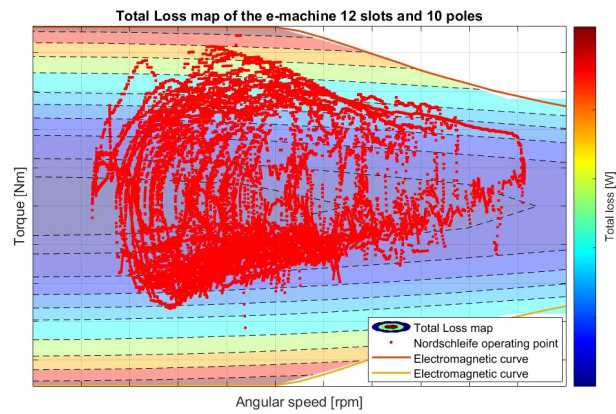


(c) Magnet loss map of the e-machine 24 slots and 20 poles

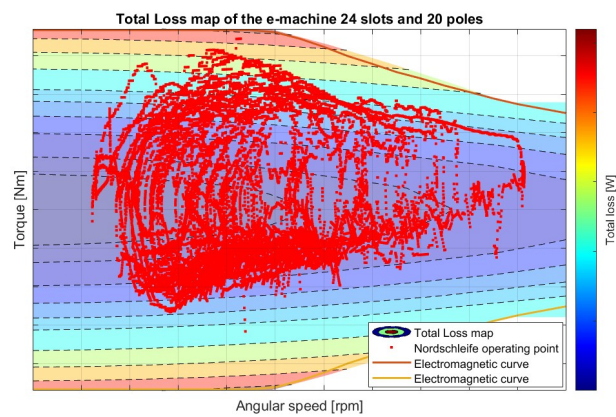
Figure 6.4: Magnet loss maps of the three electrical machines



(a) Total loss map of the e-machine 24 slots and 22 poles



(b) Total loss map of the e-machine 12 slots and 10 poles



(c) Total loss map of the e-machine 24 slots and 20 poles

Figure 6.5: Total Loss maps of the three electrical machines

It is important to highlight that AC copper, bearing losses and windage losses are not calculated from the FEA software.

6.2 Results

In the figures above, a scatter plot of torque-speed operating points from the Nordschleife driving cycle is displayed onto the loss maps. This plotting allows the determination of power loss at every operating point by using the 'interp2' function in Matlab. Given the loss maps matrices, generated through repeated FEA magnetostatic simulations as described in the previous section for different combinations of torque and speed required, the interp2 function enables linear interpolation between the loss map and each operating point.

Subsequently, it becomes feasible to compute the energy consumed by each loss component for all three machines and their cumulative energy consumption. This analysis aids in identifying which of the three machines not only fulfills the requirements of the three driving cycles but also exhibits the lowest energy consumption for race application.

	e-Motor 24 slots and 22 poles	e-Motor 12 slots and 10 poles	e-Motor 24 slots and 20 poles
Energy consumed due to DC copper loss [kWh]	76,75%	93,55%	79,72%
Energy consumed due to Eddy Current loss [kWh]	4,18%	1,64%	3,82%
Energy consumed due to Hysteresis loss [kWh]	4,51%	2,65%	4,33%
Energy consumed due to Magnet loss [kWh]	14,56%	11%	14,33%
Cumulative energy consumption [kWh]	100%	108,85%	103,21%

Table 6.1: Energy consumption of the three optimised machines for Nordschleife driving cycle

The table's results are normalised against the Cumulative energy consumption

of the electrical machine with 24 slots and 22 poles.

It is evident that DC copper loss is the predominant loss component in the e-machines compared to other types of losses. Notably, while the machines with 20 and 22 poles record the highest iron and magnet losses, overall the motor with 12 slots and 10 poles is the most energy consuming.

Furthermore, analysis of the iron and magnets loss maps above shows that, during Nordschleife driving cycles, most operating points frequently are in the mid-speed, low negative torque region where the iron and magnet loss values for all three machines are comparatively small and similar.

In addition, it is possible to perceive that the energy consumed due to Hysteresis loss is slightly larger than the one due to the Eddy current loss for the three e-motors. This occurs because, as mentioned before, most of operating points are in the mid-low speed and low torque region where the hysteresis loss prevails with respect to eddy current loss while at the high speed region, it is the contrary.

All in all, the DC copper loss map is the key factor in determining the machine with the highest energy consumption particularly, as the driving cycle considered requires frequent acceleration and decelerations, some operating points are placed in high torque and mid-speed areas. This loss depends on the amount of current supplied and the phase resistance of the windings of the three motors.

While it is detectable from the table the e-machine with minimal energy consumption that establishes the final choice for the car against the other two, it is important to recall that this assessment, conducted with the Quasi-3D FEA software, only accounts for DC copper loss, iron losses and magnet loss.

Chapter 7

Conclusion

Overall, what is shown in this thesis is the application of multi-objective optimisation problem in the electromagnetic aspect of motor design aiming to maximise the performance and efficiency and minimise the cost of the traction motor.

However, nowadays, there are car manufacturers and researchers that are developing an advance multi-objective optimisation solver able to also deal with thermal and mechanical aspects.

Genetic algorithm with the finite element analysis is considered as a good method to optimise the high-performance motors under severe constraints.

However, this method is not well suited for machines characterised by many geometrical parameters. The main reason is that, due to the independent variation of these parameters, there is a higher probability of conflict [37]. This phenomenon is well highlighted above all if the population size is very high to move well in the domain and find the global optimum easily.

It is not a good approach reducing the range of variation of the genes causing the reduction of the space domain and so, having higher probability of finding local optimum instead of global one.

Hence, new techniques are developed to successfully solve the geometrical conflicts. One proposed method is the sequential application of the genetic algorithm and a machine learning based predicted model. The task of the genetic algorithm is to optimise the range of variation of the geometrical parameters and minimising the conflicts. While the predicted model is to learn if there is a conflict for a certain value of the parameters so that later there will be generation of machines with a correct geometry.

Appendix A

Quotes of the axial flux machine

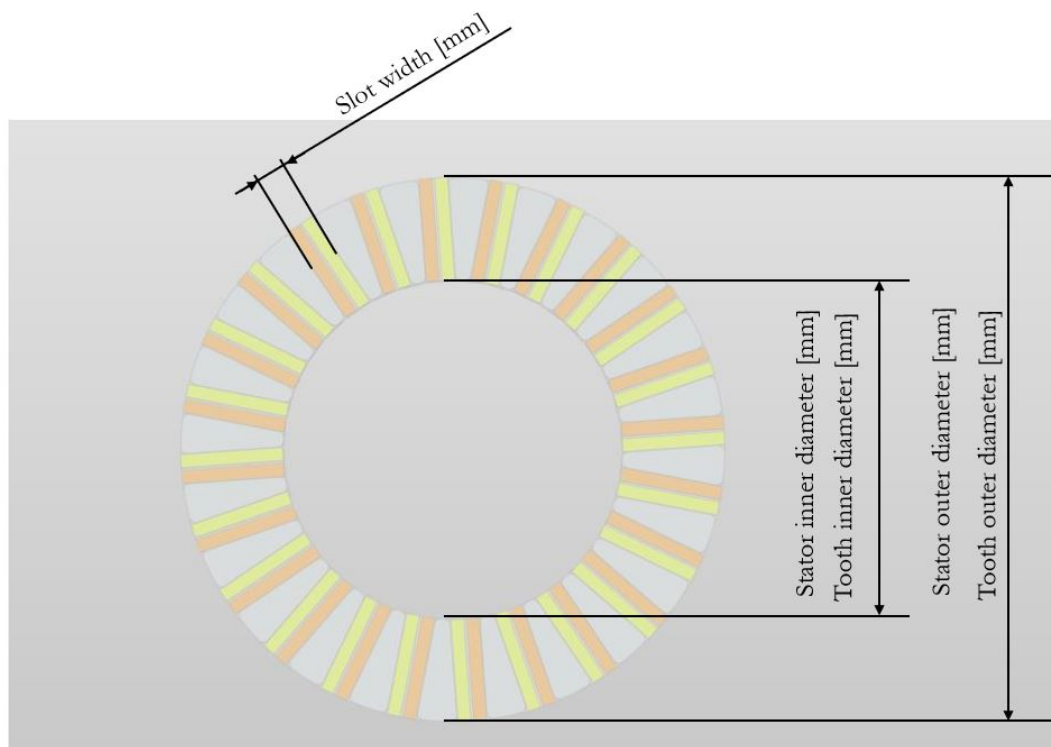


Figure A.1: Quotes on the stator disc

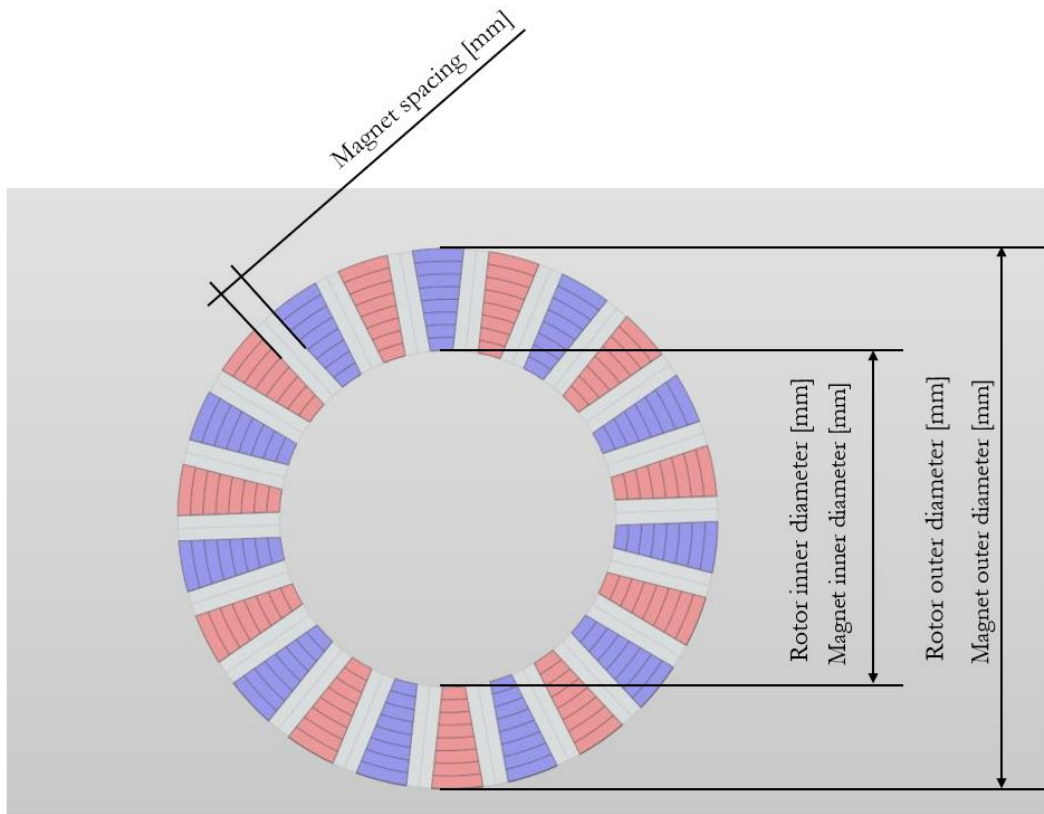


Figure A.2: Quotes on the rotor disc

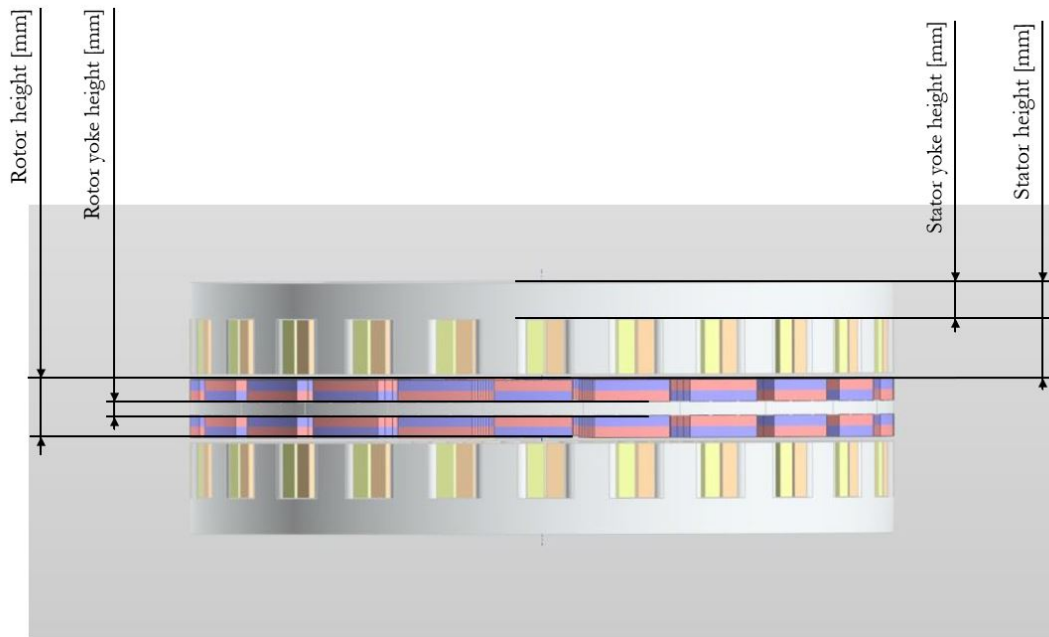


Figure A.3: Quotes on the lateral surface of the e-machine

Appendix B

Calculation of the current input and advance angle given an operating point

```
1 %% Calculation of the input current and advance angle
   given the torque and speed of an operating point
2 I_peak = I_rms_max*sqrt(2);
3 V_max = V_DC*MI/sqrt(3);
4 if Ld == Lq
5     beta_MTPA = 90;
6 else
7     cos_beta_MTPA = (-lambda_m+sqrt(lambda_m^2+(8*(
   Lq-Ld)^2*I_peak^2)))/(-4*(Lq-Ld)*I_peak);
8     beta_MTPA = acosd(cos_beta_MTPA);
9 end
10 w_el = rpm_mech*(pi/30)*PolePairs;
11 id = I_peak*cos_beta_MTPA(u):-0.01:-I_peak;
12 iq = zeros(size(id));
13 vd = zeros(size(id));
14 vq = zeros(size(id));
15 V = zeros(size(id));
16 I = zeros(size(id));
17 for i = 1:length(id)
18     iq(i) = Tem/((3/2)*PolePairs*(lambda_m+(Ld-Lq)*id(i)
   ));
```

```

19 vd(i) = -w_el*(Lq*iq(i));
20 vq(i) = w_el*((Ld*id(i))+lambda_m);
21 V(i) = sqrt(3)*sqrt(vd(i)^2+vq(i)^2);
22 if V(i) > V_DC*MI
23     iq(i) = NaN;
24     id(i) = NaN;
25     vd(i) = NaN;
26     vq(i) = NaN;
27     V(i) = NaN;
28     I(i) = NaN;
29 end
30 I(i) = sqrt(id(i)^2+iq(i)^2);
31 if I(i) > I_peak
32     iq(i) = NaN;
33     id(i) = NaN;
34     vd(i) = NaN;
35     vq(i) = NaN;
36     V(i) = NaN;
37     I(i) = NaN;
38 end
39 end
40 % Then find the combination of id and iq that provides
41 the least magnitude of the phase input current
42 [Ipeak_required,idx_min] = min(I);
43 if isnan(Ipeak_Nord)==1 % the e-machine cannot
44 operate at that operating point
45     Ipeak_required = NaN
46     idx_min = NaN
47     id_required = NaN
48     iq_required = NaN
49     beta_required = NaN
50     gamma_required = NaN
51 else
52     id_required = id(idx_min)
53     iq_required = iq(idx_min)
54     beta_required = atan2d(iq_required,id_required)
55     gamma_required = beta_required-90
56 end

```


Appendix C

Comparison of the non dominated solutions

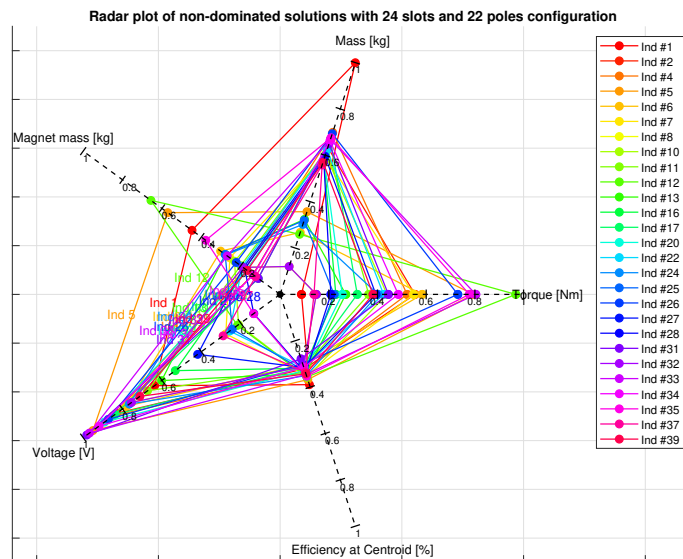


Figure C.1: E-machines with 24 slots and 22 poles

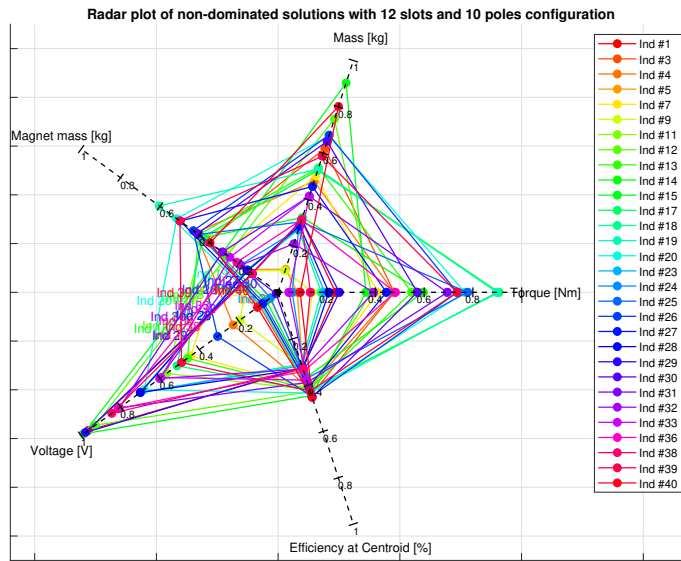


Figure C.2: E-machines with 12 slots and 10 poles

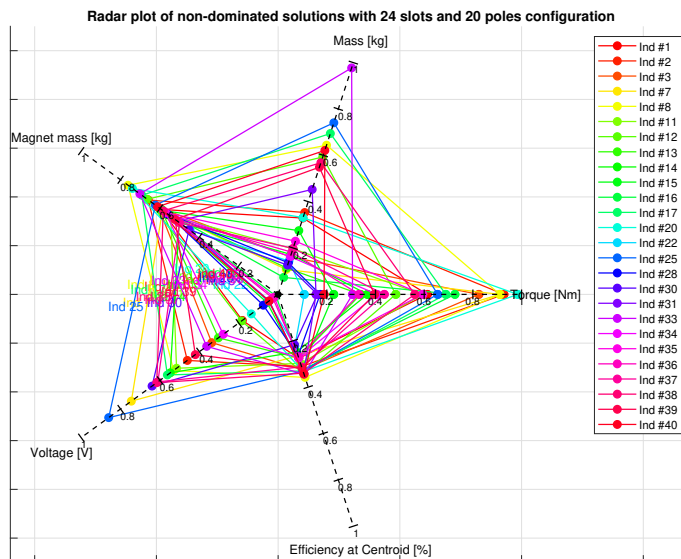


Figure C.3: E-machines with 24 slots and 20 poles

Bibliography

- [1] Mehmet Gulec and Metin Aydin. «Implementation of different 2D finite element modelling approaches in axial flux permanent magnet disc machines». In: *IET Electric Power Applications* 12.2 (2018), pp. 195–202 (cit. on p. 1).
- [2] URL: <https://motorxp.com/quasi3d-fe-modelling-of-afm/> (cit. on p. 2).
- [3] *Genetic Optimization System Engineering Toolbox 2.6*. URL: <https://engineering.purdue.edu/ECE/Research/Areas/PES/Software/genetic-optimization-toolbox-2.6> (cit. on p. 2).
- [4] Sudhoff. *GOSET For Use with MATLAB Manual version 2.3*. Purdue University School of Electrical and Computer Engineering, 2007. URL: <https://engineering.purdue.edu/~sudhoff/Software%20Distribution/GOSET%202.3%20manual.pdf> (cit. on pp. 2, 3).
- [5] Yidan Chu and Hongyang Cui. «Annual update on the global transition to electric vehicles: 2022». In: *Icct-the International Council on Clean Transportation*, (nd). <https://theicct.org/publication/global-transition-electric-vehicles-update-jun23/> (accessed July 5th, 2022) (2023) (cit. on p. 6).
- [6] Andreas Krings and Christian Monissen. «Review and trends in electric traction motors for battery electric and hybrid vehicles». In: *2020 International Conference on Electrical Machines (ICEM)*. Vol. 1. IEEE. 2020, pp. 1807–1813 (cit. on p. 6).
- [7] Masaharu Nakanishi, Kenji Hayashi, Akifumi Enomoto, Masashi Hayashiguchi, Motohiro Ando, Kazuhide Ino, Christian Felgемacher, Aly Mashaly, and Guenter Richard. «Automotive traction inverter utilizing sic power module». In: *PCIM Europe 2018; International Exhibition and Conference for Power Electronics, Intelligent Motion, Renewable Energy and Energy Management*. VDE. 2018, pp. 1–6 (cit. on p. 7).
- [8] C Peter Cho. «Permanent Magnet Motors/Generators for Automotive Applications». In: *Permanent Magnet Systems Gorham Advanced Materials Inc* (2000) (cit. on p. 7).

- [9] Jacek F Gieras, Rong-Jie Wang, and Maarten J Kamper. *Axial flux permanent magnet brushless machines*. Springer Science & Business Media, 2008 (cit. on pp. 7, 10, 11, 18, 19, 42).
- [10] Nasser Hashemnia and Behzad Asaei. «Comparative study of using different electric motors in the electric vehicles». In: *2008 18th international conference on electrical machines*. IEEE. 2008, pp. 1–5 (cit. on p. 9).
- [11] URL: <https://www.greencarcongress.com/2023/06/20230620-111.html> (cit. on p. 11).
- [12] Dana Mezher. «Modeling an Axial Flux Machine». In: (2021) (cit. on p. 12).
- [13] Amin Mahmoudi, NA Rahim, and WP Hew. «Axial-flux permanent-magnet machine modeling, design, simulation, and analysis». In: *Scientific Research and Essays* 6.12 (2011), pp. 2525–2549 (cit. on pp. 13–16).
- [14] Christian Du-Bar. «Design of an axial flux machine for an in-wheel motor application». In: *Chalmers Reproservice, Göteborg* (2011), pp. 1–2 (cit. on p. 14).
- [15] *Axial Flux Electric Motor Technology: Aerospace Motor*. 2023. URL: <https://evolito.aero/technology/> (cit. on p. 15).
- [16] Asko Parviainen et al. «Design of axial-flux permanent-magnet low-speed machines and performance comparison between radial-flux and axial-flux machines». In: (2005) (cit. on pp. 16, 18).
- [17] Mickaël Kremer. «Electromagnetic design of a disc rotor electric machine as integrated motor-generator for hybrid vehicles». PhD thesis. Université de Haute Alsace-Mulhouse, 2016 (cit. on pp. 17, 41).
- [18] URL: <https://jystator.com/axialfluxstator.html> (cit. on p. 17).
- [19] URL: <https://www.focussmc.com/soft-magnetic-composites-for-bldc-pump-motor-p19.html> (cit. on p. 17).
- [20] Alberto Tenconi. «Sistemi di propulsione elettrica per i mezzi di trasporto». In: *University lecture* (2019) (cit. on p. 17).
- [21] Florence Meier. «Permanent-magnet synchronous machines with non-overlapping concentrated windings for low-speed direct-drive applications». PhD thesis. KTH, 2008 (cit. on pp. 19, 42).
- [22] Ayman M El-Refaei, Thomas M Jahns, and Donald W Novotny. «Analysis of surface permanent magnet machines with fractional-slot concentrated windings». In: *IEEE Transactions on Energy conversion* 21.1 (2006), pp. 34–43 (cit. on p. 20).
- [23] URL: <https://www.koenigsegg.com/model/gemera> (cit. on p. 25).

- [24] Giancarlo Genta and Lorenzo Morello. *The automotive chassis: vol. 2: system design*. Springer, 2009 (cit. on p. 27).
- [25] Marah Al Halabi and Anas Al Tarabsheh. *Modelling of electric vehicles using Matlab/Simulink*. Tech. rep. SAE Technical Paper, 2020 (cit. on p. 27).
- [26] Rickard Höglund. *Modelling of a high-performance vehicle in MATLAB/Simulink and Canopy Simulations*. 2022 (cit. on p. 27).
- [27] Bharadwaj Raghuraman and Tom Gyllensten. «Electric machine design based on drive cycle analysis». In: (2019) (cit. on p. 35).
- [28] Philip Korta. «Multi-Objective Drive-Cycle Based Design Optimization of Permanent Magnet Synchronous Machines». PhD thesis. University of Windsor (Canada), 2018 (cit. on p. 35).
- [29] Shai Shalev-Shwartz and Shai Ben-David. *Understanding machine learning: From theory to algorithms*. Cambridge university press, 2014 (cit. on p. 37).
- [30] Adam Coates and Andrew Y Ng. «Learning feature representations with k-means». In: *Neural Networks: Tricks of the Trade: Second Edition*. Springer, 2012, pp. 561–580 (cit. on p. 37).
- [31] Surong Huang, Jian Luo, Franco Leonardi, and Thomas A Lipo. «A comparison of power density for axial flux machines based on general purpose sizing equations». In: *IEEE Transactions on energy conversion* 14.2 (1999), pp. 185–192 (cit. on p. 41).
- [32] BJ Chalmers and E Spooner. «An axial-flux permanent-magnet generator for a gearless wind energy system». In: *IEEE Transactions on Energy Conversion* 14.2 (1999), pp. 251–257 (cit. on p. 41).
- [33] Lubna Nasrin. *Improved Version of Energy Efficient Motor for Shell Eco Marathon: Half Weight with Higher Efficiency*. 2011 (cit. on p. 41).
- [34] Juha Pyrhonen, Valeria Hrabovcova, and R Scott Semken. *Electrical machine drives control: An introduction*. John Wiley & Sons, 2016 (cit. on p. 47).
- [35] Scott D Sudhoff. *Power magnetic devices: a multi-objective design approach*. John Wiley & Sons, 2021 (cit. on p. 60).
- [36] Jamshid Mavlonov, Sanjarbek Ruzimov, Andrea Tonoli, Nicola Amati, and Akmal Mukhitdinov. «Sensitivity Analysis of Electric Energy Consumption in Battery Electric Vehicles with Different Electric Motors». In: *World Electric Vehicle Journal* 14.2 (2023), p. 36 (cit. on p. 93).
- [37] N Schneider, M Kanamaru, H Sano, and T Yamada. «Solving geometry conflicts in GA Optimizations with large numbers of geometric parameters». In: *2022 International Conference on Electrical Machines (ICEM)*. IEEE, 2022, pp. 1034–1040 (cit. on p. 102).